Analysis of microstrip antennas in the spectral domain using a moment method

Smolders, A.B.

Award date:
1989

EINDHOVEN UNIVERSITY OF TECHNOLOGY
DEPARTMENT OF ELECTRICAL ENGINEERING
PROFESSIONAL GROUP ELECTROMAGNETISM
AND CIRCUIT THEORY

ANALYSIS OF MICROSTRIP ANTENNAS IN THE SPECTRAL DOMAIN USING A MOMENT METHOD

by: A.B. Smolders

Report no.: ET-15-89

This study has been performed in fulfilment of the requirements for the degree of Master of Science (Ir.) at the Eindhoven University of Technology from January 1989 until October 1989 under supervision of Dr. M.E.J. Jeuken.
Eindhoven, October 1989

SUMMARY

In this report a general moment method is presented to analyze an arbitrarily shaped single layered microstrip structure. This planar microstrip structure can be a single microstrip antenna or an array of microstrip antennas and can have a protective dielectric layer. Two types of excitation have been considered, namely a coaxial feed and a stripline feed.
Because the fields in the dielectric slab are calculated in the spectral domain, the method is called a spectral domain moment method.

The first step in the formulation of the method is the derivation of the exact Green's function for the dielectric slab in the spectral domain. Using this Green's function, the fields in the dielectric slab can be calculated.
Then, using the reaction theorem, an integral equation for the unknown current density on the upper conductor of the microstrip structure is obtained. This integral equation describes the relation between the current density on the upper conductor and the current density on the source.
The integral equation is transformed into a set of linear equations by expanding the current density on the upper conductor in basis functions. Solving the resulting matrix equation yields the unknown current density on the upper conductor of the microstrip antenna. Once this current density is known, the input impedance (or mutual coupling) and the resonant frequency can be calculated.
Two types of basis functions have been used in this report, namely sinusoidal entire domain basis functions and rooftop sub domain basis functions.

In this report much attention is paid to the computational and numerical problems of the spectral domain moment method. For the case of rooftop sub domain basis functions, a very efficient numerical method is presented.

For a single rectangular and for an array of rectangular microstrip antennas, the resonant frequency and input impedance have been calculated. It is concluded that for a simple rectangular microstrip antenna the best choice for the type of basis function is the entire domain sinusoidal basis function. In order to analyze a more complex microstrip structure, rooftop sub domain basis functions can be used. The prediction of the input impedance is in this case more difficult due to the simple model of the coaxial (or stripline) feed.

CONTENTS.

1. INTRODUCTION.

Over the past decade, there has been an increasing interest in microstrip antennas. Because of the flat structure of microstrip antennas they can be used for many applications for which conventional parabolic antennas are less suited. They can for example be used for mobile satellite communications in the frequency band of 1.5 $\longrightarrow$ 1.6Ghz [1]. In this case, the microstrip array antenna is positioned on a truck or boot. Another application is in the field of satellite-tv receivers at 12Ghz [2].

A great disadvantage of microstrip antennas is the small bandwidth of this resonant structure. A simple circular microstrip antenna has a VSWR-bandwidth of about 1% or less. In the case of mobile satellite communications a bandwidth of at least 6.5% is required. So in this case a simple circular microstrip antenna cannot be used. Therefore other structures have to be considered. Two possible microstrip structures with a greater bandwidth are shown in figure 1.1, namely a dual stacked microstrip antenna and a crossed slot microstrip antenna. In [3] one claims that the bandwidth requirement for mobile satellite communications using this elements can be satisfied.

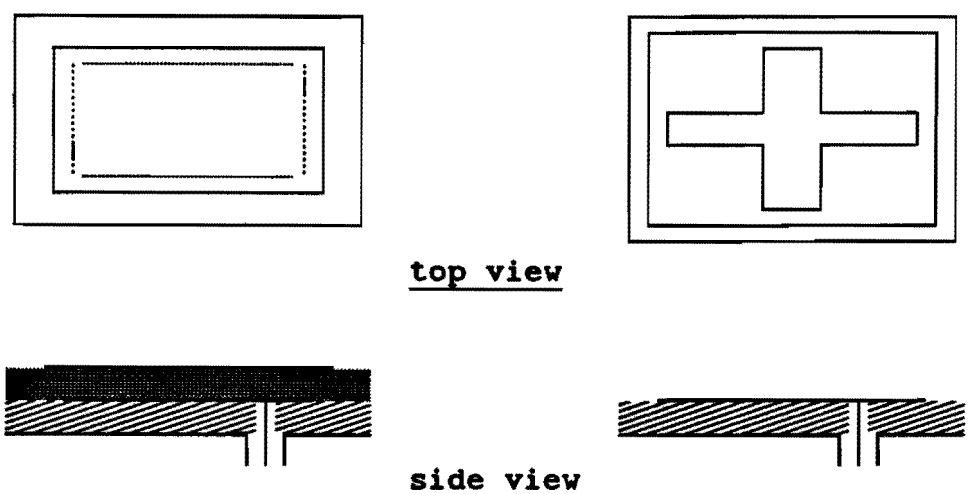

Fig 1.1: Dual stacked (a) and a crossed slot (b) microstrip antenna.

Complex microstrip structures, such as the stacked and crossed-slot microstrip antennas, cannot be analyzed using simple models, such as the cavity model [4]. A more rigorous approach has to be used in this case.

In this report a method is presented for the analysis of arbitrarily shaped single layered microstrip structures, with a protective dielectric layer. The method can also be used to analyze an array of microstrip antennas. The principles of the method were first presented in [5,6].
First we shall derive the exact Green's function for the dielectric slab in the spectral domain. Because the exact Green's function is used, the method accounts for surface waves effects.
Then an integral equation for the unknown current density on the upper conductor is obtained. This integral equation is then transformed into a set of linear equations by expanding the current density on the upper conductor in basis functions. Because the formulation is done in the spectral domain, this method is called a spectral domain moment method.

In [7] another moment method solution is presented for the analysis of dual stacked rectangular microstrip antennas. There the Green's function is calculated in the space domain.

The structure of this report is as follows. In chapter 2 the matrix equation for the unknown expansion coefficients of the expanded patch current is derived. Once this equation is solved the resonant frequency and input impedance can be obtained.
In chapter 3 the computational and numerical problems of the moment method presented here are discussed. Finally in chapter 4 some results are presented for the case of a single rectangular microstrip antenna and for the case of an array of microstrip antennas.

In this report much attention is paid to the computational problems of the spectral moment method. The resulting programs, written in FORTRAN-77, are very efficient and can therefore be used on a simple personal computer.

2. ANALYSIS OF AN ARBITRARILY SHAPED MICROSTRIP ANTENNA: A SPECTRAL DOMAIN APPROACH.

In this chapter a moment method is presented to compute the resonant frequency and input impedance of an arbitrarily shaped microstrip antenna. The method uses the exact Green's function for the dielectric slab, and thus accounts for surface waves and coupling to adjacent antenna elements.
The only approximations are made in the numerical treatment of the problem. An efficient numerical treatment is given in chapter 3 and 4. The presented method can handle edge (microstrip line) or probe (coaxial) type feeds.
Apart from the calculation of resonant frequency and input impedance, the mutual coupling between two or more microstrip antennas and the radiation pattern of a single microstrip antenna or of an array of microstrip antennas can also be analyzed using the method presented here.

2.1. Model description.

The geometry of the analytical model is illustrated in fig. 2.1. Index 1 and 2 are associated, respectively, with the dielectric substrate and with the infinite dielectric medium above the substrate.
The substrate extends to infinity in the x- and y-direction and is made of an isotropic, homogeneous and lossy material. If $\tan\delta$ is the loss tangent of the substrate material then the permittivity ε_r is complex:

$$\varepsilon_r = \varepsilon_r' - j\varepsilon_r'' = \varepsilon_r'(1 - j\tan\delta) \qquad (2.1.1)$$

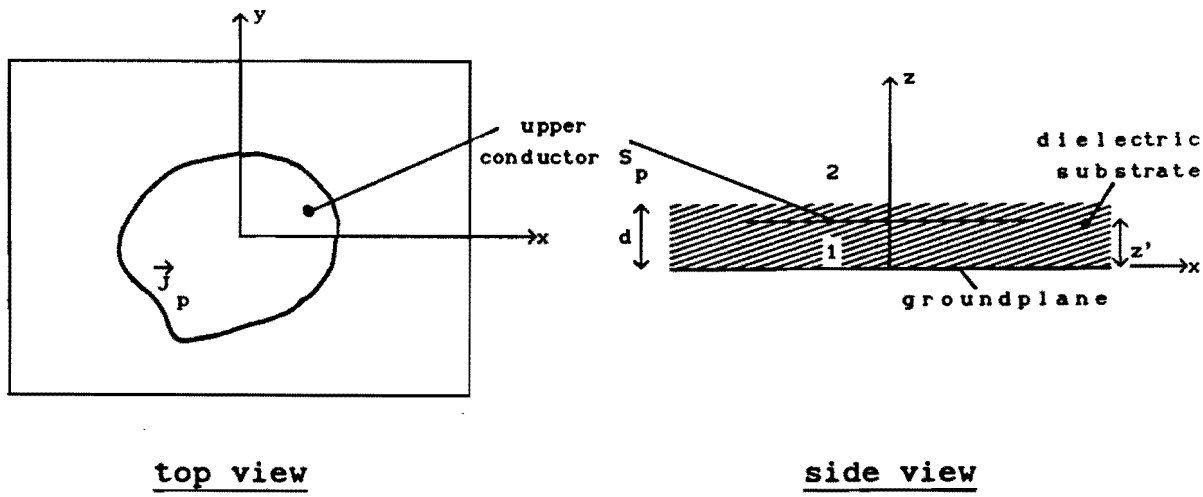

Fig. 2.1: General microstrip structure.

The ground plane and upper conductor are infinitely thin perfect electric conductors. The upper conductor is located in the z=z' plane, denoted S_p. Because the dielectric substrate has thickness d, microstrip antennas with a dielectric cover can also be analyzed.
The upper conductor is fed either by a microstrip feed line or a coaxial probe. (x_s,y_s) is the excitation point of the antenna.

2.2. Green's functions.

The fields in the dielectric slab can be calculated once the dyadic Green's function is known. Green's functions are vector potentials created by a unit source. In the case of a microstrip structure the source is a horizontally directed electric dipole located at the $z=z'$ plane. The vector potential resulting from a finite source, can then be found by dividing this source into an infinite number of elementary dipoles, and then integrating the contributions of all the elementary dipoles.
The vector potential $\vec{A}$ at the point $\vec{r}$ can be written as:

$$\vec{A} = \iint_{S_p} \overline{\overline{G}}(\vec{r},\vec{r}\,').\vec{J}_p(\vec{r}\,')\, dS \qquad (2.2.1)$$

where $\vec{J}_p(\vec{r}\,')$ is the surface current density on the upper conductor. $\vec{r}\,'$ is a point on the upper conductor.

The dyadic Green's function is a 3x3 matrix with general form:

$$\overline{\overline{G}}(\vec{r},\vec{r}\,') = \begin{bmatrix} G_{xx} & G_{xy} & G_{xz} \\ G_{yx} & G_{yy} & G_{yz} \\ G_{zx} & G_{zy} & G_{zz} \end{bmatrix} \qquad (2.2.2)$$

The subscripts 1 and 2 shall be used to indicate whether the quantity is defined in medium 1 or 2.

2.2.1 Fields from a horizontal electric dipole.

Consider a $\hat{x}$-directed infinitesimal dipole of unit strength, located at the point $\vec{r}' = (x', y', z')$. This is illustrated in fig. 2.2. The volume current density associated with this dipole is then:

$$\vec{J}_d = \vec{e}_x \, \delta(x-x')\delta(y-y')\delta(z-z') \qquad (2.2.3)$$

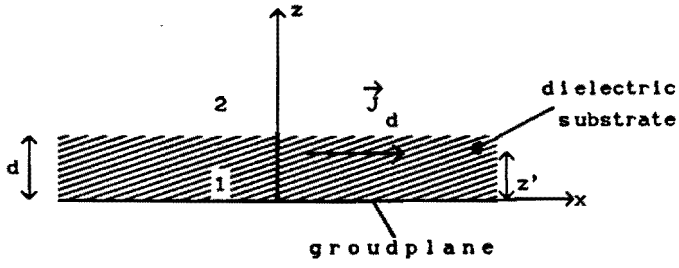

side view

Fig. 2.2: Horizontal electric dipole at (x', y', z')

With a time dependence $e^{j\omega t}$, Maxwell's equations in region 1 or region 2 take the form:

$$\nabla \times \vec{E} = -j\omega\mu_0 \vec{H}$$
$$\nabla \times \vec{H} = j\omega\varepsilon \vec{E} + \vec{J} \qquad (2.2.4)$$

where ω is the radial frequency, ε is the permittivity and μ_0 the permeability. $\vec{J}$ is the volume current density in the region of interest. The electric and magnetic fields can be written in terms of the vector potential $\vec{A}$ and scalar potential ϕ :

$$\vec{H} = \frac{1}{\mu_0} \nabla x \vec{A}$$

$$\vec{E} = -j\omega\vec{A} - \nabla\phi \qquad (2.2.5a)$$

The divergence of the vector potential $\vec{A}$ can be specified with the Lorentz Gauge [8]:

$$\nabla.\vec{A} = -j\omega\varepsilon\mu_0\phi \qquad (2.2.5b)$$

Substituting the Lorentz Gauge (2.2.5b) in equation (2.2.5a) results in:

$$\vec{E}_1 = \frac{-j\omega}{k^2}\left[k^2\vec{A}_1 + \nabla(\nabla.\vec{A}_1)\right]$$

$$\vec{H}_1 = \frac{1}{\mu_0}\nabla x \vec{A}_1 \qquad (2.2.6a)$$

(2.2.6a) may be written in the form:

$$\vec{E}_1 = \frac{-j\omega}{k^2}\Big[(k^2A_{1x} + \partial_x^2A_{1x} + \partial_x\partial_yA_{1y} + \partial_x\partial_zA_{1z})\vec{e}_x + (k^2A_{1y} + \partial_y^2A_{1y} + \partial_y\partial_xA_{1x} + \partial_y\partial_zA_{1z})\vec{e}_y + (k^2A_{1z} + \partial_z^2A_{1z} + \partial_z\partial_xA_{1x} + \partial_z\partial_yA_{1y})\vec{e}_z\Big] \qquad (2.2.6b)$$

$$\vec{H}_1 = \frac{1}{\mu_0}\Big[(\partial_yA_{1z} - \partial_zA_{1y})\vec{e}_x + (\partial_zA_{1x} - \partial_xA_{1z})\vec{e}_y + (\partial_xA_{1y} - \partial_yA_{1x})\vec{e}_z\Big]$$

If we combine the two equations (2.2.4) and (2.2.5a) with (2.2.5b) one can derive the following expression for the vector potential $\vec{A}$, in region 1 and 2, for a $\hat{x}$-directed dipole located in the z=z′ plane:

$$\begin{aligned} \nabla^2\vec{A}_1 + k^2\vec{A}_1 &= -\mu_0\vec{J}_d \qquad \text{region 1} \\ \nabla^2\vec{A}_2 + k_0^2\vec{A}_2 &= \vec{0} \qquad \text{region 2} \end{aligned} \tag{2.2.7}$$

where $k^2 = \omega^2\mu_0\varepsilon = k_0^2\varepsilon_r$ is the wave number within region 1 (=dielectric substrate) and k_0^2 is the wave number within region 2 (= free space).

In the case of a homogeneous medium the vector potential $\vec{A}$ is parallel to the $\hat{x}$-directed dipole, thus $\vec{A} = A_x\vec{e}_x$. However, it is not possible to satisfy all the boundary conditions within the microstrip structure with only a $\hat{x}$-component in $\vec{A}$. Therefore a second component, A_z, has to be present in order to satisfy all boundary conditions. With $\vec{A}(\vec{r}) = A_x(\vec{r})\vec{e}_x + A_z(\vec{r})\vec{e}_z$, the equations (2.2.7) can be written in terms of the dyadic Green's function for a $\hat{x}$-directed dipole:

region 1:

$$\begin{aligned} \nabla^2 G_{1xx} + k^2 G_{1xx} &= -\mu_0\delta(x-x')\delta(y-y')\delta(z-z') \\ \nabla^2 G_{1zx} + k^2 G_{1zx} &= 0 \end{aligned} \tag{2.2.8}$$

region 2:

$$\begin{aligned} \nabla^2 G_{2xx} + k_0^2 G_{2xx} &= 0 \\ \nabla^2 G_{2zx} + k_0^2 G_{2zx} &= 0 \end{aligned} \tag{2.2.9}$$

where G_{xx} and G_{zx} are the xx ,respectively , zx components of the dyadic Green's function $\overline{\overline{G}}(\vec{r},\vec{r}')$ in region 1 or 2. Using the boundary conditions at the interfaces z=0, z=z' and z=d, the fields created by a $\hat{x}$-directed electric dipole can be derived using equations (2.2.8) and (2.2.9).

2.2.2 Boundary conditions.

On the ground plane z=0 the following condition has to be satisfied:

$$\vec{e}_z \times \vec{E}_1 = \vec{0} \tag{2.2.10}$$

At the interface z=d between region 1 and 2 the tangential component of the fields are continuous:

$$\begin{aligned} \vec{e}_z \times \vec{E}_1 &= \vec{e}_z \times \vec{E}_2 \\ \vec{e}_z \times \vec{H}_1 &= \vec{e}_z \times \vec{H}_2 \end{aligned} \tag{2.2.11}$$

Apart from the boundary conditions at the z=0 and z=d plane, the boundary conditions at the z=z' plane must also be taken into account:

$$\begin{aligned} \lim_{\delta \to 0} \left[\vec{e}_z \times \vec{H}_1 \Big|_{z'-\delta}^{z'+\delta} \right] &= \vec{J}_d \\ \lim_{\delta \to 0} \left[\vec{e}_z \cdot \vec{H}_1 \Big|_{z'-\delta}^{z'+\delta} \right] &= \vec{0} \end{aligned} \tag{2.2.12}$$

If we place a $\hat{x}$-directed electric dipole in the z = z' plane, the boundary conditions in terms of the dyadic Green's function become:

z=0 plane:

$$G_{1xx} + \frac{1}{k^2}\left[\partial_x^2 G_{1xx} + \partial_x \partial_z G_{1zx}\right] = 0$$

$$\partial_y \partial_x G_{1xx} + \partial_y \partial_z G_{1zx} = 0$$

z=d plane:

$$G_{1xx} + \frac{1}{k^2}\left[\partial_x^2 G_{1xx} + \partial_x \partial_z G_{1zx}\right] = G_{2xx} + \frac{1}{k_0^2}\left[\partial_x^2 G_{2xx} + \partial_x \partial_z G_{2zx}\right]$$

$$\frac{1}{k^2}\left[\partial_y \partial_x G_{1xx} + \partial_y \partial_z G_{1zx}\right] = \frac{1}{k_0^2}\left[\partial_y \partial_x G_{2xx} + \partial_y \partial_z G_{2zx}\right]$$

$$\partial_y G_{1zx} = \partial_y G_{2zx} \qquad (2.2.13)$$

$$\partial_z G_{1xx} - \partial_x G_{1zx} = \partial_z G_{2xx} - \partial_x G_{2zx}$$

z=z′ plane:

$$\lim_{\delta \to 0}\left[\partial_z G_{1xx}\Big|_{z'-\delta}^{z'+\delta}\right] = -\mu_0 \delta(x-x')\delta(y-y')$$

$$\lim_{\delta \to 0}\left[\partial_y G_{1xx}\Big|_{z'-\delta}^{z'+\delta}\right] = 0$$

2.2.3 Spectral domain Green's functions.

Solutions of (2.2.8) and (2.2.9), taking into account the boundary conditions (2.2.13), can be easily obtained in the spectral domain. The solutions can be found in closed form in the spectral domain. Both sides of (2.2.8) and (2.2.9) are Fourier transformed with respect to x and y. k_x and k_y are the Fourier transform variables. For a general function F(x,y) the Fourier transform is defined as:

$$\tilde{F}(k_x,k_y) = \int\int_{-\infty}^{\infty} F(x,y)\ e^{jk_x x}\ e^{jk_y y}\ dxdy \qquad (2.2.14)$$

$$= \mathbb{F}\{F(x,y)\}$$

with inverse Fourier transform:

$$F(x,y) = \frac{1}{4\pi^2} \int\int_{-\infty}^{\infty} \tilde{F}(k_x,k_y)\ e^{-jk_x x}\ e^{-jk_y y}\ dk_x dk_y \qquad (2.2.15)$$

$$= \mathbb{F}^{-1}\{\tilde{F}(k_x,k_y)\}$$

A derative of F(x,y) with respect to x or y becomes in the spectral domain:

$$\begin{aligned} \mathbb{F}\{\partial_x F(x,y)\} &\Longrightarrow -jk_x\tilde{F}(k_x,k_y) \\ \mathbb{F}\{\partial_y F(x,y)\} &\Longrightarrow -jk_y\tilde{F}(k_x,k_y) \\ \mathbb{F}\{\partial_x^2 F(x,y)\} &\Longrightarrow -k_x^2\tilde{F}(k_x,k_y) \end{aligned} \qquad (2.2.16)$$

Equations (2.2.8) and (2.2.9) take the following form in the spectral domain:

$$\begin{aligned} \partial_z^2\tilde{G}_{1xx} + k_1^2\tilde{G}_{1xx} &= -\mu_0\delta(z-z')e^{jk_x x'}e^{jk_y y'} \\ \partial_z^2\tilde{G}_{1zx} + k_1^2\tilde{G}_{1zx} &= 0 \\ \partial_z^2\tilde{G}_{2xx} + k_2^2\tilde{G}_{2xx} &= 0 \\ \partial_z^2\tilde{G}_{2zx} + k_2^2\tilde{G}_{2zx} &= 0 \end{aligned} \qquad (2.2.17)$$

where $k_1^2 = k^2 - k_x^2 - k_y^2 \quad (\mathrm{Im}(k_1) < 0)$

$k_2^2 = k_0^2 - k_x^2 - k_y^2 \quad (\mathrm{Im}(k_2) < 0)$

The general solution of the inhomogeneous Helmholtz equations in the spectral domain are in region 1 and 2:

$$\tilde{G}_{1xx} = \begin{cases} C_{x1}e^{jk_1z} + C_{x2}e^{-jk_1z} & 0 \le z \le z' \\ C_{x3}e^{jk_1z} + C_{x4}e^{-jk_1z} & z' \le z \le d \end{cases}$$

$$\tilde{G}_{1zx} = C_{z1}e^{jk_1z} + C_{z2}e^{-jk_1z} \qquad (2.2.18)$$

$$\tilde{G}_{2xx} = C_{x5}e^{-jk_2z}$$

$$\tilde{G}_{2zx} = C_{z3}e^{-jk_2z}$$

where C_{xi} $i=1,..,5$, C_{zi} $i=1,2,3$ are constants that have to be determined. The fields in medium 2 can't have a e^{jk_2z} -dependence because of the Sommerfeld radiation conditions [9]. There are 8 unknown coefficients in (2.2.18). Naturally there are also 8 boundary conditions. The boundary conditions in the spectral domain are the same as the boundary conditions in the space domain (2.2.13), except for the fact that a derative with respect to x or y (∂_x or ∂_y) can be replaced, in the spectral domain, by a factor $-jk_x$ respectively $-jk_y$. This results in the following set boundary conditions in the spectral domain:

z=0 plane:

$$\tilde{G}_{1xx} - \frac{1}{k^2}\left[k_x^2\tilde{G}_{1xx} + jk_x\partial_z\tilde{G}_{1zx}\right] = 0$$

$$-jk_x\tilde{G}_{1xx} + \partial_z\tilde{G}_{1zx} = 0$$

z=d plane:

$$\tilde{G}_{1xx} - \frac{1}{k^2}\left[k_x^2\,\tilde{G}_{1xx} + jk_x\partial_z\tilde{G}_{1zx}\right] = \tilde{G}_{2xx} - \frac{1}{k_0^2}\left[k_x^2\tilde{G}_{2xx} + jk_x\partial_z\tilde{G}_{2zx}\right]$$

$$\frac{1}{k^2}\left[k_x\tilde{G}_{1xx} + j\partial_z\tilde{G}_{1zx}\right] = \frac{1}{k_0^2}\left[k_x\tilde{G}_{2xx} + j\partial_z\tilde{G}_{2zx}\right]$$

$$\tilde{G}_{1zx} = \tilde{G}_{2zx} \qquad (2.2.19)$$

$$\partial_z\tilde{G}_{1xx} + jk_x\tilde{G}_{1zx} = \partial_z\tilde{G}_{2xx} + jk_x\tilde{G}_{2zx}$$

z=z′ plane:

$$\lim_{\delta\to 0}\left[\partial_z\tilde{G}_{1xx}\Big|_{z'-\delta}^{z'+\delta}\right] = -\mu_0 e^{jk_x x'}e^{jk_y y'}$$

$$\lim_{\delta\to 0}\left[\tilde{G}_{1xx}\Big|_{z'-\delta}^{z'+\delta}\right] = 0$$

It can be shown by substitution of (2.2.18) in the boundary conditions (2.2.19) and carrying out a large amount of algebra, that the solution of the boundary value problem for the spectral Green's function in region 1 has the following form:

$$\tilde{G}_{1xx} = \mu_0 G_1 e^{jk_x x'}e^{jk_y y'}$$

$$\tilde{G}_{1zx} = -\mu_0 k_x G_2 e^{jk_x x'}e^{jk_y y'} \qquad (2.2.20)$$

with:

$$G_1 = \begin{cases} \dfrac{Ne\,\sin(k_1 z)}{Te\,k_1} & 0 \le z \le z' \\ \dfrac{\sin[k_1(z'-z)]}{k_1} + \dfrac{Ne\,\sin(k_1 z)}{Te\,k_1} & z' \le z \le d \end{cases}$$

$$G_2 = \frac{(\varepsilon_r - 1)\sin(k_1 z')\cos(k_1 z)}{TeTm}$$

$$Te = k_1\cos(k_1 d) + jk_2\sin(k_1 d)$$

$$Tm = k_2\varepsilon_r\cos(k_1 d) + jk_1\sin(k_1 d)$$

$$Ne = k_1\cos[k_1(d-z')] + jk_2\sin[k_1(d-z')]$$

The zeros of the complex functions Te and Tm correspond with solutions of the characteristic equation for TE, respectively, TM surface waves in a dielectric layer on a infinite conductor plate. More details about these surface waves can be found in chapter 3. The solutions for $\tilde{G}_{2xx}$ and $\tilde{G}_{2zx}$ have analog forms as (2.2.20). These components of the dyadic Green's function are not given here because they will not be used.
If we place a $\hat{y}$-directed electric dipole at (x',y',z'), the vector potential $\vec{A}$ will have a y- and z-component: $\vec{A} = A_y\vec{e}_y + A_z\vec{e}_z$. The associated Spectral domain Green's function then becomes:

$$\begin{aligned} \tilde{G}_{1yy} &= \mu_0 G_1 e^{jk_x x'} e^{jk_y y'} \\ \tilde{G}_{1zy} &= -\mu_0 k_y G_2 e^{jk_x x'} e^{jk_y y'} \end{aligned} \qquad (2.2.21)$$

The dyadic Green's function in the spectral domain for an arbitrarily directed electric dipole located in the z=z' plane can then be found by combining (2.2.20) with (2.2.21):

$$\overline{\overline{\tilde{G}}}_1 = \mu_0 e^{jk_x x'} e^{jk_y y'} \begin{bmatrix} G_1 & 0 & 0 \\ 0 & G_1 & 0 \\ -k_x G_2 & -k_y G_2 & 0 \end{bmatrix} = \mu_0 e^{jk_x x'} e^{jk_y y'}\ \overline{\overline{\tilde{G}}}_{1r} \qquad (2.2.22)$$

where $\tilde{\bar{\bar{G}}}_r$ is a function of (k_x, k_y, z, z').
The dyadic Green's function in the space domain is the obtained by taking the inverse Fourier transform of $\tilde{\bar{\bar{G}}}_1$:

$$\bar{\bar{G}}_1 = \frac{1}{4\pi^2} \iint_{-\infty}^{\infty} \tilde{\bar{\bar{G}}}_1 \, e^{-jk_x x} \, e^{-jk_y y} \, dk_x dk_y \qquad (2.2.23)$$

Note that the spectral domain dyadic Green's function has no source singularity in the excitation point (x',y',z'). However, the dyadic Green's function in the space domain has a $\frac{1}{|\vec{r} - \vec{r}'|}$ singularity [9]. Due to the Fourier transformation the source singularity is "spread out" in the spectral domain. To illustrate this, consider for example the Fourier transform of the function $f(x,y)) = \frac{1}{\sqrt{(x-x')^2 + (y-y')^2}}$:

$$\mathbb{F}[f(x,y)] = \frac{2\pi}{k_0 \beta} \, e^{jk_x x'} e^{jk_y y'} \qquad (2.2.24)$$

$$\text{with} \quad k_0 \beta = \sqrt{k_x^2 + k_y^2}$$

The Fourier transform of f(x,y) is an oscillating function with a decreasing amplitude for large values of β and has no singularities. Due to the source singularity, the integral in (2.2.23) will converge very slowly. The influence of the source singularity will be further discussed in section 3.3.

2.3 Fields in the dielectric slab.

Once the dyadic Green's function is known in the dielectric slab (region 1) the fields in this region can be calculated by using expression (2.2.6a) and (2.2.6b).
In the spectral domain the Fourier transform of the electric field $\vec{\tilde{E}}$ and magnetic field $\vec{\tilde{H}}$ in the dielectric slab are then found by:

$$\begin{aligned}\vec{\tilde{E}}_1 = \frac{-j\omega}{k^2}\Big[&[(k^2 - k_x^2)\tilde{A}_{1x} - k_x k_y \tilde{A}_{1y} - jk_x \partial_z \tilde{A}_{1z}]\vec{e}_x \\ &+ [(k^2 - k_y^2)\tilde{A}_{1y} - k_y k_x \tilde{A}_{1x} - jk_y \partial_z \tilde{A}_{1z}]\vec{e}_y \\ &+ [(k^2 + \partial_z^2)\tilde{A}_{1z} - jk_x \partial_z \tilde{A}_{1x} - jk_y \partial_z \tilde{A}_{1y}]\vec{e}_z\Big]\end{aligned} \tag{2.3.1}$$

$$\begin{aligned}\vec{\tilde{H}}_1 = \frac{1}{\mu_0}\Big[&(-jk_y \tilde{A}_{1z} - \partial_z \tilde{A}_{1y})\vec{e}_x + (\partial_z \tilde{A}_{1x} + jk_x \tilde{A}_{1z})\vec{e}_y \\ &+ (-jk_x \tilde{A}_{1y} + jk_y \tilde{A}_{1x})\vec{e}_z\Big]\end{aligned} \tag{2.3.2}$$

The vector potential in the dielectric slab can be written in the form:

$$\vec{A}_1 = \iint_{S_p} \overline{\overline{G}}_1(\vec{r},\vec{r}\,').\vec{J}_p(\vec{r}\,')dx'dy'$$

$$= \frac{1}{4\pi^2}\iint_{S_p}\Big[\int_{-\infty}^{\infty}\overline{\overline{\tilde{G}}}_1(k_x,k_y,z,\vec{r}\,')\, e^{-jk_x x}\, e^{-jk_y y}\, dk_x dk_y\Big].\vec{J}_p(\vec{r}\,')dx'dy'$$

$$= \frac{\mu_0}{4\pi^2} \int\int_{-\infty}^{\infty} \tilde{\tilde{G}}_{1r}(k_x,k_y,z,z') \cdot$$

$$\left[\iint_{S_p} \vec{J}_p(\vec{r}') \; e^{jk_x x'} e^{jk_y y'} dx'dy' \right] e^{-jk_x x} \; e^{-jk_y y} \; dk_x dk_y$$

$$= \frac{\mu_0}{4\pi^2} \int\int_{-\infty}^{\infty} \tilde{\tilde{G}}_{1r}(k_x,k_y,z,z') \cdot \tilde{\vec{J}}_p(k_x,k_y,z') e^{-jk_x x} \; e^{-jk_y y} \; dk_x dk_y$$

(2.3.3)

where $\tilde{\vec{J}}_p(k_x,k_y,z')$ is the Fourier transform of the surface current density on the upper conductor:

$$\tilde{\vec{J}}_p(k_x,k_y,z') = \iint_{S_p} \vec{J}_p(\vec{r}') \; e^{jk_x x'} e^{jk_y y'} dx'dy' \qquad (2.3.4)$$

$$= \tilde{J}_{px}\vec{e}_x + \tilde{J}_{py}\vec{e}_y$$

If we use expression (2.2.22) for the spectral domain dyadic Green's function, then the three components of the vector potential may be found by:

$$A_{1x} = \frac{\mu_0}{4\pi^2} \int\int_{-\infty}^{\infty} G_1 \; \tilde{J}_{px} \; e^{-jk_x x} \; e^{-jk_y y} \; dk_x dk_y$$

$$A_{1y} = \frac{\mu_0}{4\pi^2} \int\int_{-\infty}^{\infty} G_1 \; \tilde{J}_{py} \; e^{-jk_x x} \; e^{-jk_y y} \; dk_x dk_y \qquad (2.3.5)$$

$$A_{1z} = \frac{\mu_0}{4\pi^2} \int\int_{-\infty}^{\infty} [-k_x G_2 \tilde{J}_{px} - k_y G_2 \tilde{J}_{py}] \; e^{-jk_x x} \; e^{-jk_y y} \; dk_x dk_y$$

The general relationship between the surface current $\tilde{J}_p$ and the electric field $\vec{E}_1$ in the dielectric slab is according to (2.3.1) and (2.3.5):

$$E_{1x} = \frac{-j\omega\mu_0}{4\pi^2 k^2} \iint_{-\infty}^{\infty} \Big[[(k^2 - k_x^2)G_1 + jk_x^2 \partial_z G_2]\tilde{J}_{px} + [-k_x k_y G_1 + jk_x k_y \partial_z G_2]\tilde{J}_{py} \Big] e^{-jk_x x} e^{-jk_y y} \, dk_x dk_y$$

$$E_{1y} = \frac{-j\omega\mu_0}{4\pi^2 k^2} \iint_{-\infty}^{\infty} \Big[[-k_x k_y G_1 + jk_x k_y \partial_z G_2]\tilde{J}_{px} + [(k^2 - k_y^2)G_1 + jk_y^2 \partial_z G_2]\tilde{J}_{py} \Big] e^{-jk_x x} e^{-jk_y y} \, dk_x dk_y$$

$$E_{1z} = \frac{j\omega\mu_0}{\pi^2 k^2} \iint_{-\infty}^{\infty} \Big[[k_x k^2 G_2 + k_x \partial_z^2 G_2 + jk_x \partial_z G_1]\tilde{J}_{px} + [k_y k^2 G_2 + k_y \partial_z^2 G_2 + jk_y \partial_z G_1]\tilde{J}_{py} \Big] e^{-jk_x x} e^{-jk_y y} \, dk_x dk_y \qquad (2.3.6)$$

Expression (2.3.6) can be written in the form:

$$\vec{E}_1 = \frac{1}{4\pi^2} \iint_{-\infty}^{\infty} \vec{\tilde{E}}_1 \, e^{-jk_x x} e^{-jk_y y} \, dk_x dk_y$$

$$= \frac{1}{4\pi^2}\int_{-\infty}^{\infty}\int \overline{\overline{\tilde{Q}}}.\vec{\tilde{J}}_p \; e^{-jk_x x}\, e^{-jk_y y}\, dk_x dk_y \qquad (2.3.7)$$

where the spectral domain 3x3 matrix $\overline{\overline{\tilde{Q}}}$ has the form:

$$\overline{\overline{\tilde{Q}}} = \begin{bmatrix} \tilde{Q}_{xx} & \tilde{Q}_{xy} & 0 \\ \tilde{Q}_{yx} & \tilde{Q}_{yy} & 0 \\ \tilde{Q}_{zx} & \tilde{Q}_{zy} & 0 \end{bmatrix} \qquad (2.3.8)$$

$$\tilde{Q}_{xx} = \frac{-j\omega\mu_0}{k^2}\left[(k^2 - k_x^2)G_1 + jk_x^2\partial_z G_2\right]$$

$$\tilde{Q}_{xy} = \tilde{Q}_{yx} = \frac{-j\omega\mu_0}{k^2}\left[-k_x k_y G_1 + jk_x k_y \partial_z G_2\right]$$

$$\tilde{Q}_{yy} = \frac{-j\omega\mu_0}{k^2}\left[(k^2 - k_y^2)G_1 + jk_y^2\partial_z G_2\right]$$

$$\tilde{Q}_{zx} = \frac{j\omega\mu_0}{k^2}\left[k_x k^2 G_2 + k_x\partial_z^2 G_2 + jk_x\partial_z G_1\right]$$

$$\tilde{Q}_{zy} = \frac{j\omega\mu_0}{k^2}\left[k_y k^2 G_2 + k_y\partial_z^2 G_2 + jk_y\partial_z G_1\right]$$

A relationship between the patch current $\vec{J}_p$ and the magnetic field within the dielectric slab can be derived by substituting expression (2.3.5) in (2.3.2).

2.4 Resonant frequency and input impedance.

Two important properties of an single microstrip antenna are the resonant frequency and input impedance. Using a simple cavity model [4] the resonant frequency of a simple microstrip structure can be calculated. However, the calculation of the input impedance as a function of the frequency is with the cavity model troublesome and the accuracy depends on the thickness of the dielectric substrate, even for a simple microstrip structure.
The cavity model cannot be used to analyze an arbitrarily shaped microstrip antenna.
The only possibility to analyze a complicated microstrip structure is to use a moment method. The price we have to pay by using such a rigorous method is that the computation time will be enormous in comparison with a simple cavity model. Numerical details of the moment method presented here are discussed in chapter 3 and 4.

Before the characteristics of a microstrip antenna can be analyzed, the surface current on the upper conductor has to be known. The reaction theorem will be used to express the unknown patch current in terms of the impressed source current. This source can be either a coaxial feed probe or a microstrip feed line. The patch current is then expressed in terms of basis functions. Using the reaction theorem for each basis function, a Galerkin-type solution can be found. Because only the boundary condition for the electric field at the z=z' plane is used, the resulting integral equation is called an "electric field integral equation" (EFIE).

Also the mutual coupling between two or more microstrip antennas and the radiation pattern of a single microstrip antenna or the radiation pattern of an array of microstrip antennas, can be analyzed using the method presented here.

2.4.1 Source model.

In this section two types of sources shall be considered, namely a microstrip feed line and a coaxial feed probe. The microstrip line is assumed to be in the $z=z'$ plane. A third type of excitation often used, is the plane wave excitation. The microstrip antenna is now excited by a linearly polarized plane wave, travelling in the $-\hat{z}$ -direction. Using this type of excitation, the complex resonant frequency of a microstrip antenna can be determined [5].
Fig. 2.3 shows the two types of excitation. (x_s,y_s) is the excitation point. The microstrip antenna has in this example a rectangular shape.

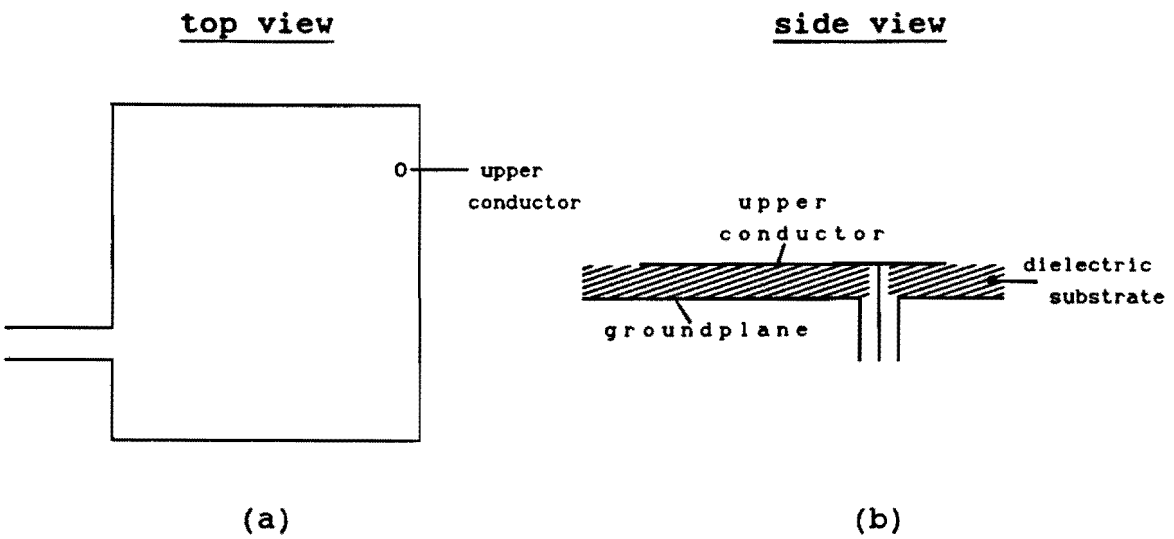

Fig. 2.3 (a) Microstrip line feed
(b) coaxial probe feed

A coaxial probe-type feed can be modeled by a cylinder with diameter equal to d_0 $(=2r_0)$. The current distribution is assumed to be uniform on the cylinder. The impressed source current is then expressed as:

$$\vec{J}_s = \frac{I_0}{2\pi r_0}\,\delta\left(\sqrt{(x-x_s)^2 + (y-y_s)^2 - r_0^2}\right)\,\vec{e}_z \qquad (2.4.1)$$

Where I_0 is the current of the source (= constant).

In the case of a microstrip feed line an equivalent current source can be obtained from the transverse magnetic field $\vec{H}_t$ at the point where the feed line connects the upper conductor. The transverse magnetic field $\vec{H}_t$ can be written as [10]:

$$\vec{H}_t = \frac{I_0}{\sqrt{w_{eff}z'}}\,\vec{e}_y \qquad (2.4.2)$$

where $w_{eff} = w + 2z'$ is the effective width of the microstrip line. The electric current source representing the feed can now be expressed as:

$$\vec{J}_s = \vec{e}_x \times \vec{H}_t$$

$$= \frac{I_0}{\sqrt{w_{eff}z'}}\,\mathrm{rect}\left[\frac{y-y_s}{w_{eff}}\right]\,\delta(x-x_s)\,\vec{e}_z \qquad (2.4.3)$$

2.4.2 Reaction theorem and integral equation.

A relationship between the unknown patch current and the source current can be found by using the reaction theorem. Consider two independent electric sources a and b (fig. 2.4). Let $\vec{E}_a$ be the electric field due to source a, and $\vec{E}_b$ the electric field caused by source b.

Fig. 2.4: Two independent electric sources a and b.

The relation between these two sources is given by the reaction theorem [11]:

$$\iiint_{\infty} [\vec{E}_a . \vec{J}_b] dV = \iiint_{\infty} [\vec{E}_b . \vec{J}_a] dV \qquad (2.4.4)$$

or: $\langle a,b \rangle = \langle b,a \rangle$

In the case of a microstrip structure the three dimensional integration becomes a two dimensional integration. $\vec{J}_a$ and $\vec{J}_b$ are now surface currents. If $\vec{J}_s$ represents the current distribution on the source and $\vec{J}_p$ the current density on the upper conductor, then the relation between these two currents may be found by:

$$\iint_{\text{source}} [\vec{E}_p . \vec{J}_s] dS = \iint_{S_p} [\vec{E}_s . \vec{J}_p] dS \qquad (2.4.5)$$

On the upper conductor S_p, the tangential component of the total electric field has to be zero. Thus:

$$(\vec{E}_p + \vec{E}_s) \times \vec{e}_z = \vec{0} \qquad \text{for } z = z' \tag{2.4.6}$$

Using this boundary condition, equation (2.4.5) represents an integral equation for the unknown patch current $\vec{J}_p$:

$$\iint_{\text{source}} [\vec{E}_p . \vec{J}_s] dS = -\iint_{S_p} [\vec{E}_p . \vec{J}_p] dS \tag{2.4.7}$$

2.4.3 Expansion of the surface current in basis functions.

The integral equation (2.4.7), where the surface current $\vec{J}_p$ is unknown, can be solved by using a moment method. The integral equation (2.4.7) is then transformed into a set of linear equations that is easily to solve with a computer. The first step in the moment method formulation is to expand the unknown patch current $\vec{J}_p$ into a set of Nmax basis functions:

$$\vec{J}_p = \sum_{j=1}^{Nmax} I_j \vec{J}_{pj} \tag{2.4.8}$$

where I_j, j=1,..,Nmax, are complex constants.
A proper choice of the basis functions is discussed in section 2.5. Now consider a test function J_{pj} on the upper conductor S_p. If $\vec{E}_{pj}$ is the electric field due to this test current, then from the integral equation (2.4.7) one obtains:

$$\iint_{source} [\vec{E}_{pj}.\vec{J}_s]dS = \iint_{S_p} [\vec{E}_p.\vec{J}_{pj}]dS \qquad (2.4.9)$$

Integral equation (2.4.9) must be satisfied for j=1,...,Nmax. $\vec{E}_p$ is the sum of all the contributions from the expansion functions $\vec{J}_{pi}$, with i = 1,..,Nmax. Thus $\vec{E}_p$ may be written as:

$$\vec{E}_p = \sum_{i=1}^{Nmax} I_i \vec{E}_{pi} \qquad (2.4.10)$$

Substitution of (2.4.10) in (2.4.9) results in the following set of equations:

$$\iint_{source} [\vec{E}_{pj}.\vec{J}_s]dS = -\sum_{i=1}^{Nmax} I_i \iint_{S_p} [\vec{E}_{pi}.\vec{J}_{pj}]dS \qquad (2.4.11)$$

where j=1,..,Nmax

In the above formulation the test functions are the same as the expansion functions. This choice is known as a Galerkin moment method solution, which ensures a fast convergence [9]. In expression (2.4.11) the magnetic field $\vec{H}_p$ is not used. Therefore the equations (2.4.11) are called "Electric Field Integral Equations" (EFIE).

2.4.4 Matrix equation

Equation (2.4.11) must apply for an arbitrarily test current $\vec{J}_{pj}$. With the notation:

$$Z_{ji} = 4\pi^2 \iint_{S_p} \vec{J}_{pj}.\vec{E}_{pi}\, dS \qquad (2.4.12a)$$

$$V_j = 4\pi^2 \iint_{source} \vec{J}_s.\vec{E}_{pj}\, dS \qquad (2.4.12b)$$

one arrives at the following matrix equation:

$$\boxed{V_j + \sum_{i=1}^{Nmax} I_i Z_{ji} = 0} \qquad j=1,..,Nmax \qquad (2.4.13)$$

Note that $\vec{E}_{pj}$ is the electric field in the dielectric slab (region 1) due to expansion current $\vec{J}_{pj}$
In matrix notation (2.4.13) becomes:

$$[V] + [Z][I] = [0]$$

The vector [I] contains the Nmax unknown complex current coefficients. The integrands of the elements of the Nmax x Nmax matrix [Z] can be written in closed form in the spectral domain:

$$Z_{ji} = 4\pi^2 \iint_{S_p} \vec{J}_{pj}.\vec{E}_{pi}\, dS$$

$$= 4\pi^2 \iint_{S_p} \vec{J}_{pj} \cdot \left[\frac{1}{4\pi^2} \int_{-\infty}^{\infty} \tilde{\vec{E}}_{pi} e^{-jk_x x}\, e^{-jk_y y}\, dk_x dk_y \right] dS$$

$$= \int_{-\infty}^{\infty} \tilde{\vec{E}}_{pi} \left[\iint_{S_p} \vec{J}_{pj} \; e^{-jk_x x} \; e^{-jk_y y} \; dxdy \right] dk_x dk_y$$

$$= \int_{-\infty}^{\infty} \tilde{\vec{E}}_{pi} . \tilde{\vec{J}}^{*}_{pj} \Big|_{z=z'} dk_x dk_y \qquad (2.4.14)$$

where $\tilde{\vec{J}}^{*}_{pj}$ is the Fourier transform of $\vec{J}^{*}_{pj}$:

$$\tilde{\vec{J}}^{*}_{pj} = \iint_{S_p} \vec{J}^{*}_{pj} \; e^{-jk_x x} \; e^{-jk_y y} \; dxdy$$

$$= \iint_{S_p} \vec{J}_{pj} \; e^{-jk_x x} \; e^{-jk_y y} \; dxdy$$

because $\vec{J}_{pj}$ is a real function of x and y. Note that $\vec{J}^{*}_{pj}$ is the complex conjugate of $\vec{J}_{pj}$.

Using (2.3.7) we observe that $\tilde{\vec{E}}_{pi} = \tilde{\overline{\overline{Q}}} . \tilde{\vec{J}}_{pi}$. Hence the coefficient Z_{ji} can be written in the form:

$$Z_{ji} = \int_{-\infty}^{\infty} [\tilde{\overline{\overline{Q}}} . \tilde{\vec{J}}_{pi}] . \tilde{\vec{J}}^{*}_{pj} \Big|_{z=z'} dk_x dk_y \qquad (2.4.15)$$

Lets consider the excitation coefficients V_j ,j=1,..,Nmax, in more detail for a coaxial-type feed. In fig. 2.5 the inner conductor of the feed is sketched.

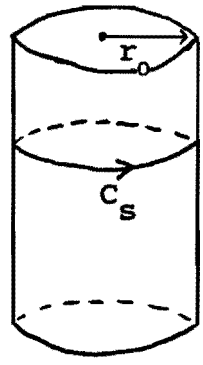

Fig. 2.5: Inner conductor of the coaxial feed.

The excitation coefficient V_j may be written as:

$$V_j = 4\pi^2 \iint_{\text{source}} \vec{J}_s . \vec{E}_{pj} \, dS$$

$$= 4\pi^2 \oint_{C_s} \int_0^{z'} \vec{J}_s . \vec{E}_{pj} \, dz \, dC_s$$

$$= \oint_{C_s} \vec{J}_s . \int_0^{z'} \left[\iint_{-\infty}^{\infty} [\tilde{\tilde{Q}} . \vec{\tilde{J}}_{pj}] e^{-jk_x x} \, e^{-jk_y y} \, dk_x dk_y \right] dz \, dC_s$$

$$= \oint_{C_s} \vec{J}_s . \iint_{-\infty}^{\infty} \int_0^{z'} [\tilde{\tilde{Q}} . \vec{\tilde{J}}_{pj}] dz \, e^{-jk_x x} \, e^{-jk_y y} \, dk_x dk_y \, dC_s$$

$$= \oint_{C_s} \vec{J}_s . \iint_{-\infty}^{\infty} [\tilde{\tilde{Q}}_v . \vec{\tilde{J}}_{pj}] \, e^{-jk_x x} \, e^{-jk_y y} \, dk_x dk_y \, dC_s \quad (2.4.16)$$

where the matrix $\overline{\overline{\tilde{Q}}}_v$ is independent of z and has the form:

$$\overline{\overline{\tilde{Q}}}_v = \begin{bmatrix} 0 & 0 & 0 \\ 0 & 0 & 0 \\ \tilde{Q}_{vzx} & \tilde{Q}_{vzy} & 0 \end{bmatrix} \qquad (2.4.17)$$

$$\tilde{Q}_{vzx} = \int_0^{z'} \tilde{Q}_{zx}\, dz$$

$$\tilde{Q}_{vzy} = \int_0^{z'} \tilde{Q}_{zy}\, dz$$

The element $\tilde{Q}_{zx}$ and $\tilde{Q}_{zy}$ are defined in (2.3.8).
The other components of $\overline{\overline{\tilde{Q}}}_v$ are zero because $\vec{J}_s$ has only a component in the z-direction. The sifting property of the delta function and expression (2.4.1) allows us to write:

$$\oint_{C_s} \vec{J}_s dC_s = \vec{e}_z \iint_{-\infty}^{\infty} \frac{I_0}{2\pi r_0} \delta\left(\sqrt{(x-x_s)^2 + (y-y_s)^2 - r_0^2}\right) dxdy \qquad (2.4.18)$$

Changing order of integration in (2.4.16) and substituting (2.4.18) gives:

$$V_j = \iint_{-\infty}^{\infty} [\overline{\overline{\tilde{Q}}}_v . \vec{\tilde{J}}_{pj}] . \vec{\tilde{J}}_s^{\,*}\, dk_x dk_y \qquad (2.4.19)$$

where $\vec{\tilde{J}}_s^{\,*}$ is the Fourier transform of the source current $\vec{J}_s^{\,*}$:

$$\vec{\tilde{J}}_s^{\,*} = \vec{e}_z \left[\iint_{-\infty}^{\infty} \frac{I_0}{2\pi r_0} \delta\left(\sqrt{(x-x_s)^2 + (y-y_s)^2 - r_0^2}\right) e^{jk_x x}\, e^{jk_y y} dxdy \right]^*$$

$$= \vec{e}_z \; I_0 J_0(r_0\sqrt{k_x^2 + k_y^2}) \; e^{-jk_x x_s} \; e^{-jk_y y_s} \qquad (2.4.20)$$

In the derivation of expression (2.4.20) the following property is used [12]:

$$\int_0^{2\pi} e^{jr\rho\cos(\phi-\psi)} d\phi = 2\pi J_0(r\rho)$$

In (2.4.20) J_0 is the Bessel function of the first kind and zero order. If the source is a microstrip line, a similar expression as (2.4.19) can be derived for the excitation coefficient V_j. The Fourier transform of $\vec{J}_s^*$ is then found by using (2.4.3):

$$\tilde{\vec{J}}_s^* = \vec{e}_z \; I_0\sqrt{w_{eff}/z'} \; \frac{2\sin(w_{eff}k_y/2)}{w_{eff}k_y} \; e^{-jk_x x_s} \; e^{-jk_y y_s} \qquad (2.4.21)$$

The resulting formulas for V_j and Z_{ji} are given in more detail in appendix 2A. This is done for two types of basis functions, namely entire domain basis functions and sub domain basis functions (see section 2.5). In order to facilitate numerical evaluation of the two dimensional integrals, a change to polar coordinates has been made in appendix 2A, such that:

$$\begin{aligned} k_x &= k_0\beta\cos\alpha \\ k_y &= k_0\beta\sin\alpha \end{aligned} \qquad (2.4.22)$$

The two dimensional infinite integrals of (2.4.15) and (2.4.19) are now transformed into one infinite integral (β) and one finite integral (α) with boundary $-\pi$ and $+\pi$. An efficient evaluation of the resulting two dimensional integral is discussed in chapter 3.

2.4.5 Resonant frequency.

The resonant frequency of a microstrip antenna can be obtained by finding a frequency f for which the determinant of the matrix [Z] is zero.
The roots of this complex determinant are in general complex. For real frequencies the determinant does not vanish, but has minimums at the points closest to the complex roots. If $f=f'+jf''$ is a complex resonant frequency of the microstrip configuration, then the quality factor of the open resonator may be defined as [13]:

$$Q = \frac{f'}{2f''} \tag{2.4.23}$$

Often the resonant frequency is defined as the frequency for which the imaginary part of the input impedance is zero [14]. Thus at resonance the input impedance is purely resistive.

2.4.6 Input impedance.

The input impedance can be calculated once the expansion coefficients I_i ,with i=1,..,Nmax, are known. Let $\vec{J}_s$ be the current distribution on the probe and I_0 the corresponding input current. Then the input impedance may be found by [11]:

$$Z_{in} = -\frac{1}{I_0^2} \iiint_{source} \vec{E}.\vec{J}_s \, dV \tag{2.4.24}$$

Where $\vec{E}$ is the total electric field from the surface current $\vec{J}_p$, caused by the source current $\vec{J}_s$. The total electric field can be written as:

$$\vec{E} = \frac{1}{4\pi^2}\int_{-\infty}^{\infty}\int_{-\infty}^{\infty}\sum_{i=1}^{Nmax} I_i[\bar{\bar{Q}}.\vec{\tilde{J}}_{pi}]\, e^{-jk_x x}\, e^{-jk_y y}\, dk_x dk_y \qquad (2.4.25)$$

The input impedance of a single microstrip antenna can now be found by substituting (2.4.25) in (2.4.24):

$$Z_{in} = -\frac{1}{4\pi^2 I_0^2}\sum_{i=1}^{Nmax} I_i V_i \qquad (2.4.26)$$

where V_i, i=1,..,Nmax, are the elements of the excitation vector [V] given in (2.4.19).
In the case of a coaxial probe feed often a somewhat artificial correction term jX_1 is added to the input impedance to account for the probe self-inductance. Where [15]:

$$X_1 = 60\sqrt{\varepsilon_r}k_0 z' \ln\left[\frac{2.25}{\sqrt{\varepsilon_r}k_0 d_0}\right] \quad \Omega \qquad (2.4.27)$$

2.4.7 Mutual coupling.

A great advantage of the spectral domain moment method is that mutual coupling between single microstrip antennas can be calculated without additional theory. The formulation is the same as in the case of isolated antennas. Consider for example the microstrip geometry shown in fig 2.6a. The shape of the microstrip antennas is chosen rectangular, but in general the antenna elements may have an arbitrarily shape. In fig.2.6b a two-port network is shown. The relation between the port voltages and source currents is:

$$\begin{bmatrix} V_1 \\ V_2 \end{bmatrix} = \begin{bmatrix} Z_{11} & Z_{12} \\ Z_{21} & Z_{22} \end{bmatrix} \begin{bmatrix} I_1 \\ I_2 \end{bmatrix} \qquad (2.4.28)$$

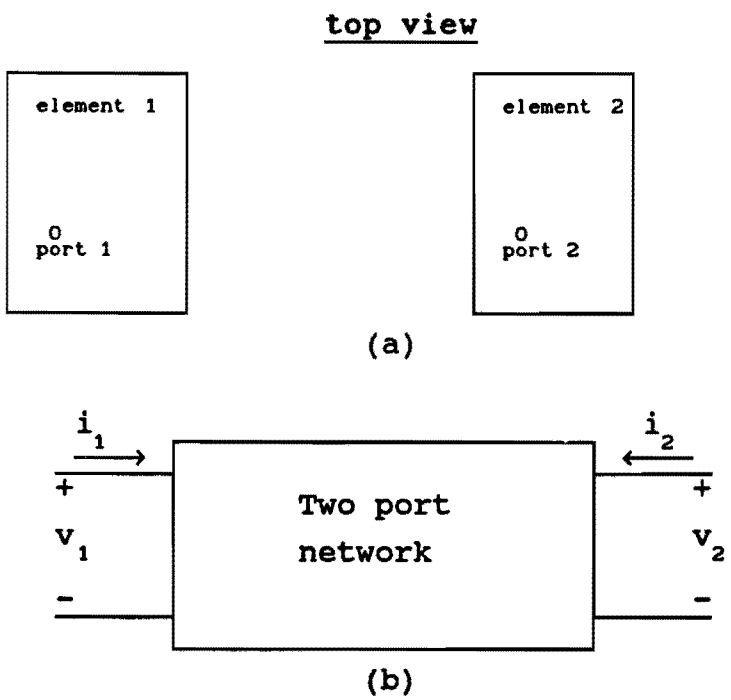

Fig. 2.6 (a) two coupled microstrip antennas
(b) two-port network

Note that the impedance matrix [z] is not the same matrix as the moment method matrix [Z]. The port voltages v_1 and v_2 should not be confused with the excitation matrix [V]. i_1 and i_2 are the source currents and not the currents on the patch. The elements of the impedance matrix [z] can be found by [11]:

$$z_{nm} = \left.\frac{v_n}{i_m}\right|_{i_n=0} = -\frac{1}{I_0^2} \iiint_V \vec{E}^{(n)} \cdot \vec{J}_s^{(m)} \, dV$$

$$= -\frac{1}{4\pi^2 I_0^2} \sum_{i=1}^{Nmax} I_i V_i^{(n)} \qquad (2.4.29)$$

where each antenna element sees the other open circuited. v_n is the voltage at port m due to a current at port n. $V_i^{(n)}$ is the excitation coefficient due to a current at port n. If we want to calculate z_{12} for example, then the expansion coefficients I_i in expression (2.4.29) should be set to zero on element 1.
Note that $z_{12} = z_{21}$.

2.5 Expansion functions.

A proper choice of basis functions in a moment method solution is of great importance. In our formulation, the surface current density on the upper conductor is expanded into a set of Nmax basis functions. The patch current can thus be written in the form:

$$\vec{J}_p = \sum_{i=1}^{Nmax} I_i \vec{J}_{pi} = \sum_{i=1}^{Nx} I_i J_{pix} \vec{e}_x + \sum_{i=Nx+1}^{Nmax} I_i J_{piy} \vec{e}_y \qquad (2.5.1)$$

where I_i are the unknown complex expansion coefficients and Nmax=Nx+Ny. Nx and Ny are, respectively, the number of expansion functions in the x- and y-direction. To find the exact solution for the patch current, Nmax should be set to infinity.
In theory there are an infinite number of basis sets. In practice, however, only a few sets can be used, because of the limited computer capacity. So we want to choose a set of basis functions with the ability to describe the unknown surface current $\vec{J}_p$ accurately, even if the number of basis functions is very small.

In general there are two classes of basis functions. The first contains the entire domain basis functions, which are nonzero for the entire domain of the unknown function. The second class is the sub domain basis function, which are defined, and thus nonzero, only over a small part of the entire domain of the unknown function.
In the next sections a few sets of basis functions that can be used for the determination of the unknown surface current $\vec{J}_p$, will be presented.

2.5.1 Entire domain basis functions.

Entire domain basis functions can only be used if the geometry of the microstrip antenna is very simple. So rectangular or circular microstrip antennas can be analysed with the use of entire domain basis functions.
For the case of a rectangular microstrip antenna a set of basis functions that is often used in moment methods is that of sinusoidal functions. The general form of the m-th basis function is:

$$f_m(x) = \begin{cases} \cos\left[\frac{(2m-1)\pi x}{Wx}\right] & -Wx/2 \le x \le Wx/2 \\ 0 & \text{elsewhere} \end{cases} \qquad (2.5.2)$$

The geometry of a rectangular microstrip antenna is shown in fig. 2.7.

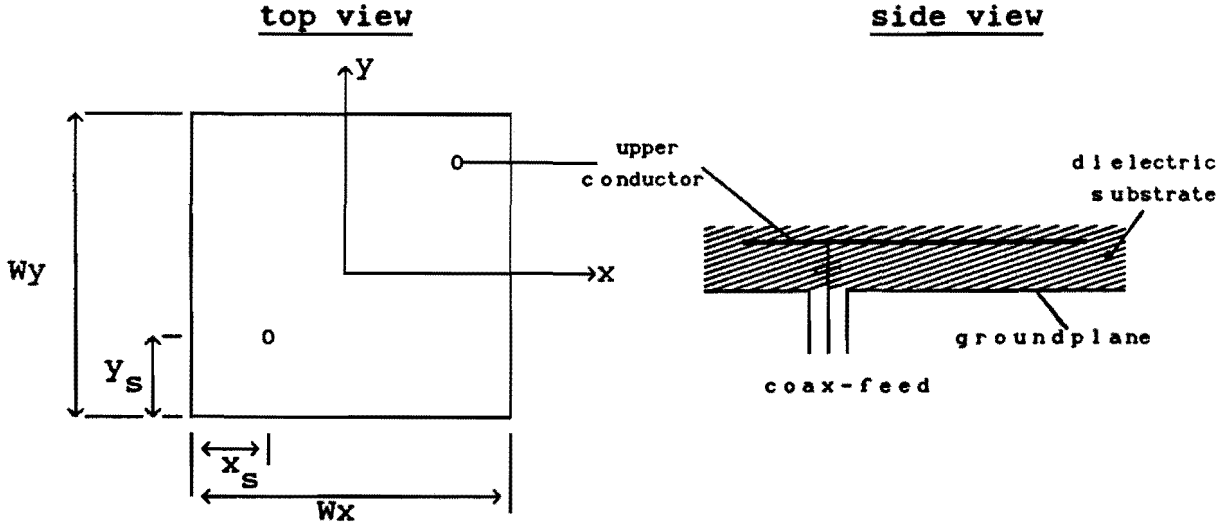

Fig. 2.7: Geometry of a rectangular microstrip antenna.

From earlier studies [5] it is known that the surface current on the upper conductor of a rectangular microstrip antenna is almost sinusoidal in the direction of current and uniform (constant) in the direction orthogonal to the current. So the patch current could be expanded in:

$$\vec{J}_p = I_1 \cos\left(\frac{\pi x}{Wx}\right)\vec{e}_x + I_2 \cos\left(\frac{\pi y}{Wy}\right)\vec{e}_y \qquad (2.5.3a)$$

with Fourier transform:

$$\vec{\tilde{J}}_p = I_1 \left[\frac{2\pi Wx \cos\left(\frac{Wxk_x}{2}x\right)}{\pi^2 - (k_x Wx)^2}\right]\left[\frac{2\sin\left(\frac{Wyk_y}{2}y\right)}{k_y}\right]\vec{e}_x$$

$$+ I_2 \left[\frac{2\pi Wy \cos\left(\frac{Wyk_y}{2}y\right)}{\pi^2 - (k_y Wy)^2}\right]\left[\frac{2\sin\left(\frac{Wxk_x}{2}x\right)}{k_x}\right]\vec{e}_y \qquad (2.5.3b)$$

If we use (2.5.3a) as a set of basis functions, the shape of the unknown patch current is independent of the type and location of the source. Only the expansion coefficients I_1 and I_2 depend on the source type and source location. So using this set of basis functions, the patch current will always be symmetric with respect to the x- and y-axis. This implies that the calculated radiation pattern of a single microstrip antenna by using (2.5.3a) as a basis, is also symmetric for an arbitrarily source location. In practice, however, the shape of the radiation pattern depends on the location of the source [15,pp.71].

To analyze an arbitrarily shaped microstrip antenna, entire domain basis functions such as (2.5.2) are less suited. The use of sub domain basis functions is in this case a better choice.

2.5.2 Sub domain basis functions.

Sub domain basis functions can be used without prior knowledge of the function they represent. So they can describe the patch current $\vec{J}_p$ of an arbitrarily shaped microstrip antenna.
Three types of sub domain basis functions will be presented here, namely piece wise constant basis functions, piece wise linear basis functions and piece wise sinusoidal basis functions. The piece wise linear functions are also called "rooftop" functions.

i) Piece wise constant (PWC)

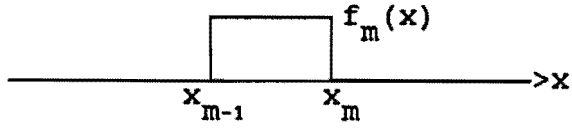

$$f_m(x) = \begin{cases} 1 & x_{m-1} \le x \le x_m \\ 0 & \text{elsewhere} \end{cases}$$

with Fourier transform:

$$\tilde{f}_m(k_x) = \frac{2\sin(k_x a/2)}{k_x} e^{jk_x(x_m+x_{m-1})/2} \qquad (2.5.4)$$

where $a = x_m - x_{m-1}$

ii) Piece wise linear (PWL).

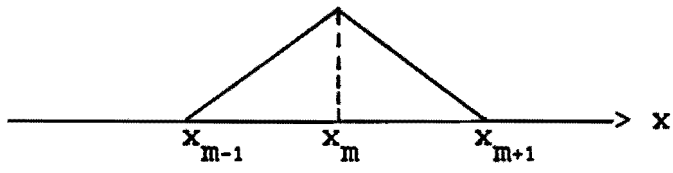

$$f_m(x) = \begin{cases} \dfrac{x - x_{m-1}}{a} & x_{m-1} \le x \le x_m \\ \dfrac{x_{m+1} - x}{a} & x_m \le x \le x_{m+1} \\ 0 & \text{elsewhere} \end{cases}$$

where $a = x_m - x_{m-1}$

The Fourier transform of this function is:

$$\tilde{f}_m(k_x) = \frac{4\sin^2(k_x a/2)}{k_x^2 a} e^{jk_x x_m} \qquad (2.5.5)$$

iii) Piece wise sinusoidal (PWS).

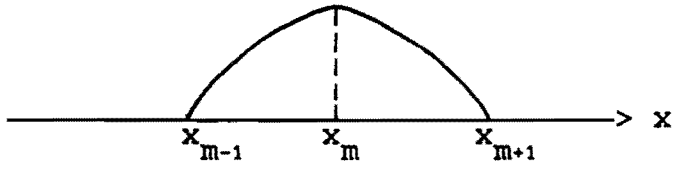

$$f_m(x) = \begin{cases} \dfrac{\sin[k(x-x_{m-1})]}{\sin(ka)} & x_{m-1} \le x \le x_m \\ \dfrac{\sin[k(x_{m+1}-x)]}{\sin(ka)} & x_m \le x \le x_{m+1} \\ 0 & \text{elsewhere} \end{cases}$$

where $a = x_m - x_{m-1}$

The Fourier transform of a PWS basis function is:

$$\tilde{f}_m(x) = \frac{2k}{\sin(ka)[k_x^2 - k^2]} (\cos(ka) - \cos(k_x a)) e^{jk_x x_m} \qquad (2.5.6)$$

The wave number k can be chosen arbitrarily.

The PWL and PWS basis functions overlap with adjacent basis functions. This implies that an approximation of a function with PWL or PWS basis functions has no discontinuities.
An example of a function represented by overlapping PWL overlapping PWL basis functions is shown in fig. 2.8.

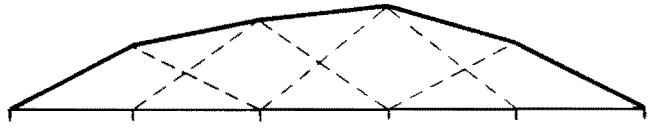

Fig. 2.8: Piece wise linear approximation of a function.

To illustrate how sub domain basis functions can be used, a rectangular microstrip antenna will be considered. The geometry is shown in fig. 2.9.

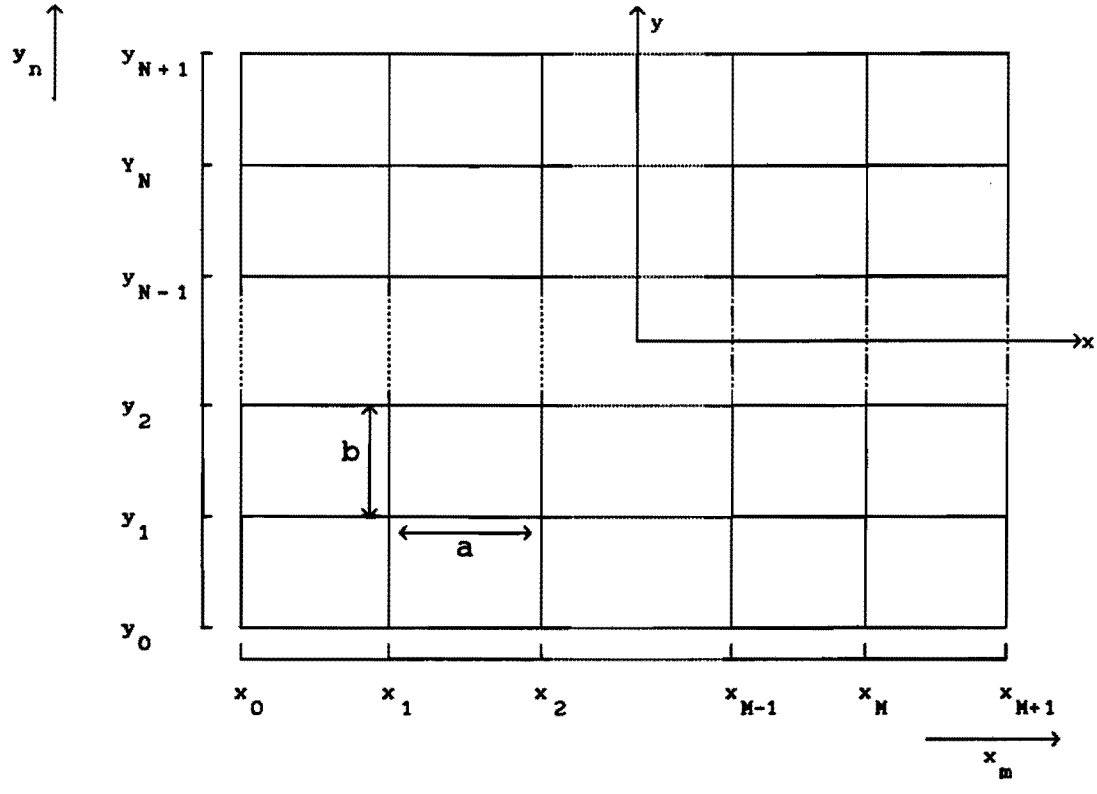

Fig 2.9: Segmentation of the patch in cells.

The upper conductor is divided in M+1 cells in the x-direction and N+1 cells in the y-direction. The patch current $\vec{J}_p$ is now expressed in terms of overlapping rooftop or PWS basis functions in the direction of current and in terms of PWC basis functions in the direction orthogonal to the current. This means that the x-directed patch current is expressed in Nx= M(N+1) basis functions and that the y-directed current is approximated by Ny=N(M+1)basis functions. The total number of basis functions is then Nmax = M(N+1) + N(M+1). In the case of overlapping rooftop basis functions in the direction of current, the Fourier transform of the patch current is given by:

$$\tilde{\vec{J}}_p = \sum_{i=1}^{Nx} I_i \tilde{J}_{pix} \vec{e}_x + \sum_{i=Nx+1}^{Nmax} I_i \tilde{J}_{piy} \vec{e}_y \qquad (2.5.7)$$

where

$$\tilde{J}_{pix} = ab\ \mathrm{sinc}^2(k_x a/2)\ \mathrm{sinc}(k_y b/2)\ e^{jk_x x_{mi}}\ e^{jk_y (y_{ni}+y_{ni-1})/2}$$

$$\tilde{J}_{piy} = ab\ \mathrm{sinc}(k_x a/2)\ \mathrm{sinc}^2(k_y b/2)\ e^{jk_y y_{ni}}\ e^{jk_x (x_{mi}+x_{mi-1})/2}$$

Note that the basis function $\tilde{J}_{pix}$ is nonzero in the interval $x_{mi-1} \le x \le x_{mi+1}$ and $y_{ni-1} \le y \le y_{ni}$ and that $\tilde{J}_{pjx}$ is nonzero for $x_{mj-1} \le x \le x_{mj}$ and $y_{nj-1} \le y \le y_{nj+1}$.
A similar expression can be derived for overlapping PWS basis functions. To improve the convergence, the wave number k for the PWS basis functions is set equal to the effective wave number of the dielectric substrate [6]:

$$k = \omega\sqrt{\mu_0 \varepsilon_{eff}} \qquad (2.5.8)$$

$$\varepsilon_{eff} = \frac{\varepsilon_r + 1}{2} + \frac{\varepsilon_r - 1}{2}\left[\frac{1}{\sqrt{1 + 10d/W}}\right]$$

APPENDIX 2A.

In this appendix the final expressions for the elements of the matrix [Z] and of the excitation vector [V] are given. This is done for rooftop sub domain basis functions and for sinusoidal entire domain basis functions. The geometry for the case of sub domain basis functions is shown in figure 2.9. The symmetry properties of the α-integrands are not used here. This is discussed in section 3.2.

An element of the matrix [Z] with a test current $\vec{J}_{pj}$ and an expansion current $\vec{J}_{pi}$ in the $\hat{x}$-direction is called a Z_{ji}^{xx} element. An element of [Z] with a test current in the $\hat{y}$-direction and an expansion current in the $\hat{x}$-direction is then a Z_{ji}^{yx} element. Thus the matrix [Z] has the general form:

$$[Z] = \begin{bmatrix} [Z^{xx}] & [Z^{xy}] \\ [Z^{yx}] & [Z^{yy}] \end{bmatrix} \qquad (2A.1)$$

where $[Z^{xx}]$ is a Nx x Nx matrix, $[Z^{xy}]$ is a Nx x Ny matrix, $[Z^{yx}]$ is a Ny x Nx matrix and $[Z^{yy}]$ is a Ny x Ny matrix (see fig. 2.9). If a test current $\vec{J}_{pj}$ is placed in the $\hat{x}$- or $\hat{y}$-direction, an element of the vector [V] is called a V_j^x, respectively, a V_j^y element. So [V] has the general form:

$$[V] = \begin{bmatrix} [V^x] \\ [V^y] \end{bmatrix} \qquad (2A.2)$$

where $[V^x]$ is a Nx x 1 matrix and $[V^y]$ is a Ny x 1 matrix.

The elements of [Z] and [V], using (2.4.14), (2.4.19) and a transformation to polar coordinates (α,β) with:

$$k_x = k_0\beta\cos\alpha$$
$$k_y = k_0\beta\sin\alpha \qquad (2A.3)$$

are then found by:

$$Z_{ji}^{xx} = \frac{\omega\mu_0 k_0^2}{\varepsilon_r}\int_0^{\infty}\int_{-\pi}^{\pi}\frac{\beta\sin(k_1 z')}{TeTmk_1}\Big[j(\beta^2\cos^2\alpha - \varepsilon_r)NeTm - \beta^2\cos^2\alpha k_1^2(\varepsilon_r-1)\sin(k_1 z')\Big]\tilde{J}_{pix}\,\tilde{J}^*_{pjx}\,d\alpha d\beta$$

$$Z_{ji}^{yx} = Z_{ij}^{xy} = \frac{\omega\mu_0 k_0^2}{\varepsilon_r}\int_0^{\infty}\int_{-\pi}^{\pi}\frac{\beta^3\sin(k_1 z')}{2TeTmk_1}\Big[jNeTm - k_1^2(\varepsilon_r-1)\sin(k_1 z')\Big]\sin 2\alpha\,\tilde{J}_{pix}\,\tilde{J}^*_{pjy}\,d\alpha d\beta$$

$$Z_{ji}^{yy} = \frac{\omega\mu_0 k_0^2}{\varepsilon_r}\int_0^{\infty}\int_{-\pi}^{\pi}\frac{\beta\sin(k_1 z')}{TeTmk_1}\Big[j(\beta^2\sin^2\alpha - \varepsilon_r)NeTm - \beta^2\sin^2\alpha k_1^2(\varepsilon_r-1)\sin(k_1 z')\Big]\tilde{J}_{piy}\,\tilde{J}^*_{pjy}\,d\alpha d\beta \qquad (2A.4)$$

$$V_j^x = \frac{j\omega\mu_0 k_0}{\varepsilon_r} \int_0^{\infty} \int_{-\pi}^{\pi} \frac{\beta^2 \tilde{J}_s' \sin(k_1 z')}{TeTmk_1} \Big[(\varepsilon_r - 1)\sin(k_1 z') k_0^2 \beta^2 + jNeTm \Big] \cos\alpha \; \tilde{J}_{pjx} \; e^{-jk_0\beta(x_s\cos\alpha + y_s\sin\alpha)} \; d\alpha d\beta$$

$$V_j^y = \frac{j\omega\mu_0 k_0}{\varepsilon_r} \int_0^{\infty} \int_{-\pi}^{\pi} \frac{\beta^2 \tilde{J}_s' \sin(k_1 z')}{TeTmk_1} \Big[(\varepsilon_r - 1)\sin(k_1 z') k_0^2 \beta^2 + jNeTm \Big] \sin\alpha \; \tilde{J}_{pjy} \; e^{-jk_0\beta(x_s\cos\alpha + y_s\sin\alpha)} \; d\alpha d\beta$$

(2A.5)

where

$$\tilde{J}_s' = J_0(r_0 k_0 \beta) \qquad \text{for a coaxial probe feed}$$

$$\tilde{J}_s' = \sqrt{w_{eff}/z'} \; \frac{2\sin(w_{eff} k_y/2)}{w_{eff} k_y} \qquad \text{for a strip line feed.}$$

$$\tilde{J}_{pjx} = \begin{cases} \left[\dfrac{2\pi(2j-1)Wx\cos(Wxk_x/2)}{[(2j-1)\pi]^2 - (k_x Wx)^2}\right]\left[\dfrac{2\sin(Wyk_y/2)}{k_y}\right] & \text{entire domain} \\ ab \; \text{sinc}^2(k_x a/2) \; \text{sinc}(k_y b/2) \; e^{[jk_x x_{mj} + jk_y(y_{nj}+y_{nj-1})/2]} & \text{PWL sub domain} \end{cases}$$

$$\tilde{J}_{pjy} = \begin{cases} \left[\dfrac{2\pi(2j-1)\,Wy\cos(Wyk_y/2)}{[(2j-1)\pi]^2 - (k_yWy)^2}\right]\left[\dfrac{2\sin(Wxk_x/2)}{k_x}\right] & \text{entire domain} \\ ab\ \mathrm{sinc}^2(k_yb/2)\ \mathrm{sinc}(k_xa/2) & \text{PWL sub domain} \\ \qquad e^{[jk_yy_{nj} + jk_x(x_{mj}+x_{mj-1})/2\ ]} & \end{cases}$$

with $a = x_{mj} - x_{mj-1}$ and $b = y_{nj} - y_{nj-1}$

$$Te = k_1\cos(k_1d) + jk_2\sin(k_1d)$$

$$Tm = k_2\varepsilon_r\cos(k_1d) + jk_1\sin(k_1d)$$

$$Ne = k_1\cos[k_1(d-z')] + jk_2\sin[k_1(d-z')]$$

$$k_1^2 = \varepsilon_r k_o^2 - k_o^2\beta^2 \qquad (\mathrm{Im}(k_1) < 0)$$

$$k_2^2 = k_o^2 - k_o^2\beta^2 \qquad (\mathrm{Im}(k_2) < 0)$$

3. COMPUTATIONAL ASPECTS.

The moment method solution presented in the previous chapter resulted in a matrix equation (2.4.13), where the elements of the matrix [Z] and the excitation vector [V] are two-dimensional integrals with infinite boundaries. If Nmax basis functions are used, we have to evaluate Nmax + $Nmax^2$ such integrals for each frequency. The calculation of the unknown surface current on the upper conductor of a microstrip antenna using for example 50 basis functions, would involve the calculation of 25,500 two-dimensional infinite integrals.
Using such a rigorous numerical approach, the use of a super computer becomes necessary. Fortunately, it is possible to reduce the number of Z_{ji}-elements that have to be evaluated, because of the Toeplitz-like symmetry of the matrix [Z]. This is discussed in section 3.4.

An efficient evaluation of the two-dimensional integrals with infinite β-boundary is possible, by extracting the source singularity from the Green's function in the dielectric slab. The integrals converge very slowly if this technique is not used. The extracted term, which represents the source singularity, can be easily evaluated in the space domain. The source-extracting technique is presented in section 3.3 for the case of rooftop basis functions.

Another computational problem is introduced by the TM- and TE-surface waves in the dielectric slab. The solutions of the characteristic equations of TM- and TE-surface waves in a grounded dielectric slab correspond to the zeros of the complex functions Te and Tm, defined in (2.2.20). The zeros of Tm and Te are the poles in the integrands of Z_{ji} and V_j. An accurate integration in the neighborhood of these singularities is discussed in section 3.1.

3.1 Surface waves

The integrands of the elements of [Z] and [V] become singular at the zeros of Tm and Te. These zeros in the complex functions Te and Tm correspond with solutions of the characteristic equation for TE, respectively, TM surface waves in a dielectric layer on an infinite conductor plate. These characteristic equations are given by:

$$Te = k_1\cos(k_1 d) + jk_2\sin(k_1 d) = 0$$

$$Tm = k_2\varepsilon_r\cos(k_1 d) + jk_1\sin(k_1 d) = 0 \qquad (3.1.1)$$

with:

$$k_1^2 = \varepsilon_r k_0^2 - k_0^2\beta^2 \qquad (\mathrm{Im}(k_1) < 0)$$

$$k_2^2 = k_0^2 - k_0^2\beta^2 \qquad (\mathrm{Im}(k_2) < 0)$$

$$k_x = k_0\beta\cos\alpha$$

$$k_y = k_0\beta\sin\alpha$$

The last two formulas transform the infinite k_x,k_y-integration into an infinite β-integration and a finite α-integration. Note that the β-integration is along the real x-axis.
The zeros in Te and Tm can cause serious numerical integration problems for the integration along the real β-axis .
In the next sections it will be shown that the integrals can be evaluated accurate, if the location of the zeros is known.

3.1.1 Location of poles in the spectral domain Green's function.

In this section a number of properties of the complex functions Te and Tm will be derived. These properties are important for an accurate calculation of the β-integrals in the neighborhood of the singularities. For the sake of simplicity, we shall assume ε_r to be real. The properties are:

i) All the zeros of Te and Tm, and thus all the poles in the spectral domain Green's function, are first-order zeros.

proof:

The elements of [Z] and [V] can be written in the general form:

$$F = \int_0^{\infty} R_1(\beta) \int_{-\pi}^{\pi} R_2(\alpha,\beta)\ d\beta d\alpha = \int_0^{\infty} R_1(\beta) h(\beta)\ d\beta d\alpha$$

where $R_1(\beta)$ has n+m poles, corresponding with n and m zeros in, respectively, Te and Tm. The inner integral can be evaluated without numerical problems and the result is called $h(\beta)$. Assume that $R_1(\beta)$ has a second-order pool in $\beta = \beta_0$. A Laurent series development of $R_1(\beta)h(\beta)$ in the vicinity of β_0 yields:

$$R_1(\beta)h(\beta) = \frac{B}{(\beta - \beta_0)^2} + \frac{A}{(\beta - \beta_0)} + g(\beta)$$

where $g(\beta)$ is analytical in $\beta = \beta_0$ and A and B are constants. In figure 3.1 a possible integration path is shown.

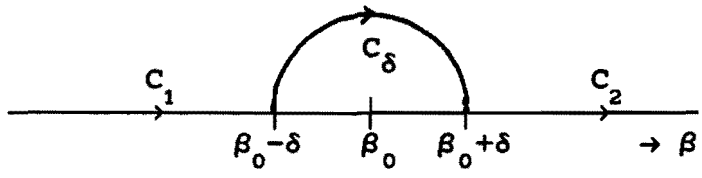

Fig. 3.1: β- integration path in the neighborhood of a pool.

The integral can now be written in the form:

$$\int_0^{\infty} R_1(\beta)h(\beta)d\beta = \int_{C_1+C_2} R_1(\beta)h(\beta)d\beta + \int_{C_\delta} R_1(\beta)h(\beta)d\beta$$

where:

$$\int_{C_\delta} R_1(\beta)h(\beta)d\beta = \int_{C_\delta} \frac{B}{(\beta - \beta_0)^2}\, d\beta + \int_{C_\delta} \frac{A}{(\beta - \beta_0)}\, d\beta + \int_{C_\delta} g(\beta)d\beta$$

Now substitute $\beta = \beta_0 + \delta e^{j\vartheta}$ in the above integrals. Then the first term of the right-hand side can be written as:

$$\int_{C_\delta} \frac{B}{(\beta - \beta_0)^2}\, d\beta = \int_0^{\pi} \frac{B}{\delta^2 e^{j\vartheta}}\, j\delta e^{j\vartheta} d\vartheta = \frac{-2B}{\delta}$$

We can now conclude that:

$$\lim_{\delta \to 0} \int_{C_\delta} \frac{B}{(\beta - \beta_0)^2} \, d\beta = \infty$$

Because the integral F is not limited in this case, the functions Te and Tm cannot have second order zeros. In a similar way it can be proved that Te and Tm cannot have third or higher order zeros.

□

ii) If the dielectric substrate is loss less, then the zeros of Te and Tm are on the real β-axis between 1 and $\sqrt{\varepsilon_r}$.

proof:

1. Assume that $\beta < 1$. The wave numbers in the z-direction in region 1 and 2 can now be written as:

$$k_1 = k_0\sqrt{\varepsilon_r - \beta^2}$$

$$k_2 = k_0\sqrt{1 - \beta^2}$$

The equations (3.1.1) then read:

$$\text{TE: } k_0\sqrt{\varepsilon_r-\beta^2}\cos(k_0 d\sqrt{\varepsilon_r-\beta^2}) + jk_0\sqrt{1-\beta^2}\sin(k_0 d\sqrt{\varepsilon_r-\beta^2}) = 0$$

$$\text{TM: } k_0\varepsilon_r\sqrt{1-\beta^2}\cos(k_0 d\sqrt{\varepsilon_r-\beta^2}) + jk_0\sqrt{\varepsilon_r-\beta^2}\sin(k_0 d\sqrt{\varepsilon_r-\beta^2}) = 0$$

The above equations have no solutions for $\beta < 1$ because both the imaginary part and the real part of the left-hand side have to be zero.

2. Consider the interval $1 \leq \beta \leq \sqrt{\varepsilon_r}$. The wave numbers are now written as:

$$k_1 = k_0\sqrt{\varepsilon_r - \beta^2}$$

$$k_2 = -jk_0\sqrt{\beta^2 - 1}$$

The equations (3.1.1) then read:

$$\text{TE: } k_0\sqrt{\varepsilon_r-\beta^2}\cos(k_0 d\sqrt{\varepsilon_r-\beta^2}) + k_0\sqrt{\beta^2-1}\sin(k_0 d\sqrt{\varepsilon_r-\beta^2}) = 0$$

$$\text{TM: } -jk_0\varepsilon_r\sqrt{\beta^2-1}\cos(k_0 d\sqrt{\varepsilon_r-\beta^2}) + jk_0\sqrt{\varepsilon_r-\beta^2}\sin(k_0 d\sqrt{\varepsilon_r-\beta^2}) = 0$$

The above equations are the characteristic equations for TE, respectively, TM surface waves in a dielectric layer on an infinite conductor plate.

3. Consider the interval $\beta > \sqrt{\varepsilon_r}$. Now we have:

$$k_1 = -jk_0\sqrt{\beta^2 - \varepsilon_r}$$

$$k_2 = -jk_0\sqrt{\beta^2 - 1}$$

The equations (3.1.1) now become:

$$\text{TE: } -jk_0\sqrt{\beta^2-\varepsilon_r}\cos(-jk_0d\sqrt{\beta^2-\varepsilon_r}) + k_0\sqrt{\beta^2-1}\sin(-jk_0d\sqrt{\beta^2-\varepsilon_r} = 0$$

$$\text{TM: } -jk_0\varepsilon_r\sqrt{\beta^2-1}\cos(-jk_0d\sqrt{\beta^2-\varepsilon_r}) + k_0\sqrt{\beta^2-\varepsilon_r}\sin(-jk_0d\sqrt{\beta^2-\varepsilon_r}) = 0$$

In this case no solutions are possible for $\beta^2 > \sqrt{\varepsilon_r}$.

□

iii) If $k_0d\sqrt{\varepsilon_r-1} < \pi/2$ then the function Te has no zeros and the function Tm has 1 zero. In this case, only one surface wave can exist in the dielectric slab.

proof:

The zeros of Te can be found by solving the equation:

$$-\tan[k_0d\sqrt{\varepsilon_r-\beta^2}] = \sqrt{\frac{\varepsilon_r-\beta^2}{\beta^2-1}} \qquad \text{with } 1 \le \beta \le \sqrt{\varepsilon_r}$$

Let

$$f_e(\beta) = -\tan[k_0d\sqrt{\varepsilon_r-\beta^2}]$$

$$g_e(\beta) = \sqrt{\frac{\varepsilon_r-\beta^2}{\beta^2-1}}$$

The functions $f_e(\beta)$ and $g_e(\beta)$ are sketched in fig. 3.2.

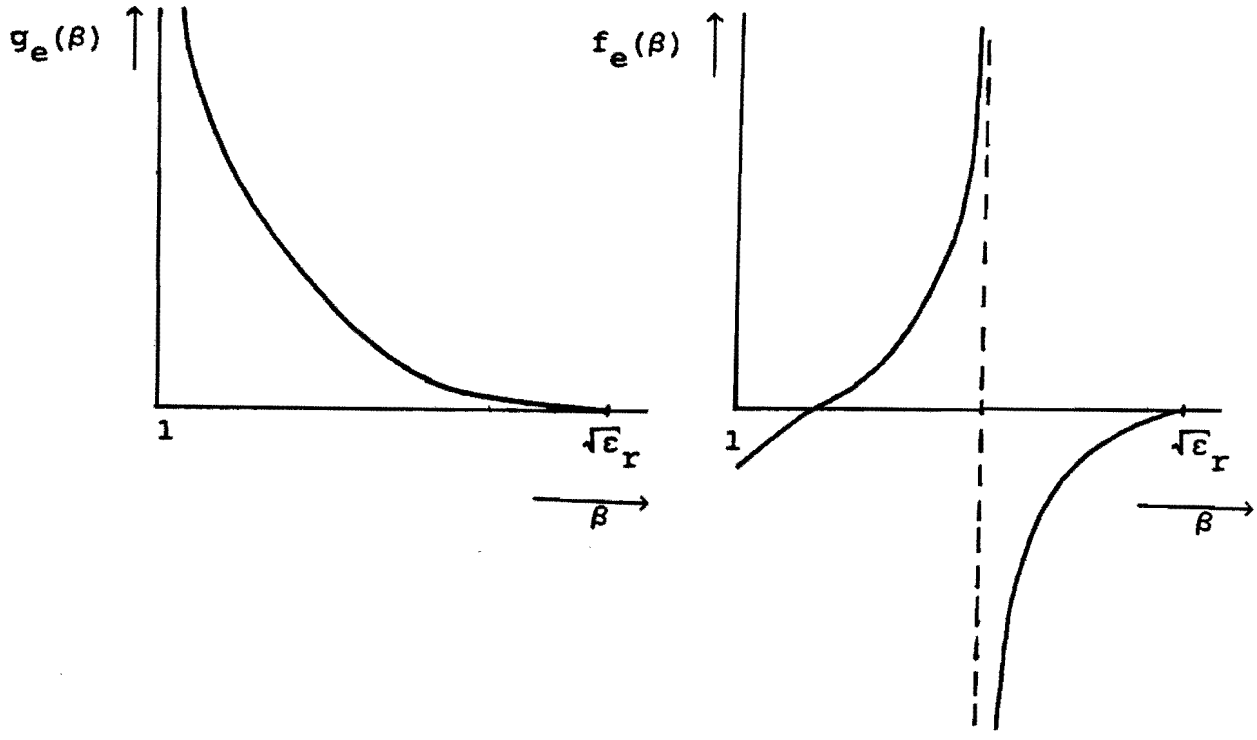

Fig. 3.2 Graphical solution of the characteristic equation for TE surface waves in a grounded dielectric slab.

For $a < 0$, the functions $f_e(\beta)$ and $g_e(\beta)$ do not intersect. We can therefore conclude that no TE surface waves can exist in a grounded dielectric slab if the following condition is satisfied:

$$k_0 d\sqrt{\varepsilon_r - 1} < \pi/2$$

For the case of TM surface waves, the characteristic equation can be written as:

$$\tan[k_0 d\sqrt{\varepsilon_r - \beta^2}] = \varepsilon_r \sqrt{\frac{\beta^2 - 1}{\varepsilon_r - \beta^2}} \qquad \text{with } 1 \le \beta \le \sqrt{\varepsilon_r}$$

Let

$$f_m(\beta) = \tan[k_0 d\sqrt{\varepsilon_r - \beta^2}]$$

$$g_m(\beta) = \varepsilon_r\sqrt{\frac{\beta^2 - 1}{\varepsilon_r - \beta^2}}$$

The functions $f_m(\beta)$ and $g_m(\beta)$ are sketched in fig. 3.3.

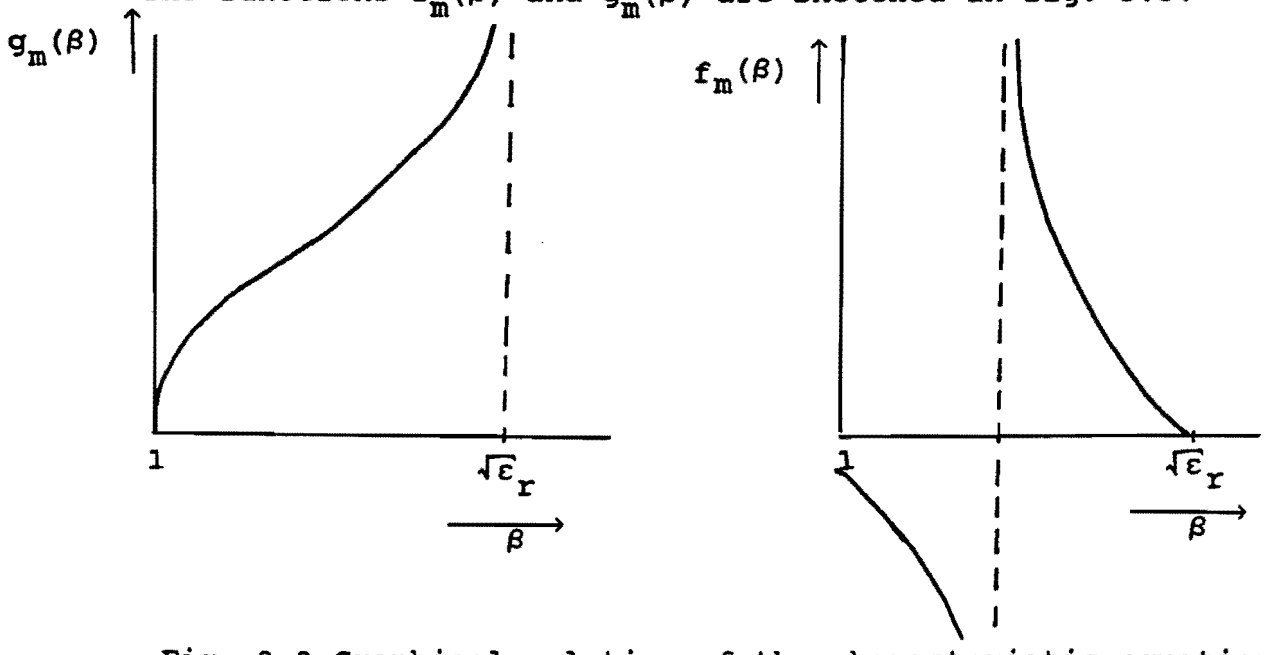

Fig. 3.3 Graphical solution of the characteristic equation for TM surface waves in a grounded dielectric slab.

The functions $g_m(\beta)$ and $f_m(\beta)$ always intersect, which implies that Tm has always one or more zeros. Tm has only one zero if the condition

$$k_0 d\sqrt{\varepsilon_r - 1} \geq \pi$$

is satisfied.

We can conclude that there exists only one surface wave in the dielectric slab if:

$$k_0 d\sqrt{\varepsilon_r - 1} < \pi/2 \qquad (3.1.2)$$

A practical example is ε_r=2.5, d=1.59mm. Then condition (3.1.2) is satisfied if the frequency f < 38Ghz.

□

In practice, the relative permittivity of the dielectric substrate will be complex. The values of β for which Te or Tm are zero are in this case also complex:

$$\beta_p = \beta_0 + j\nu \qquad (3.1.3)$$

where $\nu < 0$.
An accurate location of a zero β_p can be calculated by using numerical techniques. An efficient and accurate numerical method for the determination of all the zeros in Te and Tm, is the Powell-hybrid method [16].
The accuracy of the numerical method used is of great importance, since we want to extract the singularities caused by Te and Tm, from the integrands of Z_{ji} and V_j. This "extracting" technique is discussed in the next section.

3.1.2 Extraction of singularities.

The integrands of the two-dimensional integrals Z_{ji} and V_j are singular when the complex functions Te or Tm are zero. These singularities must be avoided when integrating from $\beta = 0$ to ∞. If the dielectric substrate is lossy, the poles move into the fourth quadrant. However, for low loss dielectric substrates, the imaginary part of such a pole β_p is very small. This can cause serious numerical integration problems.
To avoid these difficulties, a number of techniques are developed [6,17,18]. In [6] the integration along the real β-axis from $\beta_0-\delta$ to $\beta_0+\delta$, where $\delta \approx 0.001$, is approximated analytical. A more accurate method is used in [17]. Here the singularities are extracted from the integrands of Z_{ji} and V_j. The extracted singular function F_{sing} can be integrated analytically. For simplicity and from a practical point of view, we shall assume that condition (3.1.2) is satisfied, i.e. there is only one zero in Tm and there are no zeros in Te.
The integrand of Z_{ji} or of V_j can be written in the form:

$$F(\beta) = \frac{h(\beta)}{Te(\beta)Tm(\beta)} \qquad (3.1.4)$$

where the α-integral is calculated numerically and is included in the analytical function $h(\beta)$. The integration from $\beta = 1$ to $\beta = \sqrt{\varepsilon'_r}$ may be written in the form:

$$\int_1^{\sqrt{\varepsilon'_r}} F(\beta)\, d\beta = \int_1^{\sqrt{\varepsilon'_r}} [F(\beta) - F_{sing}(\beta)]\, d\beta + \int_1^{\sqrt{\varepsilon'_r}} F_{sing}(\beta)\, d\beta \qquad (3.1.5)$$

where

$$F_{sing}(\beta) = \frac{R}{\beta - \beta_p} \qquad (3.1.6)$$

In (3.1.6) $\beta_p = \beta_o + j\nu$ ($\nu<0$) is the complex zero of Tm and R is the residue of $F(\beta)$ at $\beta = \beta_p$. This residue R can be found by:

$$R = \lim_{\beta\to\beta_p} (\beta - \beta_p)F(\beta)$$

$$= \frac{h(\beta_p)}{Te(\beta_p)} \lim_{\beta\to\beta_p} (\beta - \beta_p)/Tm(\beta) \qquad (3.1.7)$$

$Tm(\beta)$ can be expanded in a Taylor series about $\beta = \beta_p$:

$$Tm(\beta) = \frac{dTm(\beta)}{d\beta}\bigg|_{\beta=\beta_p} (\beta - \beta_p) + \text{...higher order terms} \qquad (3.1.8)$$

Substituting (3.1.8) in (3.1.7) yields:

$$R = \frac{h(\beta_p)}{Te(\beta_p)} \lim_{\beta\to\beta_p} \left[\frac{(\beta - \beta_p)}{\frac{dTm(\beta)}{d\beta}\Big|_{\beta=\beta_p} (\beta - \beta_p) + \ldots.} \right]$$

$$= \frac{h(\beta_p)}{Te(\beta_p)Tm'(\beta_p)} \qquad (3.1.9)$$

with $Tm'(\beta_p) = \frac{dTm(\beta)}{d\beta}\Big|_{\beta=\beta_p}$

The first integral of the right-hand side of (3.1.5) can easily be obtained numerically, because the singularity in $\beta = \beta_p$ is extracted from the integrand. The extracted function F_{sing} can be integrated analytically as:

$$\int_1^{\sqrt{\varepsilon'_r}} F_{sing}(\beta)\, d\beta = R\{ \ln(\sqrt{\varepsilon'_r} - \beta_p) - \ln(1 - \beta_p)\}$$

$$= R \ln\left[\frac{\sqrt{\varepsilon_r'} - \beta_0 - j\nu}{1 - \beta_0 - j\nu}\right]$$

$$= \frac{R}{2} \ln\left[\frac{(\sqrt{\varepsilon_r'} - \beta_0)^2 + \nu^2}{(1 - \beta_0)^2 + \nu^2}\right]$$

$$+ jR \arctan\left[\frac{\sqrt{\varepsilon_r'} - \beta_0}{\nu}\right] + jR \arctan\left[\frac{\beta_0 - 1}{\nu}\right] \qquad (3.1.10)$$

Fig. 3.4 shows the real parts of the original integrand $F(\beta)$ and of the extracted integrand $F(\beta) - F_{sing}$. The integral over the function $F(\beta) - F_{sing}$ can now easily be evaluated numerically.

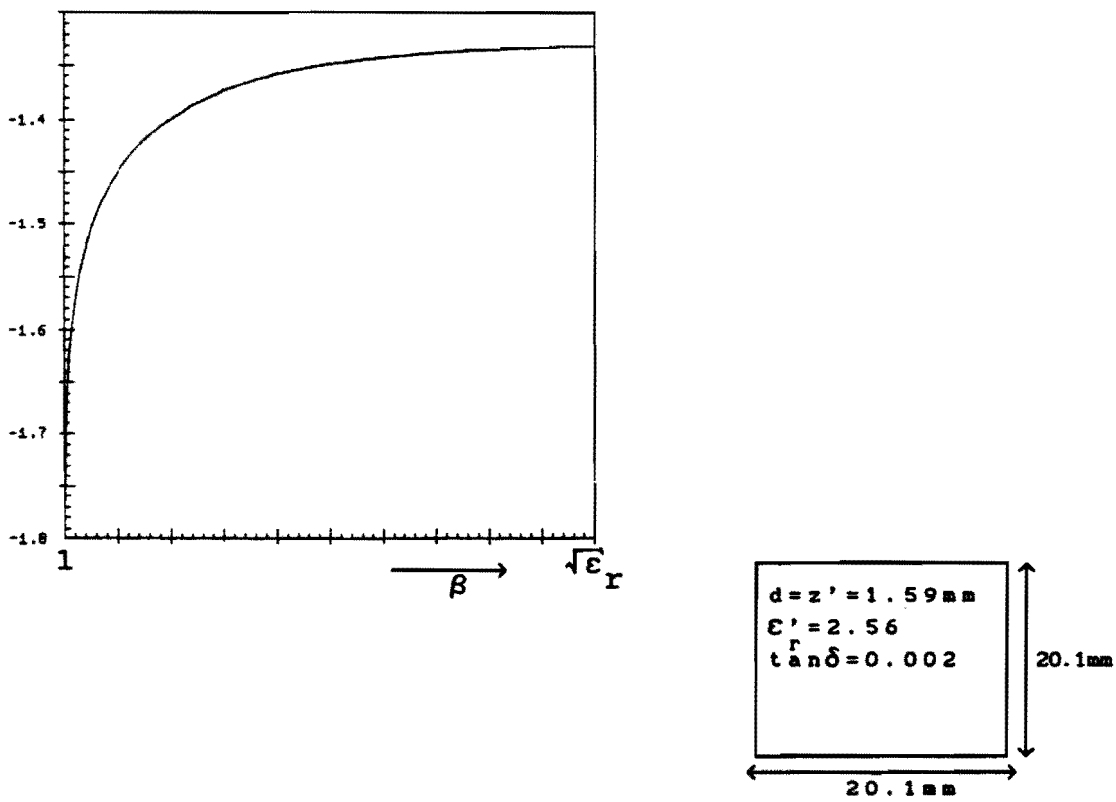

Fig. 3.4: Real part of $F(\beta) - F_{sing}(\beta)$
Frequency f=4.4Ghz. PWL basis functions,
M=9,N=0, i=j=1.

3.2 Symmetry properties of the integrands of the matrix elements.

As mentioned in chapter 2, the infinite k_x, k_y integrations are converted to polar coordinates β and α, with integration range $0\rightarrow\infty$, respectively, $0\rightarrow 2\pi$.
It is possible to reduce the α integration range to $0\rightarrow\pi/2$, by using the even and odd properties of the integrands of Z_{ji} and V_j. Consider for example an element of the matrix [Z] with a test current $\vec{J}_{pj}$ and an expansion current $\vec{J}_{pi}$ in the $\hat{x}$-direction. Thus $\vec{J}_{pj} = J_{pjx}\,\vec{e}_x$ and $\vec{J}_{pi} = J_{pix}\,\vec{e}_x$. This element of the [Z] matrix is called a Z_{ji}^{xx} element. A Z_{ji}^{yx} element is then an element of [Z] with a test current in the $\hat{y}$-direction and an expansion current in the $\hat{x}$ direction.
According to Appendix 2A a Z_{ji}^{xx} element can be written as:

$$Z_{ji}^{xx} = \frac{\omega\mu_0 k_0^2}{\varepsilon_r}\int_0^{\infty}\frac{\beta\sin(k_1 z')}{TeTmk_1}\int_{-\pi}^{\pi}\Big[j(\beta^2\cos^2\alpha - \varepsilon_r)NeTm - \beta^2\cos^2\alpha k_1^2(\varepsilon_r-1)\sin(k_1 z')\Big]\tilde{J}_{pix}\,\tilde{J}_{pjx}^{*}\,d\alpha d\beta \qquad (3.2.1)$$

The product term $\tilde{J}_{pix}\,\tilde{J}_{pjx}^{*}$ has the general form:

$$\tilde{J}_{pix}\,\tilde{J}_{pjx}^{*} = \tilde{J}'_{pix}\,\tilde{J}'_{pjx}\,e^{jaxx}\,e^{jbxx} \qquad (3.2.2)$$

If we use entire domain basis functions we have according to (2.5.2) and (2.5.3):

$$\tilde{J}'_{pix}\,\tilde{J}'_{pjx} = \left[\frac{2\pi(2i-1)Wx\cos(Wxk_x/2)}{[(2i-1)\pi]^2-(k_xWx)^2}\right]\left[\frac{2\pi(2j-1)Wx\cos(Wxk_x/2)}{[(2j-1)\pi]^2-(k_xWx)^2}\right]$$

$$\left[\frac{2\sin(Wyk_y/2)}{k_y}\right]^2 \qquad (3.2.3a)$$

$$axx = 0$$
$$bxx = 0$$

where $k_x = k_0\beta\cos\alpha$ and $k_y = k_0\beta\sin\alpha$.

For sub domain basis functions, with overlapping rooftop basis functions in the direction of current and piece-wise constant (PWC) basis functions in the direction orthogonal to the current, we find by using expression (2.5.7):

$$\tilde{J}'_{pix}\,\tilde{J}'_{pjx} = (ab)^2\mathrm{sinc}^4(k_0\beta\cos\alpha a/2)\mathrm{sinc}^2(k_0\beta\sin\alpha b/2) \qquad (3.2.3b)$$

$$axx = (x_{mi} - x_{mj})k_0\beta\cos\alpha$$
$$bxx = (y_{ni} - y_{nj})k_0\beta\sin\alpha$$

where x_{mi}, y_{ni}, x_{mj} and x_{nj} are the sub domain coordinates of the i-th, respectively, j-th sub domain (see fig. 2.9).
Now consider the integral Ixx, defined as:

$$Ixx = \int_{-\pi}^{\pi} f(\alpha,\beta)\; e^{jaxx}\; e^{jbxx}\; d\alpha \qquad (3.2.4)$$

where $f(\alpha,\beta)\; e^{jaxx}\; e^{jbxx}$ is the integrand of (3.2.1).

This integral may be written in the form:

$$Ixx = \int_{-\pi}^{\pi} f(\alpha,\beta)[\cos(axx+bxx) + j\sin(axx+bxx)]d\alpha$$

$$= \int_{-\pi}^{\pi} f(\alpha,\beta)[(\text{cosaxxcosbxx} - \text{sinaxxsinbxx}) + j(\text{sinaxxcosbxx} + \text{cosaxxsinbxx})]d\alpha$$

The above integral can be divided in two integrals with ranges $0 \rightarrow \pi$ and $-\pi \rightarrow 0$. Substituting $\alpha' = -\alpha$ in the second integral and using the properties:

$$\begin{aligned} axx(-\alpha) &= axx(\alpha) \\ bxx(-\alpha) &= -bxx(\alpha) \\ f(-\alpha,\beta) &= f(\alpha,\beta) \end{aligned}$$

then yields:

$$Ixx = 2\int_{0}^{\pi} f(\alpha,\beta)[\text{cosaxxcosbxx} + j\text{sinaxxcosbxx}]d\alpha$$

Substitute $\alpha' = \alpha - \pi/2$ in the above integral. Using the even and odd properties:

$$\begin{aligned} axx(-\alpha') &= -axx(\alpha') \\ bxx(-\alpha') &= bxx(\alpha') \\ f(-\alpha',\beta) &= f(\alpha',\beta) \end{aligned}$$

and using the inverse substitution $\alpha = \alpha' + \pi/2$ then yields:

$$Ixx = 4\int_{0}^{\pi/2} f(\alpha,\beta)\text{cosaxxcosbxx}\ d\alpha \qquad (3.2.5)$$

An element Z_{ji}^{xx} can now be written as

$$Z_{ji}^{xx} = \frac{4\omega\mu_0 k_0^2}{\varepsilon_r} \int_0^{\infty} \frac{\beta \sin(k_1 z')}{TeTmk_1} \int_0^{\pi/2} \Big[j(\beta^2 \cos^2\alpha - \varepsilon_r) NeTm$$

$$- \beta^2 \cos^2\alpha k_1^2 (\varepsilon_r - 1) \sin(k_1 z') \Big] \tilde{J}'_{pix} \tilde{J}'_{pjx} \cos axx \cos bxx \, d\alpha d\beta$$

(3.2.6)

The α-integration ranges of the other elements of [Z] and of the excitation vector [V] can also be reduced to $0 \rightarrow \pi/2$, by using the even and odd properties of the integrands. The resulting expressions can be written in the form:

$$Z_{ji}^{yx} = Z_{ij}^{xy} = - \frac{4\omega\mu_0 k_0^2}{\varepsilon_r} \int_0^{\infty} \frac{\beta^3 \sin(k_1 z')}{2TeTmk_1} \Big[jNeTm - k_1^2 (\varepsilon_r - 1) \sin(k_1 z') \Big]$$

$$\int_0^{\pi/2} \tilde{J}'_{pix} \tilde{J}'_{pjx} \sin 2\alpha \, \sin ayx \sin byx \, d\alpha d\beta \qquad (3.2.7a)$$

with:

$$\left.\begin{aligned} ayx &= [(x_{mi} + x_{mi-1})/2 - x_{mj}] k_0 \beta \cos\alpha \\ byx &= [y_{ni} - (y_{nj} + y_{nj-1})/2] k_0 \beta \sin\alpha \end{aligned}\right\} \text{subdomain basis functions}$$

$ayx = byx = 0$ for entire domain basis functions.

$$Z_{ji}^{yy} = \frac{4\omega\mu_0 k_0^2}{\varepsilon_r} \int_0^{\infty} \frac{\beta \sin(k_1 z')}{TeTmk_1} \int_0^{\pi/2} \Big[j(\beta^2 \sin^2\alpha - \varepsilon_r) NeTm$$

$$- \beta^2 \sin^2\alpha k_1^2 (\varepsilon_r - 1) \sin(k_1 z') \Big] \tilde{J}'_{piy} \tilde{J}'_{pjy} \cos ayy \cos byy \, d\alpha d\beta$$

(3.2.7b)

with:

$$\left.\begin{aligned} ayy &= (x_{mi} - x_{mj})k_0\beta\cos\alpha \\ byy &= (y_{ni} - y_{nj})k_0\beta\sin\alpha \end{aligned}\right\} \quad \text{subdomain basis functions}$$

$ayy = byy = 0$ for entire domain basis functions.

Note that the terms Z_{ji}^{yx} and Z_{ji}^{xy} are always zero for the case of entire domain basis functions.
In the case of a coaxial probe feed the elements of the excitation matrix [V] become:

$$V_j^x = \frac{4\omega\mu_0 k_0}{\varepsilon_r} \int_0^{\infty} \frac{J_0(r_0 k_0\beta)\beta^2 \sin(k_1 z')}{TeTmk_1} \left[(1-\varepsilon_r)\sin(k_1 z')k_0^2\beta^2 - jNeTm\right]$$

$$\int_0^{\pi/2} \tilde{J}'_{pjx} \cos\alpha \ \text{sinaxcosbx} \ d\alpha d\beta \qquad (3.2.7c)$$

$$V_j^y = \frac{4\omega\mu_0 k_0}{\varepsilon_r} \int_0^{\infty} \frac{J_0(r_0 k_0\beta)\beta^2 \sin(k_1 z')}{TeTmk_1} \left[(1-\varepsilon_r)\sin(k_1 z')k_0^2\beta^2 - jNeTm\right]$$

$$\int_0^{\pi/2} \tilde{J}'_{pjy} \sin\alpha \ \text{cosaysinby} \ d\alpha d\beta \qquad (3.2.7d)$$

where

$$\left.\begin{aligned} ax &= (x_{mj} - x_s)k_0\beta\cos\alpha \\ bx &= [(y_{nj}+y_{nj-1})/2 - y_s]k_0\beta\sin\alpha \\ ay &= [(x_{mj}+x_{mj-1})/2 - x_s]k_0\beta\cos\alpha \\ by &= (y_{nj} - y_s)k_0\beta\sin\alpha \end{aligned}\right\} \quad \text{sub domain basis functions}$$

$$\left.\begin{aligned} ax &= ay = x_s k_0 \beta \cos\alpha \\ bx &= by = y_s k_0 \beta \sin\alpha \end{aligned}\right] \quad \text{entire domain basis functions.}$$

(x_s, y_s) is the excitation point.
In the above expressions the functions $\tilde{J}_{pix}$ and $\tilde{J}_{piy}$ have the form (see Appendix 2A):

$$\tilde{J}_{pix} = \begin{cases} \tilde{J}'_{pix} & \text{entire domain basis functions} \\ \tilde{J}'_{pix}\, e^{[jk_x x_{mi} + jk_y (y_{ni}+y_{ni-1})/2]} & \text{PWL sub domain basis functions} \end{cases}$$

$$\tilde{J}_{piy} = \begin{cases} \tilde{J}'_{piy} & \text{entire domain basis functions} \\ \tilde{J}'_{piy}\, e^{[jk_y y_{ni} + jk_x (x_{mi}+x_{mi-1})/2]} & \text{PWL sub domain basis functions} \end{cases}$$

where $\tilde{J}'_{pix}$ and $\tilde{J}'_{piy}$ have the form:

$$\tilde{J}'_{pix} = \begin{cases} \left[\dfrac{2\pi(2i-1)Wx\, \cos(Wxk_x/2)}{[(2i-1)\pi]^2 - (k_x Wx)^2}\right]\left[\dfrac{2\sin(Wyk_y/2)}{k_y}\right] & \text{entire domain basis functions} \\ ab\, \mathrm{sinc}^2(k_x a/2)\, \mathrm{sinc}(k_y b/2) & \text{PWL sub-domain basis functions} \end{cases}$$

$$\tilde{J}'_{piy} = \begin{cases} \left[\dfrac{2\pi(2i-1)Wy\, \cos(Wyk_y/2)}{[(2i-1)\pi]^2 - (k_y Wy)^2}\right]\left[\dfrac{2\sin(Wxk_x/2)}{k_x}\right] & \text{entire domain basis functions} \\ ab\, \mathrm{sinc}^2(k_y b/2)\, \mathrm{sinc}(k_x a/2) & \text{PWL sub-domain basis functions} \end{cases}$$

with $a = x_{mi} - x_{mi-1}$ and $b = y_{ni} - y_{nj-1}$

3.3 Extraction of the source singularity.

Using sub domain basis functions the number of matrix elements of [Z] and [V] that have to be determined, can become very large. It is therefore of great importance that these elements are calculated with a minimum use of computing time. As mentioned in section 2.2.3, the β-integrand of [Z] and of [V] converge very slowly. In the next sections it will be shown that the source of this slow convergence is the source singularity $\frac{1}{|\vec{r} - \vec{r}'|}$ in the Green's function. In the spectral domain this singularity is "spread out", causing a slow convergence of the β-integrands for large values of β.

A method of extracting the source singularity is presented here. The extracted term, which represents the contribution of the currents in a homogeneous medium of relative permittivity $\varepsilon_h = (\varepsilon_r+1)/2$ (ε_r is the rel. permittivity of the dielectric slab), can be calculated very efficiently in the space domain. The remaining β-integral now converges relatively quickly. In the next sections overlapping rooftop basis functions are used in the direction of the current and PWC basis functions are used in the direction orthogonal to the current. The method presented here can also be used for the case of overlapping PWS basis functions in the direction of current. This is done in [19].
For entire domain basis functions the number of matrix elements is usually very small, so an efficient evaluation of these elements is less important then in the case of sub domain basis functions.

The method works only well if the upper conductor of the microstrip antenna is located in the $z = d$ plane. Furthermore it is assumed that the source is a coaxial-type probe.

3.3.1 Convergence of matrix elements without extraction of source singularity.

The infinite β-integrals are terminated at $\beta = \beta_{max}$. An accurate result of these integrals requires that $\beta_{max} = 200$ or more. The elements of [Z] converge more slowly as the distance between the two subsections under consideration increases.
So for off-diagonal elements an accurate result often requires that $\beta_{max} = 400$ or more [19]. Another problem is caused by the fact that the α-integration requires more sample points for large values of β. This effect is illustrated in fig 3.5, where the real part of the α-integrand of a Z_{11}^{xx} element is shown for $\beta = 5$ and $\beta = 50$.

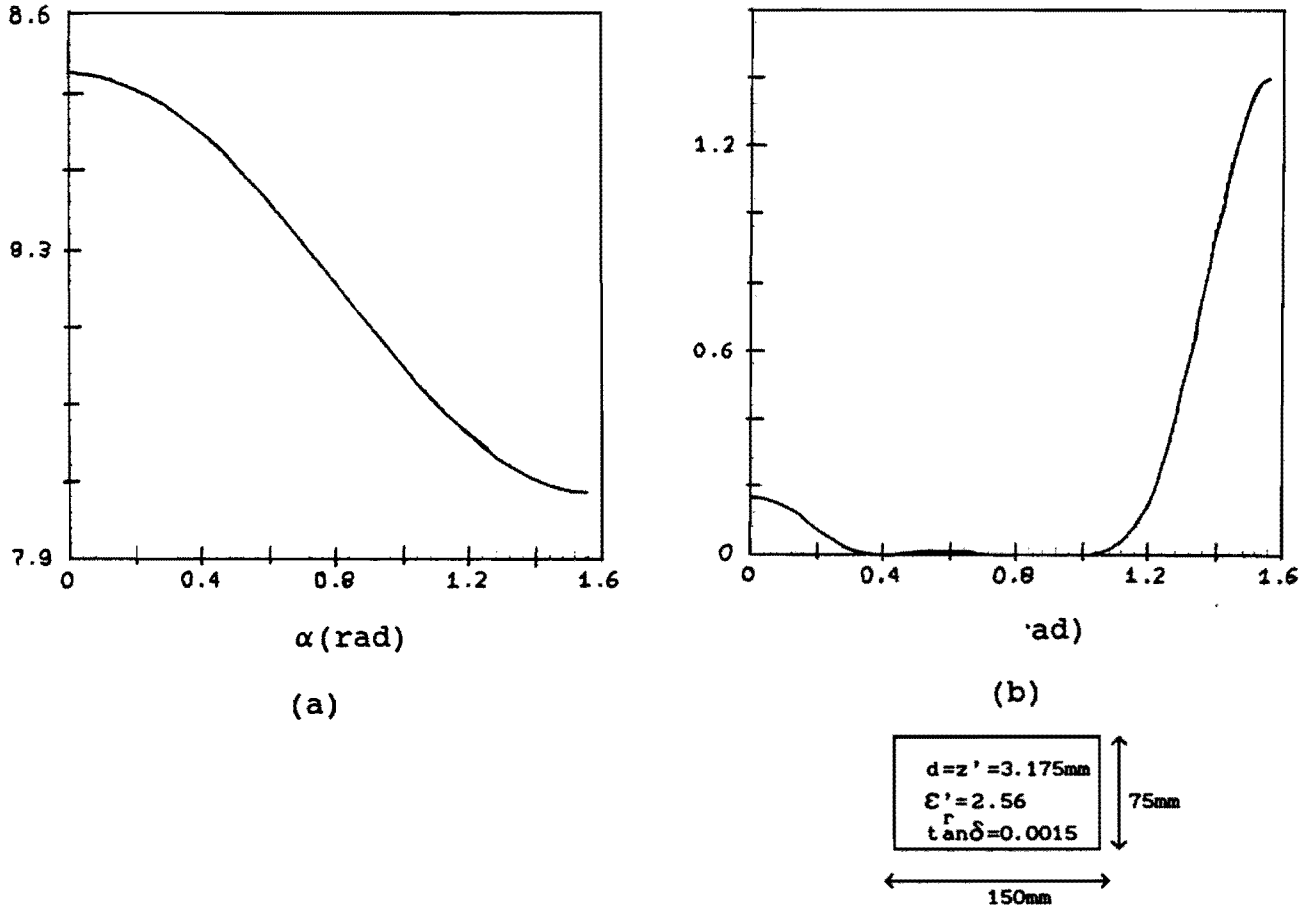

Fig 3.5: α-integrand of Z_{11}^{xx} for (a) $\beta = 5$ and (b) $\beta = 50$.
Frequency: 630 Mhz.

3.3.2 Asymptotic behavior of the integrands.

In this section the asymptotic forms of the β-integrands of a Z_{ji}^{xx} and V_j^x element are derived. Similar asymptotic forms can be derived for the other elements of the matrices [Z] and [V]. If the upper conductor is located in the z = d plane, a Z_{ji}^{xx} element has then according to Appendix 2A the form:

$$Z_{ji}^{xx} = \int_0^{\infty} \int_{-\pi}^{\pi} \tilde{Q}_{xx} \tilde{J}_{pix} \tilde{J}^*_{pjx} \, k_0^2 \beta d\alpha d\beta \qquad (3.3.1)$$

where

$$\tilde{Q}_{xx} = \frac{\omega \mu_0 \sin(k_1 d)}{\varepsilon_r TeTmk_1} \left[j(\beta^2 \cos^2\alpha - \varepsilon_r) NeTm \right.$$

$$\left. - \beta^2 \cos^2\alpha k_1^2 (\varepsilon_r - 1) \sin(k_1 d) \right]$$

For large values of β we can write:

$$\begin{aligned}
k_1 &\approx -jk_0\beta \\
k_2 &\approx -jk_0\beta \\
\cos(k_1 d) &\approx \tfrac{1}{2} e^{k_0\beta d} \\
\sin(k_1 d) &\approx -\tfrac{j}{2} e^{k_0\beta d} = -j\cos(k_1 d) \qquad (3.3.2) \\
Te &= k_1 \cos(k_1 d) + jk_2 \sin(k_1 d) \approx 2k_0\beta \sin(k_1 d) \\
Tm &= k_2 \varepsilon_r \cos(k_1 d) + jk_1 \sin(k_1 d) \approx k_0\beta(\varepsilon_r + 1)\sin(k_1 d) \\
Ne &= k_1 \cos[k_1(d - z')] + jk_2 \sin[k_1(d - z')] \approx k_1
\end{aligned}$$

Substituting the above asymptotic expressions in (3.3.1) yields for the asymptotic form of the function $\tilde{Q}_{xx}$:

$$\tilde{Q}_{xx} \approx - \frac{\omega\mu_0 \sin(k_1 d)}{2j\varepsilon_r(\varepsilon_r+1)k_0^3\beta^3\sin^2(k_1 d)} \left[(\beta^2\cos^2\alpha - \varepsilon_r)k_0^2\beta^2(\varepsilon_r+1)\sin(k_1 d) + k_0^2\beta^4\cos^2\alpha(\varepsilon_r-1)\sin(k_1 d)\right]$$

$$= \frac{-j\omega\mu_0}{2k_0^3\beta}\left[k_0^2 - \frac{2k_0^2\beta^2\cos^2\alpha}{(\varepsilon_r+1)}\right]$$

$$= \frac{-j\omega\mu_0}{2k_0^3\beta}\left[k_0^2 - \frac{2k_x^2}{(\varepsilon_r+1)}\right] \qquad (3.3.3)$$

where $k_x = k_0\beta\cos\alpha$

An element of the excitation vector [V] with a test current in the $\hat{x}$-direction can be written in the form for z = d (see Appendix 2A):

$$V_j^x = \int_0^{\infty}\int_{-\pi}^{\pi} \tilde{Q}_{vzx}\tilde{J}_{pix}\,\tilde{J}_s^*\,k_0^2\beta\,d\alpha\,d\beta \qquad (3.3.4)$$

where

$$\tilde{Q}_{vzx} = \frac{j\omega\mu_0 k_0\beta\cos\alpha\sin(k_1 d)}{\varepsilon_r k_0^2 TeTmk_1}\left[(\varepsilon_r-1)\sin(k_1 d)k_0^2\beta^2 + jNeTm\right]$$

Using the asymptotic expressions (3.3.2), it can be shown that $\tilde{Q}_{zvx}$ has then following asymptotic form for large values of β:

$$\tilde{Q}_{vzx} \approx \frac{-\omega\mu_0\cos\alpha}{k_0^2(\varepsilon_r+1)} = \frac{-\omega\mu_0 k_x}{k_0^3\beta(\varepsilon_r+1)} \qquad (3.3.5)$$

3.3.3 Fields from a dipole in a homogeneous medium.

Now consider a $\hat{x}$-directed electric dipole, located at (x',y',d) in a homogeneous medium with relative permittivity ε_h. If we leave the $e^{-jk|\vec{r} - \vec{r}'|}$ -dependence of the fields out of consideration, i.e. $|\vec{r} - \vec{r}'|$ is very small, the xx-component of the dyadic Green's function of the homogeneous medium in the observation point (x,y,z) becomes:

$$G_h^{xx}(x',y',x,y,z) = \frac{\mu_0}{4\pi|\vec{r} - \vec{r}'|} = \frac{\mu_0}{4\pi\sqrt{(x-x')^2 + (y-y')^2 + (z-d)^2}}$$

$$= \frac{\mu_0}{4\pi\sqrt{(x-x')^2 + (y-y')^2}} \quad \text{for } \underline{z = d} \qquad (3.3.6)$$

where $\vec{r} = (x,y,z)$
$\vec{r}' = (x',y',d)$

The Fourier transform of G_h^{xx} has the form for the case that z = d:

$$\tilde{G}_h^{xx}(x',y',k_x,k_y,d) = \frac{\mu_0}{4\pi}\int_{-\infty}^{\infty}\int \frac{1}{\sqrt{(x-x')^2 + (y-y')^2}} e^{jk_x x} e^{jk_y y}\, dxdy$$

$$= \frac{\mu_0}{2k_0\beta} e^{jk_x x'} e^{jk_y y'} \qquad (3.3.7)$$

where $k_0^2\beta^2 = k_x^2 + k_y^2$

If we place a $\hat{x}$-directed electric current $J_{px}\,\vec{e}_x$ in the z = d plane in this homogeneous medium, the x component of the electric field E_h^x at (x,y,d) is then according to (2.2.6b) and (2.2.1):

$$E_h^x(x,y,d) = -\frac{j\omega}{k_h^2}\left[k_h^2 A_h^x(x,y,d) + \partial_x^2 A_h^x(x,y,d)\right] \qquad (3.3.8a)$$

where A_h^x is the vector potential at (x,y,d):

$$A_h^x(x,y,d) = \iint_{S_p} G_h^{xx}(x',y',x,y,d)\, J_{px}(x',y')dx'dy' \qquad (3.3.8b)$$

k_h^2 is the wave number of the homogeneous medium: $k_h^2 = \varepsilon_h k_0^2$ and S_p is the region where the current $\vec{J}_{px}$ is nonzero.
In terms of the Green's function in the spectral domain $\tilde{G}_h^{xx}$ the vector potential becomes at z = d:

$$A_h^x(x,y,d) = \iint_{S_p}\left[\frac{1}{4\pi^2}\int_{-\infty}^{\infty}\tilde{G}_h^{xx}(x',y',k_x,k_y,d)e^{-jk_x x}\, e^{-jk_y y}dk_x dk_y\right]$$

$$J_{px}(x',y')dx'dy'$$

$$= \frac{1}{4\pi^2}\int_{-\infty}^{\infty}\frac{\mu_0}{2k_0\beta}\left[\iint_{S_p} J_{px}(x',y')e^{jk_x x'}e^{jk_y y'}dx'dy'\right]e^{-jk_x x}\, e^{-jk_y y}dk_x dk_y$$

$$= \frac{1}{4\pi^2}\int_{-\infty}^{\infty}\frac{\mu_0}{2k_0\beta}\,\tilde{J}_{px}(k_x,k_y)\, e^{-jk_x x}\, e^{-jk_y y}\, dk_x dk_y \qquad (3.3.9)$$

where $\tilde{J}_{px}(k_x,k_y)$ is the Fourier transform of $J_{px}(x',y')$.
According to (3.3.8) and (3.3.9) the electric field at (x,y,d) may now be found by:

$$E_h^x(x,y,d) = -\frac{j\omega}{k_h^2}\left[k_h^2 A_h^x(x,y,d) + \partial_x^2 A_h^x(x,y,d)\right]$$

$$= \frac{-j\omega}{4\pi^2 k_h^2}\int_{-\infty}^{\infty}(k_h^2 - k_x^2)\frac{\mu_0}{2k_0\beta}\,\tilde{J}_{px}(k_x,k_y)\, e^{-jk_x x}\, e^{-jk_y y}\, dk_x dk_y \qquad (3.3.10)$$

Now place the $\hat{x}$-directed electric currents J_{pix} and J_{pjx} in the z=d plane in the homogeneous medium. Note that J_{pix} is nonzero in subsection i and J_{pjx} is nonzero in subsection j. Let E^x_{hpi} be the $\hat{x}$-directed electric field at (x,y,d) due to current J_{pix}. Introduce the function Z^{xx}_{hji} which is defined as:

$$Z^{xx}_{hji} = 4\pi^2 \iint_{S_p} J_{pjx}\, E^x_{hpi}\, dS \qquad (3.3.11)$$

Z^{xx}_{hji} has the same form as Z^{xx}_{ji} defined in (2.4.12a).
Substituting expression (3.3.10) in (3.3.11) and changing order of integration results in:

$$Z^{xx}_{hji} = -\frac{j\omega\mu_0}{k_h^2} \int_{-\infty}^{\infty}\int (k_h^2 - k_x^2)\frac{1}{2k_0\beta}\, \tilde{J}_{pix}\tilde{J}^*_{pjx}\, dk_x dk_y \qquad (3.3.12)$$

where $\tilde{J}^*_{pjx}$ is the complex conjugate of the Fourier transform of J_{pjx}. If we choose the relative permittivity of the homogeneous medium ε_h equal to $(\varepsilon_r + 1)/2$, (3.3.12) becomes:

$$Z^{xx}_{hji} = -\frac{j\omega\mu_0}{k_0^2} \int_{-\infty}^{\infty}\int \frac{1}{2k_0\beta}\left[k_0^2 - \frac{2k_x^2}{(\varepsilon_r+1)} \right] \tilde{J}_{pix}\tilde{J}^*_{pjx}\, dk_x dk_y$$

$$= \int_0^{\infty}\int_{-\pi}^{\pi} \tilde{Q}_{hxx}\tilde{J}_{pix}\, \tilde{J}^*_{pjx}\, k_0^2\beta\, d\alpha d\beta \qquad (3.3.13)$$

where

$$\tilde{Q}_{hxx} = \frac{-j\omega\mu_0}{2k_0^3\beta}\left[k_0^2 - \frac{2k_x^2}{(\varepsilon_r+1)} \right]$$

$$k_x = k_0\beta\cos\alpha$$
$$k_y = k_0\beta\sin\alpha$$

We now observe that $\tilde{Q}_{hxx}$ has the same asymptotic form as $\tilde{Q}_{xx}$ of (3.3.1).

In a similar way we can derive for $\varepsilon_h = (\varepsilon_r + 1)/2$ that:

$$V_{hj}^{x} = 4\pi^2 \iint_{\text{source}} J_s(x,y)\ E_{hpj}^{z}(x,y,z)\ dS$$

$$= -\frac{4j\pi^2\omega}{k_h^2} \oint_{C_s} \int_0^d J_s(x,y)\ (\partial_z \partial_x A_{hj}^{x}(x,y,z))\ dz dC_s$$

$$= -\frac{j\pi\omega\mu_0}{k_h^2} \oint_{C_s} \partial_x \iint_{S_j} \int_0^d \partial_z \left[\frac{1}{\sqrt{(x-x_j)^2 + (y-y_j)^2 + (z-d)^2}}\right] dz$$

$$J_s(x,y)\ dx_j dy_j\ dC_s$$

$$= -\frac{j\pi\omega\mu_0}{k_h^2} \oint_{C_s} \partial_x \iint_{S_j} \left[\frac{1}{\sqrt{(x-x_j)^2 + (y-y_j)^2}}\right] J_s(x,y)\ dx_j dy_j\ dC_s$$

$$+ \frac{j\pi\omega\mu_0}{k_h^2} \oint_{C_s} \partial_x \iint_{S_j} \left[\frac{1}{\sqrt{(x-x_j)^2 + (y-y_j)^2 + d^2}}\right] J_s(x,y)\ dx_j dy_j\ dC_s$$

$$= -\frac{\omega\mu_0}{k_h^2} \iint_{-\infty}^{\infty} \frac{k_x}{k_0\beta(\varepsilon_r+1)}\ \tilde{J}_{pjx}\tilde{J}_s^*\ dk_x dk_y + I_{vh}$$

$$= \int_0^{\infty} \int_{-\pi}^{\pi} \tilde{Q}_{hvzx} \tilde{J}_{pjx} \tilde{J}_s^* k_o^2 \beta d\alpha d\beta + I_{vh} \qquad (3.3.14)$$

where

$$\tilde{Q}_{hvzx} = \frac{-\omega\mu_o k_x}{k_o^3 \beta(\varepsilon_r+1)}$$

$\tilde{J}_s^*$ is given in (2.4.20) for an coaxial probe feed and the contour C_s and height d of this probe feed are shown in fig. 2.5. Note that E^z_{hpj} is the $\hat{z}$-directed electric field from the $\hat{x}$-directed current J_{pjx}:

$$\vec{E}^z_{hpj}(x,y,z) = -\frac{j\omega}{k_h^2}[\partial_z \partial_x A^x_{hj}(x,y,z)]\vec{e}_z \qquad (3.3.14a)$$

We observe that $\tilde{Q}_{hvzx}$ has the same asymptotic form as $\tilde{Q}_{vzx}$ of (3.3.4). The integrand of the integral I_{vh} has no singularity at the source and is therefore of no importance for the technique described in this section. The term I_{vh} is given by:

$$I_{vh} = \frac{j\pi\omega\mu_o}{k_h^2} \oint_{C_s} \partial_x \iint_{S_j} \left[\frac{1}{\sqrt{(x-x_j)^2 + (y-y_j)^2 + d^2}}\right] J_s(x,y)\, dx_j dy_j\, dC_s$$

3.3.4 Source term removal.

In the space domain the dyadic Green's function in the dielectric slab $\overline{\overline{G}}_1(\vec{r},\vec{r}')$ has a $\frac{1}{|\vec{r}-\vec{r}'|}$ singularity [Mosig]. This source singularity is responsible for the asymptotic behavior of the Green's function in the spectral domain. In the previous section it is shown that the asymptotic form of the spectral domain Green's function in the grounded dielectric slab is identical to the spectral domain Green's function (3.3.7) of a homogeneous medium with relative permittivity $\varepsilon_h = (\varepsilon_r+1)/2$.

Now consider a Z^{xx}_{ji} element of the matrix [Z]. If $\tilde{Q}_{hxx}$ of (3.3.13) is subtracted from $\tilde{Q}_{xx}$ of (3.3.1), the resulting integral converges more quickly then the original integral. Thus writing Z^{xx}_{ji} in the form:

$$Z^{xx}_{ji} = Z^{xx}_{hji} + \int_0^{\infty}\int_{-\pi}^{\pi} [\tilde{Q}_{xx} - \tilde{Q}_{hxx}]\tilde{J}_{pix}\,\tilde{J}^*_{pjx}\,k_0^2\beta d\alpha d\beta \qquad (3.3.15)$$

results in a term Z^{xx}_{hji}, that can efficiently be evaluated in the space domain for the case of rooftop basis functions (see section 3.3.5), and in an integral that converges relatively quickly. Note that Z^{xx}_{hji} is given by expression (3.3.11).
The improved convergence of the second term of the right-hand side of (3.3.15) is illustrated in fig 3.6. In this figure the imaginary part of the function

$$f_1(\beta) = \int_{-\pi}^{\pi} \tilde{Q}_{xx}\tilde{J}_{pix}\,\tilde{J}^*_{pjx}\,k_0^2\beta d\alpha$$

and the imaginary part of the function

$$f_2(\beta) = \int_{-\pi}^{\pi} [\tilde{Q}_{xx} - \tilde{Q}_{hxx}]\tilde{J}_{pix}\,\tilde{J}^{*}_{pjx}\,k_0^2\beta d\alpha$$

are drawn for the case of rooftop basis functions and i=j=1. The real parts of $f_1(\beta)$ and $f_2(\beta)$ have a similar form as the imaginary parts.

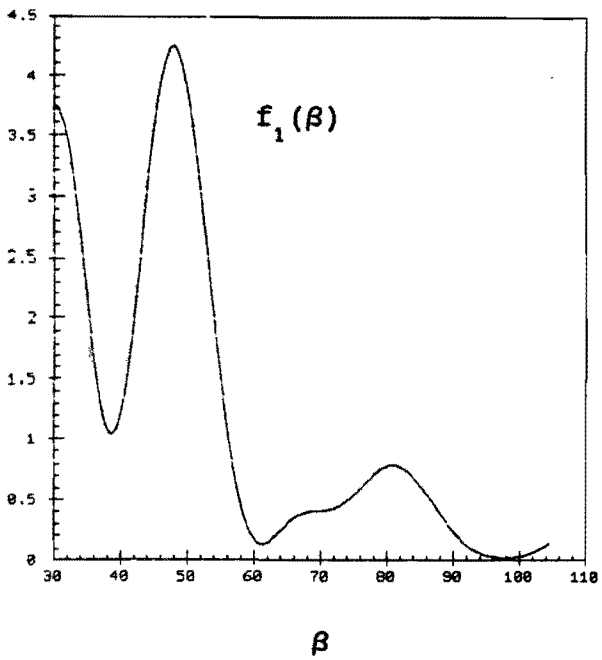

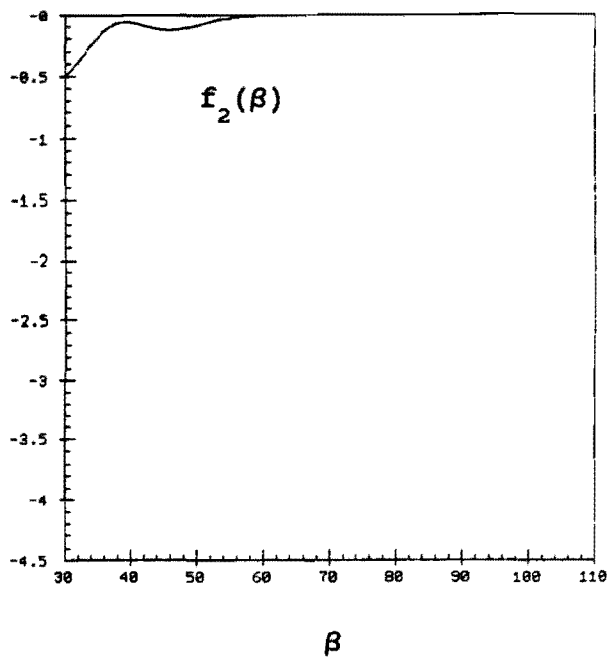

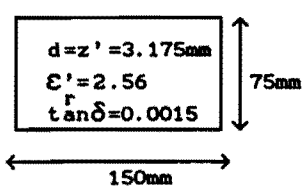

Fig 3.6: Imaginary part of $f_1(\beta)$ and $f_2(\beta)$ for i = j = 1.
Frequency f = 630Mhz

From fig 3.6 it is obvious that the β-integral over $f_2(\beta)$ converges more quickly then the β-integral over $f_1(\beta)$.
A V_j^x element of the excitation vector [V] can also be written as a sum of a term representing the contribution from the source singularity and a quickly converging integral:

$$V_j^x = [V_{hj}^x - I_{vh}] + \int_0^{\infty} \int_{-\pi}^{\pi} [\tilde{Q}_{vzx} - \tilde{Q}_{hvzx}] \tilde{J}_{pjx} \, \tilde{J}_s^* \, k_0^2 \beta d\alpha d\beta \qquad (3.3.16)$$

where V_{hj}^x and I_{vh} are given in (3.3.14).

3.3.5 Computation of the extracted source term.

Using the technique described in the previous section, the elements of the matrix [Z] and of the excitation vector [V] can be calculated very efficiently. This, of course, on the condition that the extracted terms Z_{hji} and V_{hj} can be calculated efficiently.
The best way to calculate the extracted terms is to evaluate them in the space domain. This is done in this section for Z_{hji}^{xx} and V_{hj}^x. The derivation for the other element can be done in a similar way. The final expressions for all the elements of [Z] and [V] are given in Appendix 3A. We shall assume that the patch current $\vec{J}_p$ is expressed in terms of overlapping rooftop functions in the direction of current and in terms of Piece-wise constant (PWC) functions in the direction orthogonal to the current. In [19], where a similar source extracting technique is used, overlapping Piece-wise sinusoidal functions are used to describe the patch current in the direction of current.

Now lets consider a Z_{hji}^{xx} element. According to (3.3.11) and (3.3.8) this element can be written as:

$$Z^{xx}_{hji} = 4\pi^2 \iint_{S_j} J_{pjx}\, E^{x}_{hpi}\, dS$$

$$= -\frac{4j\pi^2\omega}{k_h^2} \iint_{S_j} [k_h^2 A^{x}_{hi}(x_j,y_j,d) + \partial^2_{x_j} A^{x}_{hi}(x_j,y_j,d)]J_{pjx}\, dS$$

$$= -\frac{4j\pi^2\omega}{k_h^2} \iint_{S_j} \left[\iint_{S_i} [k_h^2 + \partial^2_{x_j}] G^{xx}_h(x_i,y_i,x_j,y_j,d) \right.$$

$$\left. J_{pix}(x_i,y_i)\, dx_i dy_i \right] J_{pjx}(x_j,y_j) dx_j dy_j \qquad (3.3.17)$$

where $G^{xx}_h(x_i,y_i,x_j,y_j,d)$ is defined in (3.3.6), S_i and S_j represent sub domain i, respectively, sub domain j and $k_h^2 = k_0^2(\varepsilon_r+1)/2$. In the case of rooftop basis functions, J_{pix} and J_{pjx} have the form (see section (2.5.2):

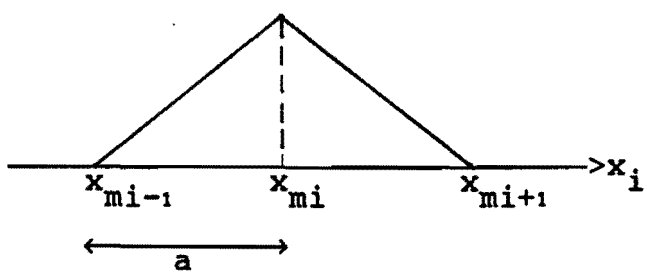

$$J_{pix}(x_i,y_i) = \begin{cases} \dfrac{a - |x_{mi}-x_i|}{a} & \text{for } \begin{cases} x_{mi-1} \le x_i \le x_{mi+1} \\ y_{ni-1} \le y_i \le y_{ni} \end{cases} \\ 0 & \text{elsewhere} \end{cases} \qquad (3.3.18)$$

where $a = x_{mi} - x_{mi-1}$
$b = y_{ni} - y_{ni-1}$

We shall assume that a and b are constants, which means that all the subsections have equal dimensions. Using rooftop basis functions, the inner two-dimensional integral of (3.3.17) can be found in closed form. Carrying out a huge amount of algebra, the final result for Z^{xx}_{hji} is then:

$$\iint_{S_i} [k_h^2 + \partial^2_{x_j}] G_h^{xx}(x_i,y_i,x_j,y_j,d) J_{pix}(x_i,y_i)\,dx_i\,dy_i$$

$$= [k_h^2 A^x_{hi}(x_j,y_j,d) + \partial^2_{x_j} A^x_{hi}(x_j,y_j,d)] \qquad (3.3.19a)$$

with

$$A^x_{hi}(x_j,y_j,d) = \frac{\mu_0}{4\pi a}\Bigg[\frac{1}{2}\, y_1 \left(\sqrt{x_{10}^2+y_1^2} + \sqrt{x_{30}^2+y_1^2} - 2\sqrt{x_{20}^2+y_1^2} \right)$$

$$+ (2x_{20}^2 - x_{10}^2 - x_{30}^2)\ln 2$$

$$- \tfrac{1}{2}x_{10}^2 \ln[y_1+\sqrt{x_{10}^2+y_1^2}] - \tfrac{1}{2}x_{30}^2 \ln[y_1+\sqrt{x_{30}^2+y_1^2}]$$

$$+ x_{20}^2 \ln[y_1+\sqrt{x_{20}^2+y_1^2}] - x_{10}y_1 \ln[x_{10}+\sqrt{x_{10}^2+y_1^2}]$$

$$- x_{30}y_1 \ln[x_{30}+\sqrt{x_{30}^2+y_1^2}] + 2x_{20}y_1 \ln[x_{20}+\sqrt{x_{20}^2+y_1^2}] \Bigg] \Bigg|_{y_{10}}^{y_{20}}$$

(3.3.19b)

$$\partial^2_{x_j} A^x_{hi}(x_j,y_j,d) = \frac{\mu_0}{4\pi a}\Big[\, 2\ln[y_1+\sqrt{x_{20}^2+y_1^2}\,] - \ln[y_1+\sqrt{x_{10}^2+y_1^2}\,]$$

$$- \ln[y_1+\sqrt{x_{30}^2+y_1^2}\,]\Big]\Big|_{y_{10}}^{y_{20}} \qquad (3.3.19c)$$

with $x_{10} = x_j - x_{mi-1}$
$x_{20} = x_j - x_{mi}$
$x_{30} = x_j - x_{mi+1}$
$y_{10} = y_j - y_{ni-1}$
$y_{20} = y_j - y_{ni}$

The outer two-dimensional integral of (3.3.17) can now be obtained using a numerical integration routine. The integrand given by expression (3.3.19a) is a very smooth function of x_j and y_j if subsection i and subsection j are not touching each other. However, if the distance between the two subsections becomes very small, expression (3.3.19c) has a logarithmic singularity which hinders a direct numerical integration. Fortunately it is possible to calculate the x_j-integral over (3.3.19c) analytically. The result of this one-dimensional integration is given in Appendix 3A. The resulting integrand has no singularities and can very easily be integrated numerically.

An advantage of the use of rooftop basis functions instead of PWS basis functions is that the inner integral (3.3.19a) for the case of PWS basis functions cannot be evaluated in closed form, but in terms of exponential integrals [19]. An (simple) analytical integration of the logarithmic singularity is in this case not possible.

In a similar way an element V^x_{hj} can be determined in the space domain. The resulting integral is an one-dimensional integral, which can be evaluated very easily using a simple numerical

integration routine. According to (3.3.14) V^x_{hj} can be written as:

$$V^x_{hj} = 4\pi^2 \iint_{source} J_s \, E^z_{hpj} \, dS$$

$$= - \frac{4j\pi^2\omega}{k_h^2} \oint_{C_s} \int_0^d J_s \, \partial_z \partial_x A^x_{hj}(x,y,z) \, dz dC_s$$

$$= - \frac{4j\pi^2\omega}{k_h^2} \oint_{C_s} J_s \partial_x \left[\iint_{S_j} G_h^{xx}(x_j,y_j,x,y,d) J_{pjx}(x_j,y_j) dx_j dy_j \right] dC_s + I_{vh} \qquad (3.3.20)$$

where $\vec{J}_s = J_s \vec{e}_z = \frac{I_0}{2\pi r_0} \vec{e}_z$ on a cylinder with contour C_s and with diameter $d_0 = 2r_0$ and height d (see fig. 2.5). (x,y,z) are coordinates on the source surface. Using rooftop basis functions (3.3.20) finally becomes:

$$V^x_{hj} = - \frac{j\omega\mu_0}{2k_h^2 a} \int_0^{2\pi} f_{vh}(r_0,\phi) d\phi + I_{vh} \qquad (3.3.21)$$

with

$$f_{vh}(r_0,\phi) = \Big(2x_{20} \ln[y_1 + \sqrt{x_{20}^2 + y_1^2}] - x_{10} \ln[y_1 + \sqrt{x_{10}^2 + y_1^2}]$$

$$- x_{30} \ln[y_1 + \sqrt{x_{30}^2 + y_1^2}] + 2y_1 \ln[x_{20} + \sqrt{x_{20}^2 + y_1^2}]$$

$$- y_1 \ln[x_{10} + \sqrt{x_{10}^2 + y_1^2}] - y_1 \ln[x_{30} + \sqrt{x_{30}^2 + y_1^2}] \Big) \Big|_{y_{10}}^{y_{20}}$$

$$x_{10} = r_0\cos\phi + x_s - x_{mj-1}$$
$$x_{20} = r_0\cos\phi + x_s - x_{mj}$$
$$x_{30} = r_0\cos\phi + x_s - x_{mj+1}$$
$$y_{10} = r_0\sin\phi + y_s - y_{nj-1}$$
$$y_{20} = r_0\sin\phi + y_s - y_{nj}$$

(x_s, y_s) is the excitation point. Note that the integrand $f_{vh}(r_0, \phi)$

has no logarithmic singularities. As mentioned before , the integral I_{vh} is of no importance, because this term falls off in expression (3.3.16).
Note that the integrands of (3.3.17) and (3.3.21) are frequency independent, which means that these two-dimensional integrals have to be evaluated only once for a specific microstrip structure.

3.4 Toeplitz-type symmetry of the matrix [Z].

Due to the Toeplitz-type symmetry of the matrix [Z] not all the elements of the matrix [Z] have to be evaluated. From (3.2.6) and (3.2.7) it can be seen that an arbitrarily element Z_{ji} depends on the distance between sub domain i and sub domain j. In the case of a Z_{ji}^{xx} or a Z_{ji}^{yy} element, only the absolute distance, specified by $|x_{mj} - x_{mi}|$ and $|y_{nj} - y_{ni}|$, is relevant. The Toeplitz-type symmetry of [Z] is illustrated with the following simple example.

Consider a rectangular microstrip antenna with dimension Wx x Wy. Expand the unknown patch current in 12 basis functions. The basis functions are now expressed in terms of overlapping rooftop functions in the direction of current and in terms of piece-wise constant (PWC) functions in the direction orthogonal to the current. In fig. 3.7 the geometry of this microstrip structure is shown.

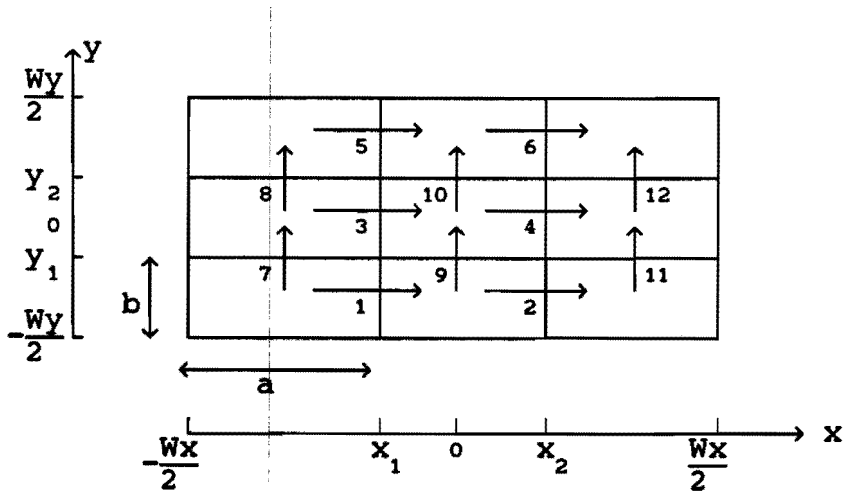

Fig. 3.7: Dividing the microstrip antenna in 12 subsections.

Basis function 1 is a $\hat{x}$-directed current and is nonzero for $-\frac{Wx}{2} \leq x \leq x_1$ & $\frac{Wy}{2} \leq y \leq y_1$, and is expressed in terms of a rooftop function along the x-axis and is constant along the y-axis in the specified interval.

Basis function 1 up to and including 6 represent the $\hat{x}$-directed patch current and basis function 7 up to and including 12 represent the $\hat{y}$-directed patch current.

The symmetric 12x12 matrix [Z] now has the form:

$$\begin{bmatrix}
Z_{1,1} & \cdot & \cdot & \cdot & \cdot & \cdot & \cdot & \cdot & \cdot & \cdot & \cdot & \cdot \\
Z_{2,1} & Z_{1,1} & \cdot & \cdot & \cdot & \cdot & \cdot & \cdot & \cdot & \cdot & \cdot & \cdot \\
Z_{3,1} & Z_{4,1} & Z_{1,1} & \cdot & \cdot & \cdot & \cdot & \cdot & \cdot & \cdot & \cdot & \cdot \\
Z_{4,1} & Z_{3,1} & Z_{2,1} & Z_{1,1} & \cdot & \cdot & \cdot & \cdot & \cdot & \cdot & \cdot & \cdot \\
Z_{5,1} & Z_{6,1} & Z_{3,1} & Z_{4,1} & Z_{1,1} & \cdot & \cdot & \cdot & \cdot & \cdot & \cdot & \cdot \\
Z_{6,1} & Z_{5,1} & Z_{4,1} & Z_{3,1} & Z_{2,1} & Z_{1,1} & \cdot & \cdot & \cdot & \cdot & \cdot & \cdot \\
Z_{7,1} & -Z_{11,1} & -Z_{7,1} & Z_{11,1} & -Z_{8,1} & Z_{12,1} & Z_{7,7} & \cdot & \cdot & \cdot & \cdot & \cdot \\
Z_{8,1} & -Z_{12,1} & Z_{7,1} & -Z_{11,1} & -Z_{7,1} & Z_{11,1} & Z_{8,7} & Z_{7,7} & \cdot & \cdot & \cdot & \cdot \\
Z_{9,1} & Z_{7,1} & Z_{7,1} & -Z_{7,1} & -Z_{10,1} & Z_{10,1} & Z_{9,7} & Z_{10,7} & Z_{7,7} & \cdot & \cdot & \cdot \\
Z_{10,1} & -Z_{10,1} & -Z_{7,1} & Z_{7,1} & Z_{7,1} & -Z_{7,1} & Z_{10,7} & Z_{9,7} & Z_{8,7} & Z_{7,7} & \cdot & \cdot \\
Z_{11,1} & -Z_{7,1} & -Z_{11,1} & Z_{7,1} & -Z_{12,1} & -Z_{10,1} & Z_{11,7} & Z_{12,7} & Z_{9,7} & Z_{10,7} & Z_{7,7} & \cdot \\
Z_{12,1} & Z_{10,1} & Z_{11,1} & -Z_{7,1} & -Z_{11,1} & Z_{7,1} & Z_{12,7} & Z_{11,7} & Z_{10,7} & Z_{9,7} & Z_{8,7} & Z_{7,7}
\end{bmatrix}$$

In this example only 18 of the 144 elements have to be calculated (for each frequency).

APPENDIX 3A.

In this appendix the final expressions for the extracted source terms are given for the case of rooftop basis functions, defined in (3.3.18). The geometry is shown in fig 2.9. The relative permittivity of the homogeneous medium $\varepsilon_h = (\varepsilon_r+1)/2$. The resulting expressions are then with $k_h^2 = k_0^2\varepsilon_h$:

i. Z_{ji}^{xx}

Spectral domain.

$$Z_{hji}^{xx} = \frac{-j\omega\mu_0}{k_0^2} \int\int_{-\infty}^{\infty} \frac{1}{2k_0\beta}\left[k_0^2 - \frac{2k_x^2}{(\varepsilon_r+1)}\right] \tilde{J}_{pix}\, \tilde{J}^*_{pjx}\, dk_x dk_y \qquad (3A.1)$$

Space domain.

$$Z_{hji}^{xx} = -\frac{4j\pi^2\omega}{k_h^2}\int\int_{S_j}[k_h^2 A^x_{hi}(x_j,y_j) + \partial^2_{x_j} A^x_{hi}(x_j,y_j)]J_{pjx}(x_j,y_j)dx_j dy_j \qquad (3A.2)$$

with

$$A^x_{hi}(x_j,y_j) = \frac{\mu_0}{4\pi a}\Bigg[\frac{1}{2}\, y_1\left(\sqrt{x_{10}^2+y_1^2} + \sqrt{x_{30}^2+y_1^2} - 2\sqrt{x_{20}^2+y_1^2}\right)$$

$$+ (2x_{20}^2 - x_{10}^2 - x_{30}^2)\ln 2$$

$$- \tfrac{1}{2}x_{10}^2 \ln[y_1+\sqrt{x_{10}^2+y_1^2}] - \tfrac{1}{2}x_{30}^2 \ln[y_1+\sqrt{x_{30}^2+y_1^2}]$$

$$+ x_{20}^2 \ln[y_1+\sqrt{x_{20}^2+y_1^2}] - x_{10}y_1 \ln[x_{10}+\sqrt{x_{10}^2+y_1^2}]$$

$$- x_{30}y_1 \ln[x_{30}+\sqrt{x_{30}^2+y_1^2}] + 2x_{20}y_1 \ln[x_{20}+\sqrt{x_{20}^2+y_1^2}] \Big]\Big|_{y_{10}}^{y_{20}}$$

$$\partial_{x_j}^2 A_{hi}^x(x_j,y_j) = \frac{\mu_0}{4\pi a}\Big[2\ln[y_1+\sqrt{x_{20}^2+y_1^2}] - \ln[y_1+\sqrt{x_{10}^2+y_1^2}]$$

$$- \ln[y_1+\sqrt{x_{30}^2+y_1^2}]\Big]\Big|_{y_{10}}^{y_{20}}$$

$$x_{10} = x_j - x_{mi-1}$$
$$x_{20} = x_j - x_{mi}$$
$$x_{30} = x_j - x_{mi+1}$$
$$y_{10} = y_j - y_{ni-1}$$
$$y_{20} = y_j - y_{ni}$$
$$a = x_{mi} - x_{mi-1}$$

ii. Z_{hji}^{yx} and Z_{hij}^{xy}.

Spectral domain.

$$Z_{hji}^{yx} = Z_{hij}^{xy} = \frac{j\omega\mu_0}{k_0^2} \int\int_{\infty} \frac{k_x k_y}{k_0\beta(\varepsilon_r+1)} \tilde{J}_{pix} \tilde{J}_{pjy}^* \, dk_x dk_y \qquad (3A.3)$$

Space domain.

$$Z_{hji}^{yx} = Z_{hij}^{xy} = -\frac{4j\pi^2\omega}{k_h^2} \iint_{S_j} \partial_{x_j}\partial_{y_j} A_{hi}^x(x_j,y_j) \; J_{pjy}(x_j,y_j) dx_j dy_j \qquad (3A.4)$$

with

$$\partial_{x_j}\partial_{y_j} A^x_{hi}(x_j,y_j) = \frac{\mu_0}{4\pi a}\left[2\ln[x_{20}+\sqrt{x_{20}^2+y_1^2}] - \ln[x_{10}+\sqrt{x_{10}^2+y_1^2}] - \ln[x_{30}+\sqrt{x_{30}^2+y_1^2}]\right]\Bigg|_{y_{10}}^{y_{20}}$$

$$x_{10} = x_j - x_{mi-1}$$
$$x_{20} = x_j - x_{mi}$$
$$x_{30} = x_j - x_{mi+1}$$
$$y_{10} = y_j - y_{ni-1}$$
$$y_{20} = y_j - y_{ni}$$
$$a = x_{mi} - x_{mi-1}$$

iii. V^x_j.

Spectral domain.

$$V^x_{hj} = -\frac{\omega\mu_0}{k_0^2}\int_{-\infty}^{\infty}\frac{k_x}{k_0\beta(\varepsilon_r+1)}\tilde{J}_{pjx}\,\tilde{J}^*_s\,dk_x dk_y + Ivh \qquad (3A.5)$$

where $\tilde{J}^*_s$ is given in (2.4.20) and the term Ivh is a term that is not used in the source extracting technique (see section 3.3.3).

Space domain.

$$V^x_{hj} = -\frac{j\omega\mu_0}{2k_h^2 a}\int_0^{2\pi} f_{vh}(r_0,\phi)\,d\phi + I_{vh} \qquad (3A.6)$$

with

$$f_{vh}(r_0,\phi) = \Big[2x_{20}\ln[y_1+\sqrt{x_{20}^2+y_1^2}\,] - x_{10}\ln[y_1+\sqrt{x_{10}^2+y_1^2}\,]$$

$$- x_{30}\ln[y_1+\sqrt{x_{30}^2+y_1^2}\,] + 2y_1\ln[x_{20}+\sqrt{x_{20}^2+y_1^2}\,]$$

$$- y_1\ln[x_{10}+\sqrt{x_{10}^2+y_1^2}\,] - y_1\ln[x_{30}+\sqrt{x_{30}^2+y_1^2}\,]\Big|_{y_{10}}^{y_{20}}$$

$$x_{10} = r_0\cos\phi + x_s - x_{mj-1}$$
$$x_{20} = r_0\cos\phi + x_s - x_{mj}$$
$$x_{30} = r_0\cos\phi + x_s - x_{mj+1}$$
$$y_{10} = r_0\sin\phi + y_s - y_{nj-1}$$
$$y_{20} = r_0\sin\phi + y_s - y_{nj}$$
$$a = x_{mj} - x_{mj-1}$$

(x_s,y_s) is the excitation point of the coaxial-type probe feed and r_0 is the radius of the inner conductor of the feed.

The elements Z^{yy}_{hji} and V^{y}_{hj} have the same form as (3A.1) and (3A.2), respectively, (3A.5) and (3A.6), if a change of x- and y-coordinates is made in these expressions.

From expression (3A.2) it is clear that $\partial^2_{x_j} A^x_{hi}$ has a logarithmic singularity if the two subsections i and j are touching. Some parts of the x_j-integral over $(\partial^2_{x_j} A^x_{hi})J_{pjx}$ can be done analytically, which means that the logarithmic singularity can be removed. The result of this x_j-integration is:

$$\int_{x_j} [\partial^2_{x_j} A^x_{hi}(x_j,y_j)] J_{pjx}(x_j,y_j)\,dx_j$$

$$= \frac{\mu_0}{4\pi a^2} \Bigg[\int_{x_{mj-1}}^{x_{mj}} 2x_{20}\ln[y_1+\sqrt{x_{20}^2+y_1^2}] - x_{10}\ln[y_1+\sqrt{x_{10}^2+y_1^2}] - x_{30}\ln[y_1+\sqrt{x_{30}^2+y_1^2}]\Big|_{y_{10}}^{y_{20}} dx_j$$

$$+ \int_{x_{mj}}^{x_{mj+1}} -2x_{20}\ln[y_1+\sqrt{x_{20}^2+y_1^2}] + x_{10}\ln[y_1+\sqrt{x_{10}^2+y_1^2}] + x_{30}\ln[y_1+\sqrt{x_{30}^2+y_1^2}]\Big|_{y_{10}}^{y_{20}} dx_j$$

$$+ 2(x_{mi}-x_{mj}+a)\Bigg[x_{20}\left(\ln[y_1+\sqrt{x_{20}^2+y_1^2}] - 1\right) + y_1\ln[2x_{20}+2\sqrt{x_{20}^2+y_1^2}]\Big|_{y_{10}}^{y_{20}}\Bigg]\Bigg|_{x_{mj-1}-x_{mi}}^{x_{mj}-x_{mi}}$$

$$+ 2(x_{mj}-x_{mi}+a)\Bigg[x_{20}\left(\ln[y_1+\sqrt{x_{20}^2+y_1^2}] - 1\right) + y_1\ln[2x_{20}+2\sqrt{x_{20}^2+y_1^2}]\Big|_{y_{10}}^{y_{20}}\Bigg]\Bigg|_{x_{mj}-x_{mi}}^{x_{mj+1}-x_{mi}}$$

$$- (x_{mi-1}-x_{mj}+a)\left[x_{10}\left(\ln[y_1+\sqrt{x_{10}^2+y_1^2}\,] - 1\right)\right.$$

$$\left. + y_1\ln[2x_{10}+2\sqrt{x_{10}^2+y_1^2}\,]\Big|_{y_{10}}^{y_{20}}\right] \Bigg|_{x_{mj-1}-x_{mi-1}}^{x_{mj}-x_{mi-1}}$$

$$- (x_{mj}-x_{mi-1}+a)\left[x_{10}\left(\ln[y_1+\sqrt{x_{10}^2+y_1^2}\,] - 1\right)\right.$$

$$\left. + y_1\ln[2x_{10}+2\sqrt{x_{10}^2+y_1^2}\,]\Big|_{y_{10}}^{y_{20}}\right] \Bigg|_{x_{mj}-x_{mi-1}}^{x_{mj+1}-x_{mi-1}}$$

$$- (x_{mi+1}-x_{mj}+a)\left[x_{30}\left(\ln[y_1+\sqrt{x_{30}^2+y_1^2}\,] - 1\right)\right.$$

$$\left. + \quad y_1\ln[2x_{30}+2\sqrt{x_{30}^2+y_1^2}\,]\Big|_{y_{10}}^{y_{20}}\right] \Bigg|_{x_{mj-1}-x_{mi+1}}^{x_{mj}-x_{mi+1}}$$

$$- (x_{mj}-x_{mi+1}+a)\left[x_{30}\left(\ln[y_1+\sqrt{x_{30}^2+y_1^2}\,] - 1\right)\right.$$

$$\left. + y_1\ln[2x_{30}+2\sqrt{x_{30}^2+y_1^2}\,]\Big|_{y_{10}}^{y_{20}}\right] \Bigg|_{x_{mj}-x_{mi+1}}^{x_{mj+1}-x_{mi+1}}$$

(3A.7)

Some parts of the y_j-integral over $(\partial_{x_j}\partial_{y_j}A^x_{hi})J_{pjy}$ in (3A.4) can also be calculated analytically, and thus removing the logarithmic singularity.

4. RESULTS.

In this chapter some numerical results of the method presented in chapter 2 and chapter 3 are given. Using the FORTRAN programs described in Appendix 4A, the resonant frequency and the input impedance are calculated for the case of a single rectangular microstrip antenna and for the case of an array of rectangular microstrip antennas. This is done for two types of basis functions, namely for sinusoidal entire domain basis functions (see section 2.5.1) and for Piece-wise linear (PWL) sub domain basis functions. The excitation can be either a stripline feed or a coaxial probe feed.
Note that the source extracting technique, described in section 3.3, can only be used for the case of PWL sub domain basis functions.
In all the results presented here the correction term jX_1 of (2.4.27) for the case of a coaxial probe feed, is not added to the input impedance.

4.1 Single rectangular microstrip antenna.

In order to determine the accuracy of the method, a simple rectangular microstrip antenna is analyzed. The geometry of this microstrip antenna is shown in fig 4.1.

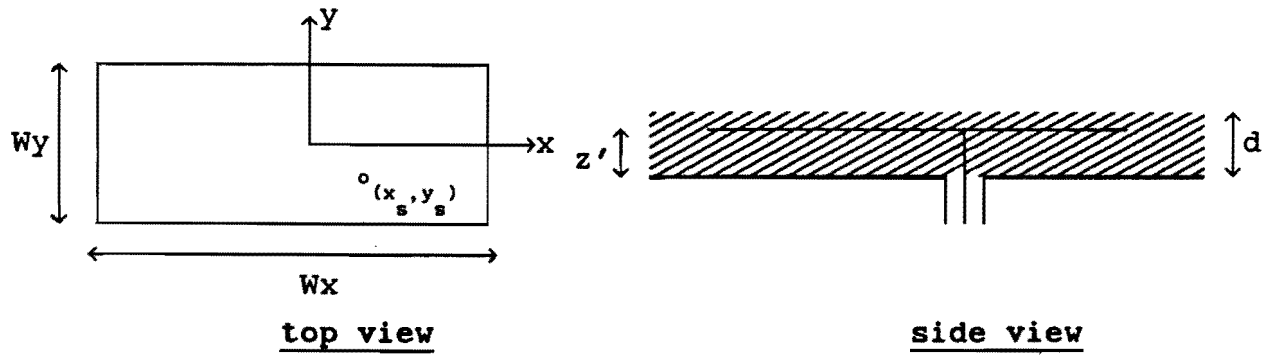

Fig. 4.1: Geometry of a rectangular microstrip antenna

4.1.1 Entire domain basis functions.

From [10] it is known that the current distribution on the patch is almost sinusoidal in the direction of current and almost uniform in the direction orthogonal to the current. This would mean that the shape of the patch current is independent of the location of the source. In the next section, however, it will be shown that this is only true for the imaginary part of the surface current.

In spite of the fact that the shape of the real part of the patch current is not entirely sinusoidal, the use of just one sinusoidal entire domain basis function does give good results for the case of a rectangular microstrip antenna. The patch current is thus expanded in the form:

$$\vec{J}_p = I_1 \cos\left(\frac{\pi x}{Wx}\right)\vec{e}_x + I_2 \cos\left(\frac{\pi y}{Wy}\right)\vec{e}_y \qquad (4.1.1)$$

A great advantage of the use of entire domain basis functions for the analysis of a rectangular microstrip antenna is that the matrix [Z] is very small (2x2 matrix) and that the off-diagonal elements of [Z] are zero (see expression (3.2.7a)).

From expression (3.2.7c) and (3.2.7d) it can be seen that if the excitation point (x_s,y_s) is on the x- or y-axis, the excitation vector [V] has only one component, i.e. if $x_s = 0$ then $V_1 = 0$ and if $y_s = 0$ then $V_2 = 0$.

Using (4.1.1) and the matrix equation [V] + [Z][I] = [0], the resonant frequency and input impedance of a microstrip antenna can be determined. Some results are shown in fig 4.2. ⟶ fig. 4.4.
The resonant frequency is now obtained by finding a frequency f_r for which the determinant of the matrix [Z] has a minimum. Note that for $f = f_r$ the imaginary part of the input impedance is zero.

Fig. 4.2. shows the determinant of [Z] and the input impedance of a coax fed rectangular microstrip antenna. The excitation is situated on the x-axis, so only one component of (4.1.1) has to be used in the calculations. The agreement between these calculations and that of [10,fig.7] is very good.
The results for an rectangular microstrip antenna fed by a stripline are shown in fig 4.3. Again, agreement between these results and that of [6,fig.4 and 10,fig.2] is very good.
Fig. 4.4 shows the determinant of [Z] and the input impedance for an off-center fed rectangular microstrip antenna. The source is a coaxial feed probe. Because the excitation is not situated on one of the axis, both the expansion functions in (4.1.1) have to be used in the calculations. Again the results are in good agreement with earlier results [10,fig.6].

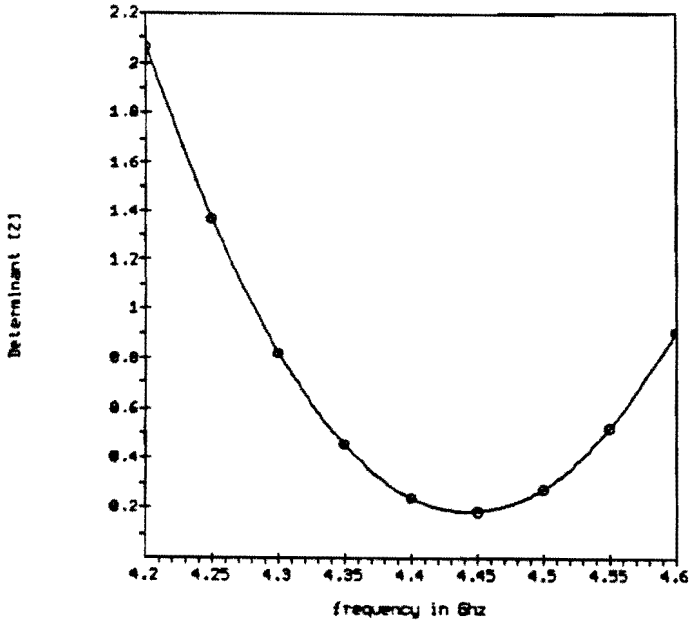

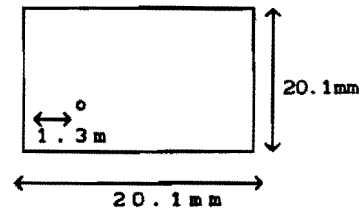

$d = z' = 1.59mm$

$\varepsilon_r' = 2.55 \quad \tan\delta = 0.002$

(a)

increment: 50Mhz
(increasing clockwise)

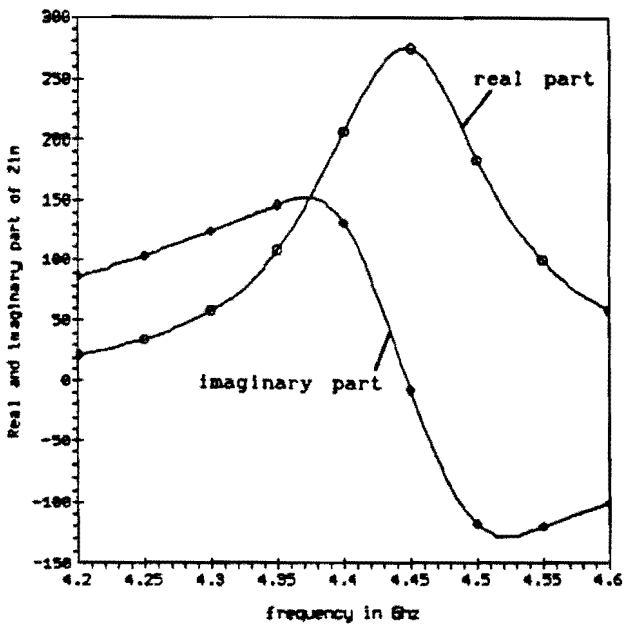

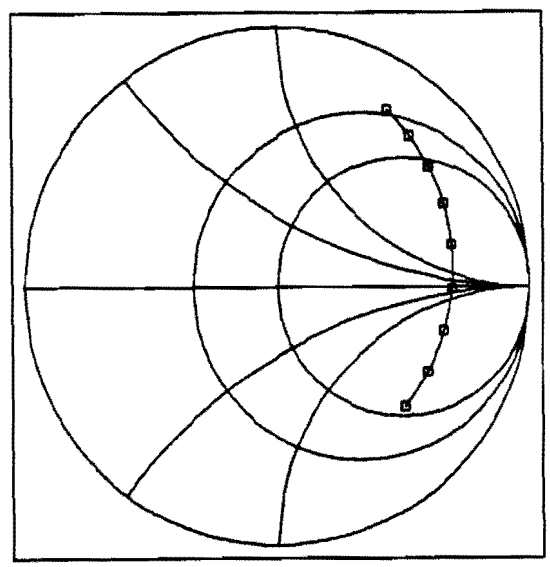

(b)

Fig. 4.2: Determinant of [Z] (a) and input impedance (b) of a rectangular microstrip antenna fed by an coax. Frequency band 4.2 ⟶ 4.6Ghz.

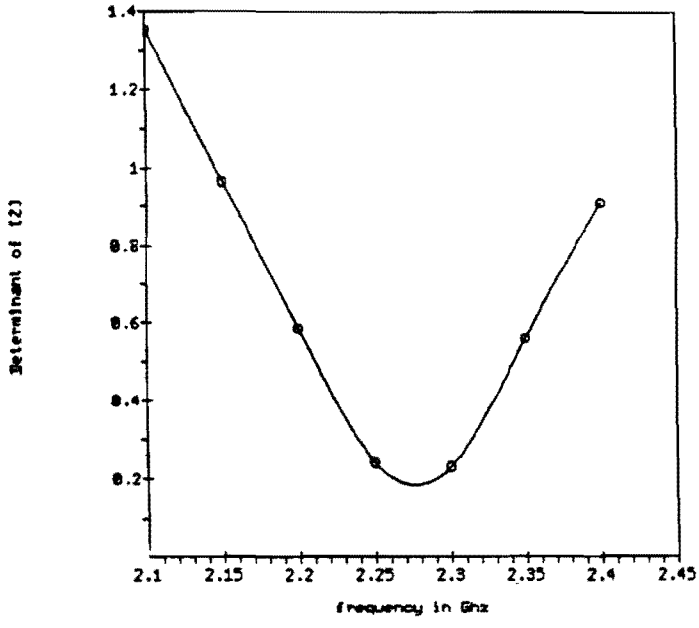

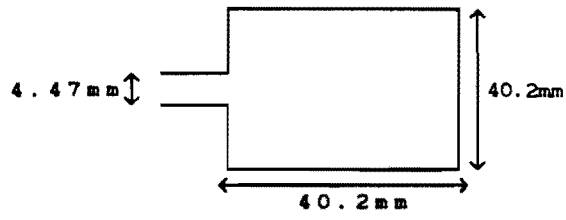

d=z'=1.59mm

ε_r' = 2.55 tanδ=0.002

(a)

increment: 50Mhz
(increasing clockwise)

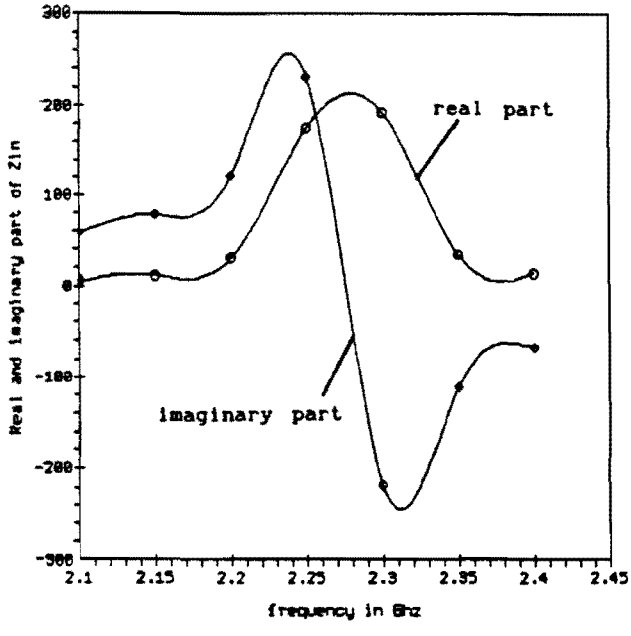

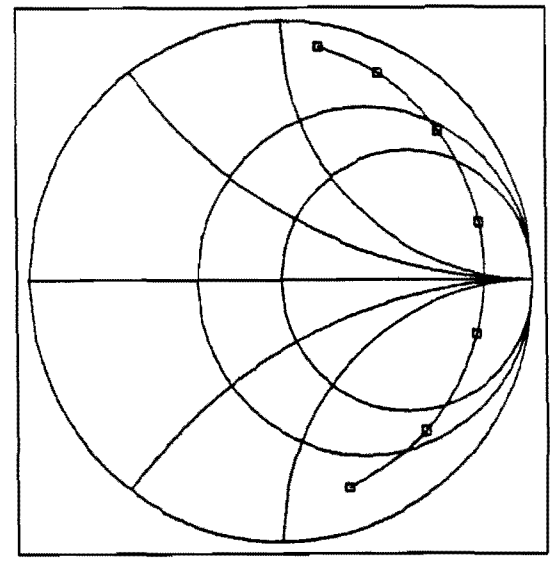

(b)

Fig. 4.3: Determinant of [Z] (a) and input impedance (b) of a rectangular microstrip antenna fed by a stripline. Frequency band 2.1 ⟶ 2.4Ghz

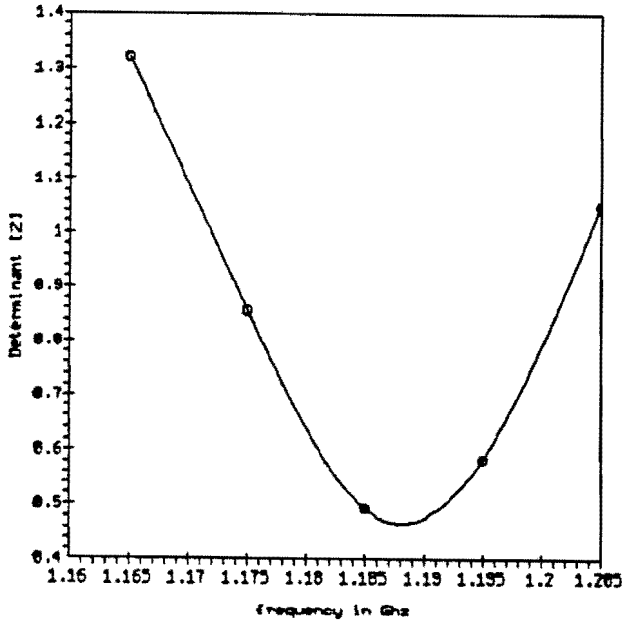

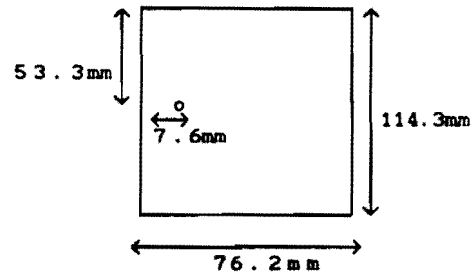

d=z'=1.59mm

ε_r' = 2.64 tanδ=0.003

(a)

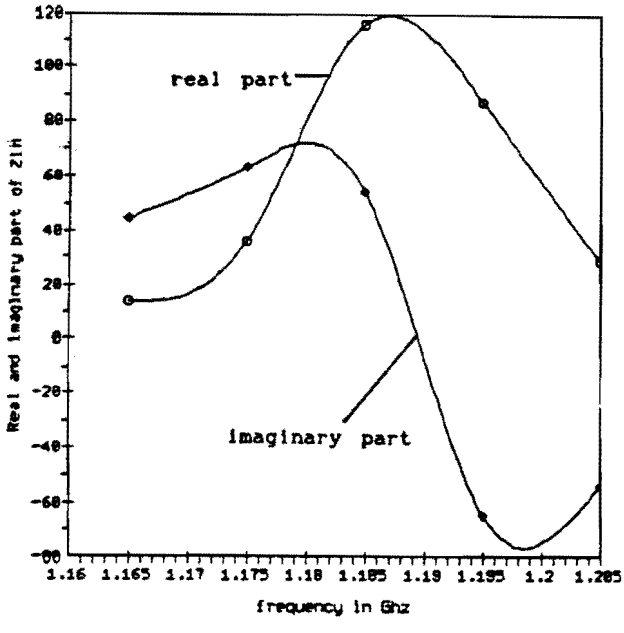

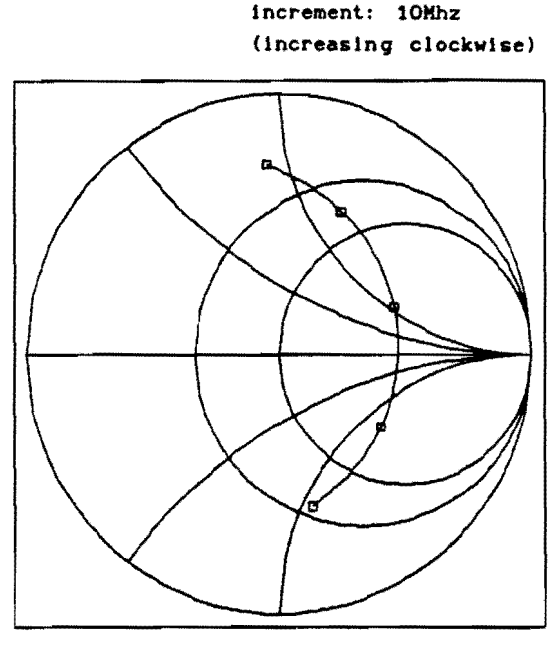

(b)

Fig. 4.4: Determinant of [Z] (a) and input impedance (b) of an off-center fed rectangular microstrip antenna. Frequency band 1.165 ⟶ 1.205Ghz.

4.1.2 Sub domain basis functions.

Sub domain basis functions are more flexible to use than sinusoidal entire domain basis functions, i.e. arbitrarily shaped microstrip antennas can relatively easily be analyzed using this type of basis functions. In this section a simple rectangular microstrip antenna is analyzed using Piece-wise linear (=rooftop) basis functions.

The upper conductor of the microstrip antenna is now divided in M+1 cells along the x-axis and N+1 cells along the y-axis (see fig 2.9). The patch current is then expressed in M(N+1) + N(M+1) rooftop basis functions. As the number of cells increases, the calculated solution converges, in theory, towards the real solution. The convergence is illustrated in fig.4.5 where the calculated resonant frequency as a function of the number of cells along the x-axis is shown. The number of cells along the y-axis N+1 = 1. Note that in this case only $\hat{x}$-polarized basis functions are used.

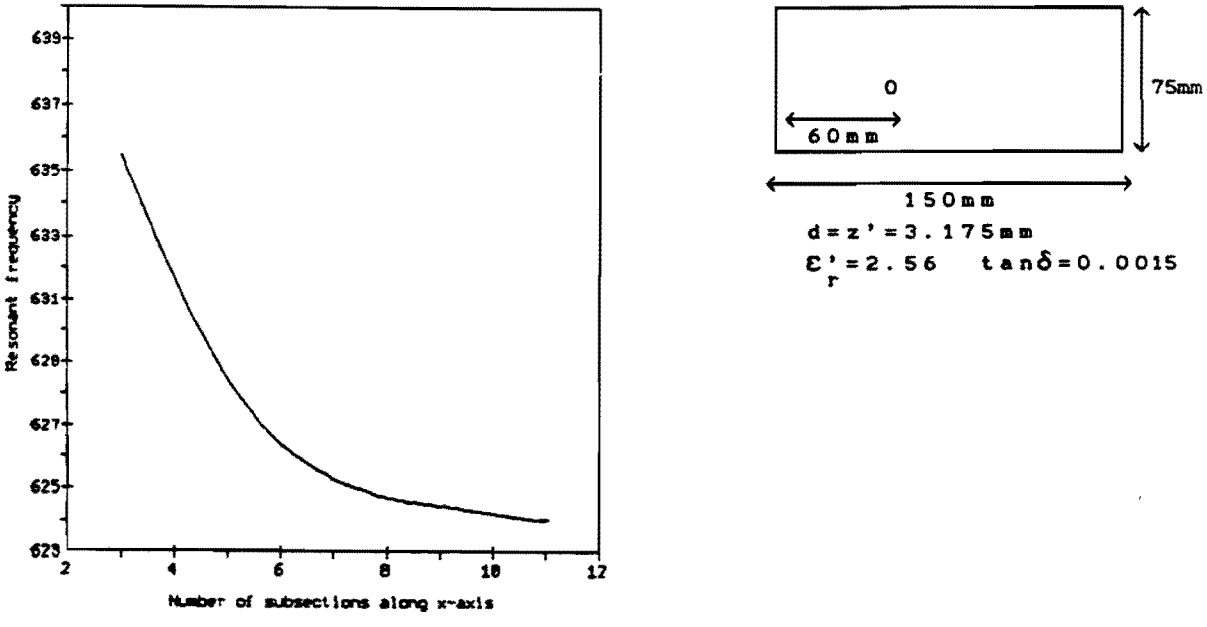

Fig 4.5: convergence of resonant frequency using rooftop sub domain basis functions.

In order to calculate the input impedance, the matrix equation [V] + [Z][I] = [0] has to be solved. Once the vector [I] is known, the current distribution on the upper conductor can be calculated. This is shown in figure 4.6, where the real and imaginary part of the patch current is drawn for y = 0 and f = 625Mhz ($f > f_r$). The number of cells along the x-axis is 10 and the number of cells along the y-axis is 1. Also is the function $f(x) = \cos(\frac{\pi x}{wx})$ drawn in figure 4.6. The microstrip antenna has the same dimensions as the antenna of fig.4.5.

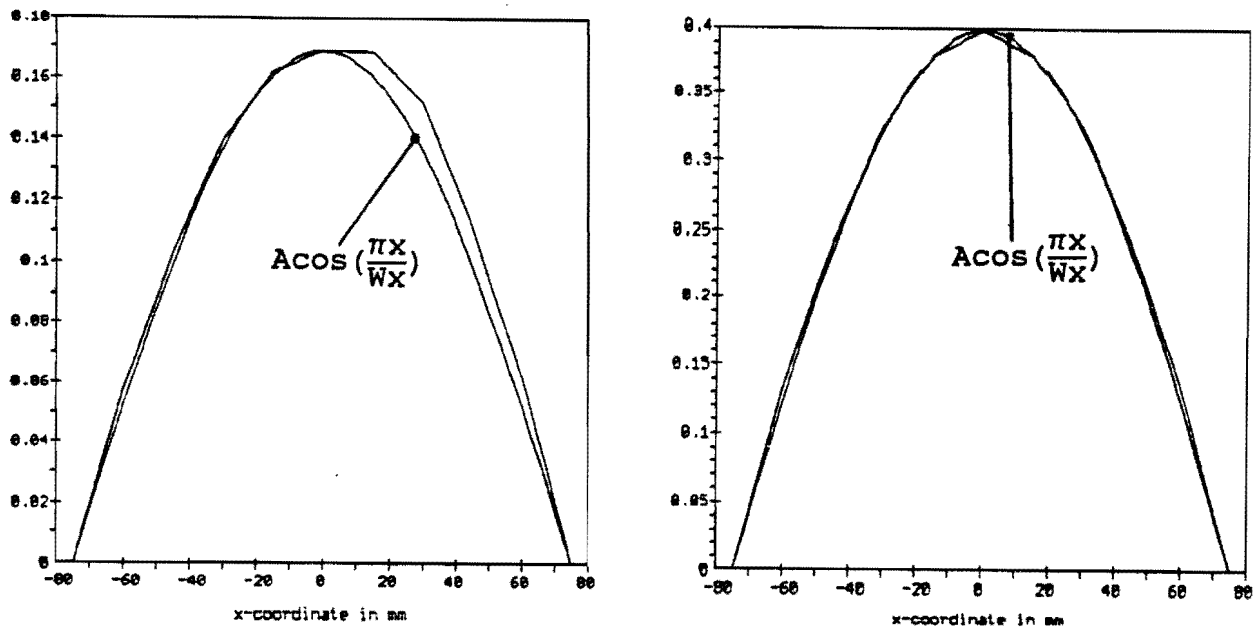

real part

imaginary part

Fig. 4.6: Calculated patch current using rooftop basis functions. Frequency f = 625Mhz.

From fig 4.6 it is obvious that the real part of the patch current is not independent of the location of the excitation. On the other hand, the imaginary part of the patch current is independent of the position of the excitation and is almost sinusoidal along the x-axis. It should be noted that the imaginary part of the patch current is negligible if the frequency is not near resonance. Near resonance, however, the imaginary part of the patch current is dominant. Thus near resonance the patch current will be almost sinusoidal along the x-axis (in this example). From fig. 4.6 one can also conclude that the shape of the radiation pattern of a single rectangular microstrip antenna depends on the location of the excitation. In [15,pp.71] this effect is verified experimentally.

In order to analyze the convergence of the input impedance a microstrip antenna with the same dimensions as the antenna of figure 4.5 was analyzed. In fig. 4.7 some results are shown. From this figure it is clear that the imaginary part of the input impedance strongly depends on the number of cells along the x-axis. In this example the best choice for the number of subsections along the x-axis Mx = 9, i.e. the excitation point is located in the middle of the 6-th subsection. In [22] a similar technique was used in order to obtain good results. The bad prediction of the input impedance using sub domain basis functions can possibly be improved if a better source model is used. In [23] this was also suggested.

In figure 4.8 an example is shown for the case that the number of cells along the y-axis is not equal 1. In this case there are 9 cells along the x-axis and 4 cells along the y-axis. The total number of basis functions is thus 59, i.e. 32 $\hat{x}$-directed expansion functions and 27 $\hat{y}$-directed expansion functions. The excitation is now located in the point (x_s,y_s) = (25mm,0mm). The other dimensions are the same as in figure 4.5.

It may be concluded that for the case of an rectangular microstrip antenna the best choice for the basis functions are the sinusoidal entire domain basis functions. Using this type of basis functions good results can be obtained be using only 2 basis functions (see (4.1.1)). The computing time for the calculation of the matrix [Z] and vector [V] is in this case relative small.

However, if one wants to analyze an arbitrarily shaped microstrip antenna, sub domain basis functions have to be used. Due to the simple source model, the determination of the input impedance will be difficult. The best choice for the excitation point is in this case in the middle of a subsection. To improve the moment method for the case of sub domain basis functions, more research has to be done on the modeling of the source.

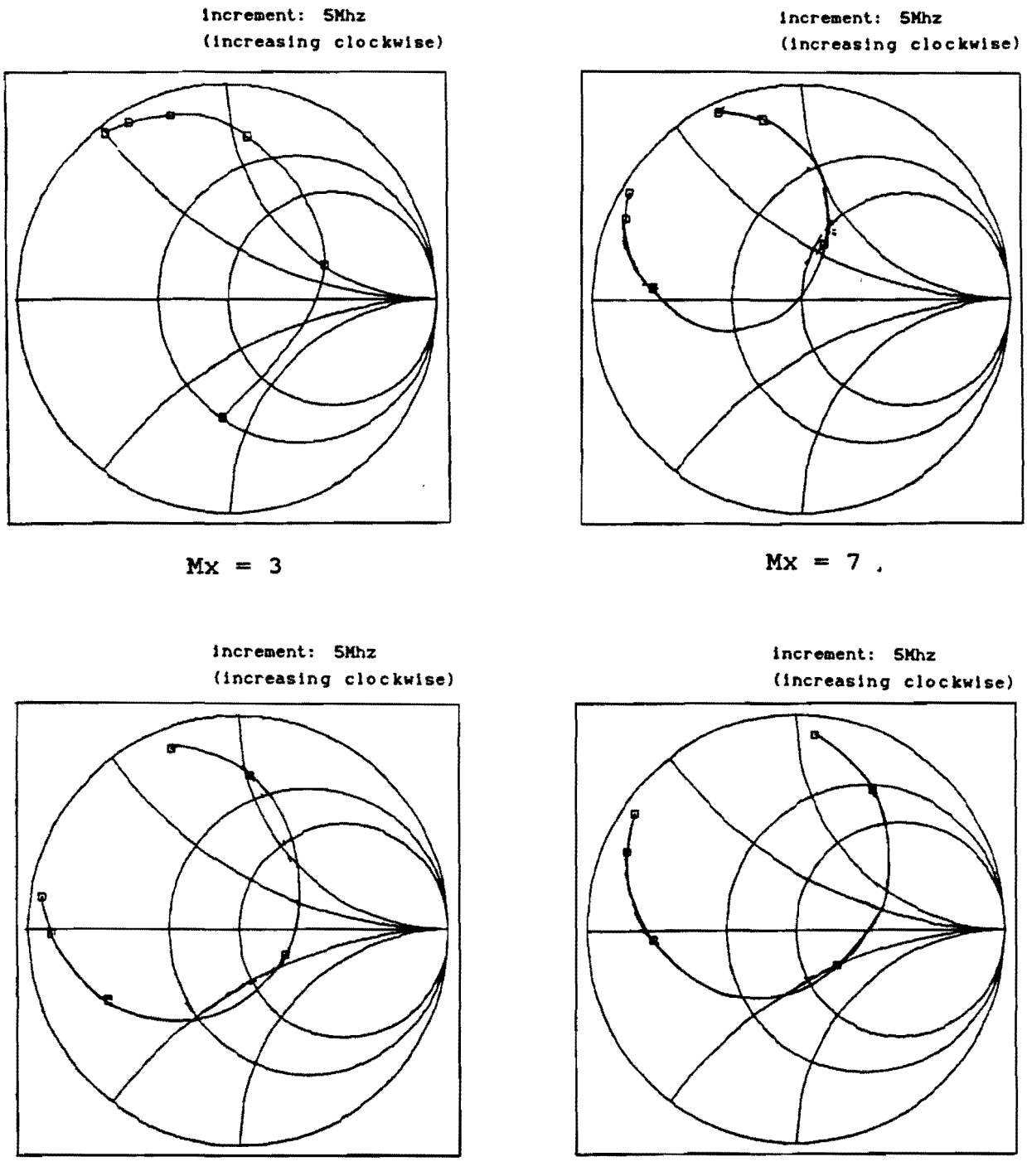

Fig. 4.7: Input impedance of a rectangular microstrip antenna as a function of the number of cells along the x-axis. dimensions: see fig.4.5. Frequency band 615 ⟶ 640Mhz.

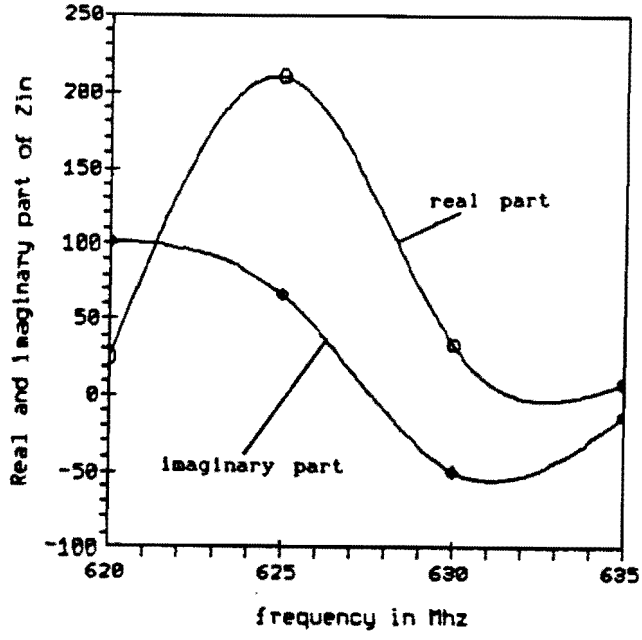

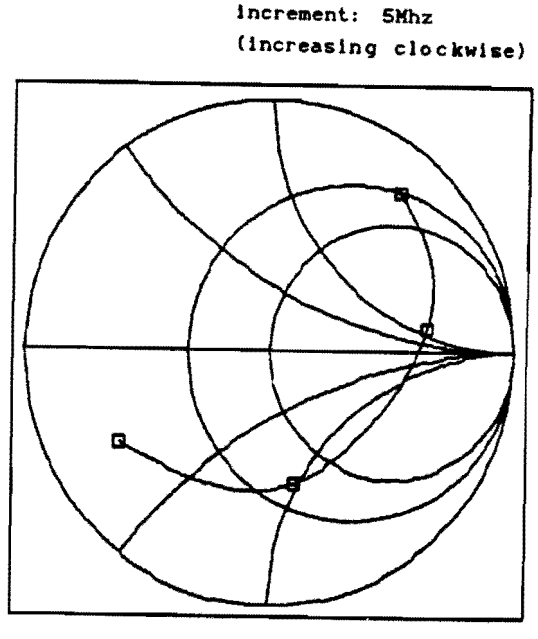

Fig. 4.8: Input impedance of a rectangular microstrip antenna using 59 rooftop basis functions, with 9 cells along the x-axis and 4 cells along the y-axis.
Dimensions :see fig. 4.5, except (x_s, y_s)=(25mm,0mm).
Frequency band 620 ⟶ 635Mhz.

4.2 Array of rectangular microstrip antennas.

With the moment method presented in this report, arrays of microstrip antennas can be analyzed. These arrays may have a dielectric cover. Because the analytical formulation of the method is exact, surface waves effects and coupling to adjacent antenna elements are taken into account. As an example of the mutual coupling in microstrip arrays, the array of fig 4.9 will be considered. The total array consists of 5 rectangular microstrip antennas with a element spacing s_x. Element 1 is excited by a coaxial feed probe. In order to determine the influence of the 4 coupled elements, five different situations have been analyzed. First an array containing 1 element was analyzed. Then an array containing 2 elements, 3 elements, 4 elements and finally an array containing 5 elements was analyzed. In each case the excitation was located at the first element.
In order to limit the computing time entire domain basis functions were used. On each element two basis functions were used to describe the unknown patch current.
The calculated input impedance for these 5 arrays are shown in fig. 4.10.

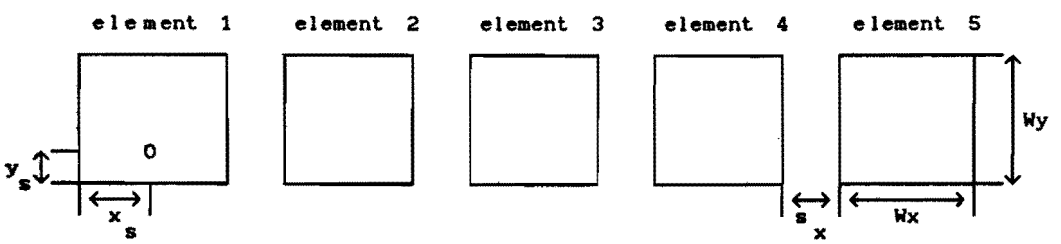

Example: Wx=20mm d=z'=1.58mm (no dielectric cover)
Wy=22.3mm ε_r'=2.2 tanδ=0.002
s_x=5mm
x_s=10mm
y_s=6.8mm

Fig. 4.9: Geometry of the microstrip array antenna.

increment: 30Mhz
(increasing clockwise)

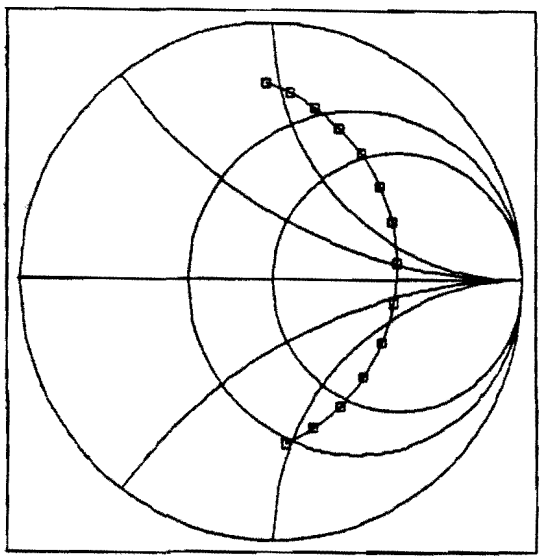

(a)

increment: 30Mhz
(increasing clockwise)

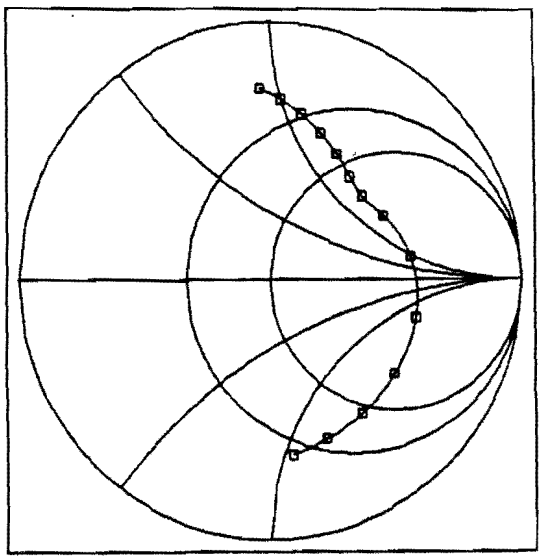

(b)

increment: 30Mhz
(increasing clockwise)

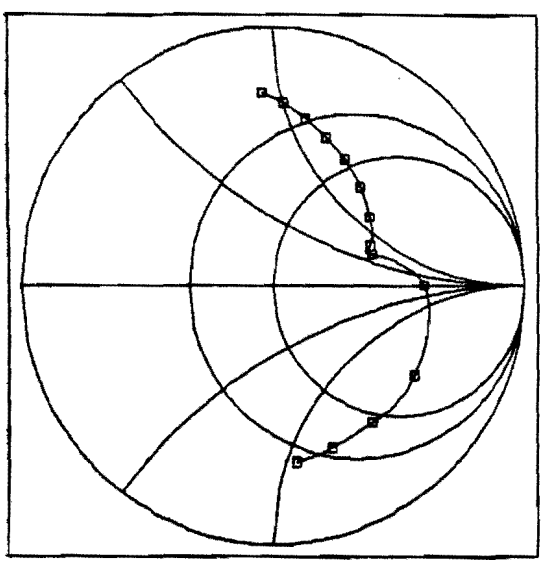

(c)

increment: 30Mhz
(increasing clockwise)

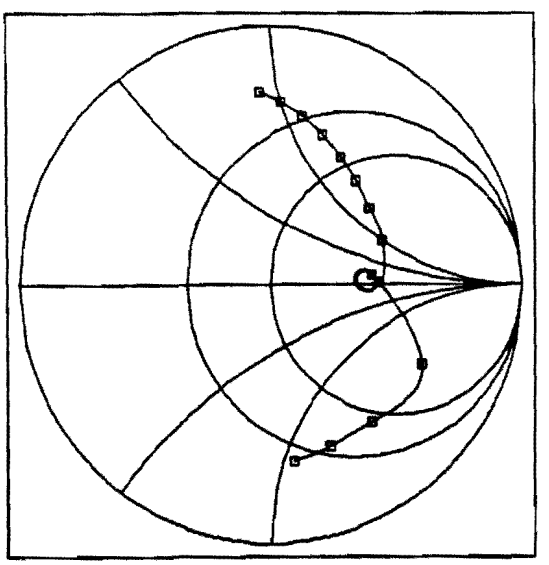

(d)

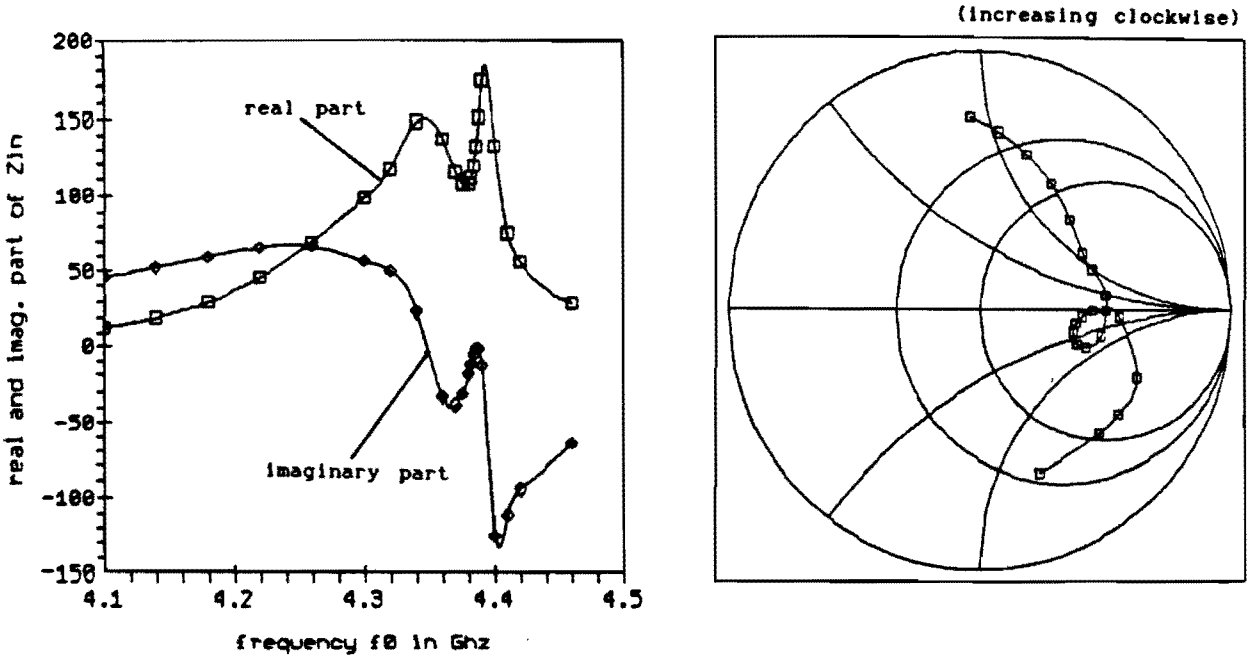

(e)

Fig. 4.10: Input impedance of an array containing (a) 1 element, (b) 2 elements, (c) 3 elements, (d) 4 elements, (e) 5 elements. In each case element 1 (see fig 4.7) is excited with a coaxial probe. Frequency band 4.1 ⟶ 4.49Ghz.

It should be noted that the element spacing s_x is in this example relative small, which means that the mutual coupling in an practical array will be smaller then in this example.
From fig. 4.10 it is clear that the impedance locus changes dramatically if one or more elements are placed in the neighbourhood of element 1. One can also conclude that not only element 2 has a strong influence on the current distribution on element 1, but that all four capacitive coupled elements have a strong influence.

APPENDIX 4A: SOFTWARE USER GUIDE.

In this appendix a description of the developed software is given. Because a large amount of programs is developed, the source listings of these programs are not added to this report. All programs are written in standard FORTRAN-77 and can therefore be used with a great number of FORTRAN compilers. The programs are easy to use and can be easily adjusted, because all the programs and subroutines are provided with text-blocks in which the structure of the program/subroutine under consideration is stated. All programs use double precision variables.

The software can be run on a XT- or AT-personal computer in combination with a RM-FORTRAN or MS-FORTRAN compiler. The computing time to calculate the matrix [Z] and the excitation vector [V] depends of course on the number of basis functions that are used. The calculation of one [Z] or [V] element is in the order of 3 minutes on a XT (8.7Mhz with mathematical co-processor) computer. The computing time needed for solving the matrix equation [Z][I]=-[V] is very small in comparison with the time needed to calculate the matrices [Z] and [V].

In figure A.1 the main programs MSSUB and MSLUD and all the important subroutines are shown.
On the next pages a brief description of each program/subroutine is given.

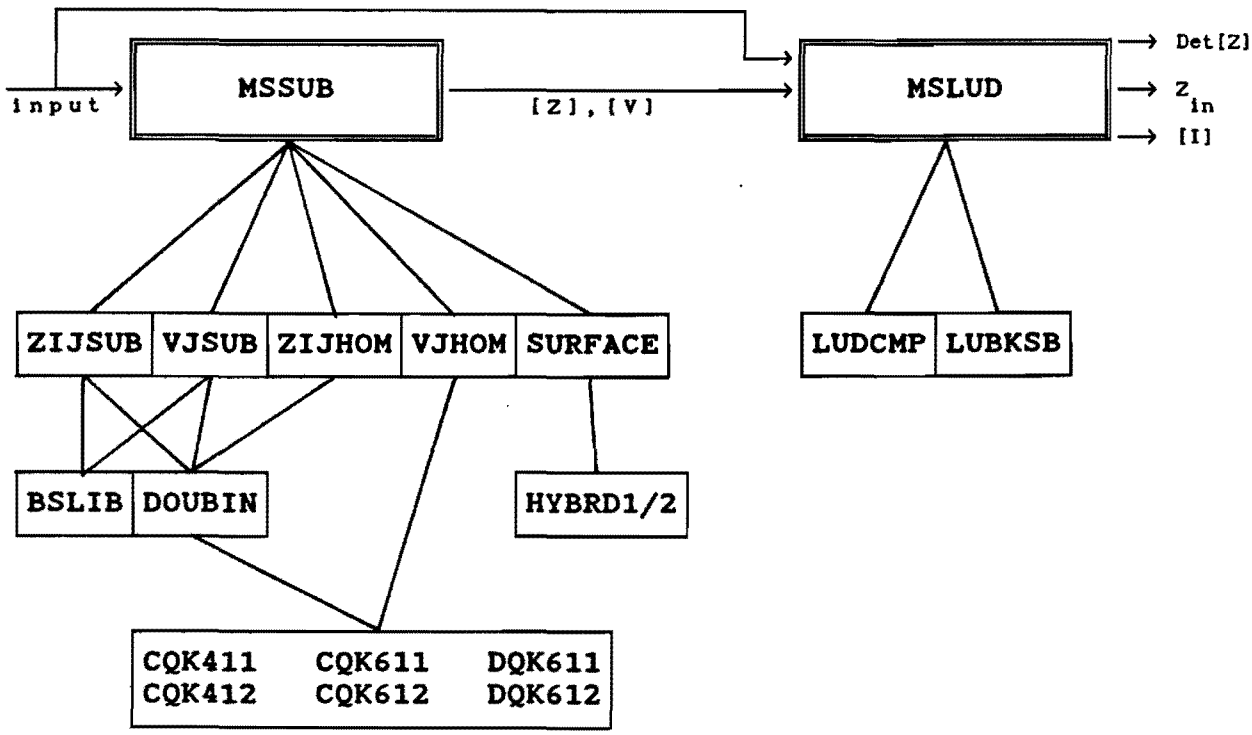

Fig. A.1: Relationship between the programs and subroutines.

MSSUB.

MSSUB is a program that calculates all the relevant elements of the matrix [Z] and of the excitation vector [V]. The Toeplitz-type symmetry of the matrix [Z] is taken into account. The output files are:

ZIJ.dat : contains all relevant elements of [Z]
VJ.dat : contains all elements of the excitation vector [V]
ERRZ.dat: contains the absolute errors in the computed [Z] elements
ERRV.dat: contains the absolute errors in the computed [V] elements.

The user is asked for the following input parameters:

Subdomain (1) or entire domain (0) basis functions :
Number of sub sections along the x-axis (Mx) :
Number of sub sections along the y-axis (Nx) :
Stripline (0) or coax (1) feed :
Source position (x_s,y_s) in mm :
Width of stripline (w) or radius (r_0) of coax in mm :
Real part of permittivity of the substrate (ε'_r) :
Dielectric loss (tanδ) :
Distance (z') between ground plane and patch in mm :
Thickness (d) of dielectric substrate in mm :
x-dimension (Wx) of microstrip antenna :
y-dimension (Wy) of microstrip antenna :
Start frequency in Ghz :
Number of frequency evaluations :
Distance between two frequencies in Ghz :

MSLUD.

This program solves the matrix equation

$$[Z][I] = -[V]$$

where the vector [I] contains the unknown current coefficients. Before this equation can be solved, the matrix [Z] is filled in a proper way taking into account the Toeplitz-type symmetry of [Z] (see section 3.4). The output files are:

DETZ.dat : determinant of [Z]
REZIN.dat : real part of input impedance
IMZIN.dat : imaginary part of input impedance.

The user is asked for the following parameters:

Only x- (0) or x- and y-components (1) in the patch current:
Number of sub sections along the x- and y-axis (Mx,Nx) :
Start frequency in Ghz :
Number of frequency evaluations :
Distance between two frequencies in Ghz :

ZIJSUB.

This subroutine calculates a (Z_{ji} - Z_{hji}) element for the case of PWL subdomain basis functions and a Z_{ji} element for the case of sinusoidal entire domain basis functions. Z_{hji} is a term that represents the extracted source singularity (see section 3.3)

VJSUB.

This subroutine calculates a (V_j-V_{hj}) element for the case of PWL subdomain basis functions and a V_j element for the case of sinusoidal entire domain basis functions. V_{hj} is a term that represents the extracted source singularity (see section 3.3).

ZIJHOM.

This subroutine calculates a Z_{hji} element for the case of PWL subdomain basis functions.

VJHOM.

This subroutine calculates a V_{hj} element for the case of PWL subdomain basis functions.

SURFACE.

Subroutine SURFACE calculates the location of a zero in the complex function Tm (see equation (3.1.1)). The zeros can be found be using the minpack [16] subroutine HYBRD.

HYBRD1/2.

This minpack routine tries to find a zero of a system of n nonlinear functions in n variables by using a modification of the Powell hybrid method [16]. In our case n = 2, because both the real and imaginary parts of equation (3.1.1) have to be zero.

BSLIB.

This file contains a number of subroutines and functions that are frequently used by the other subroutines.

DOUBIN.

Subroutine DOUBIN calculates a two-dimensional integral. A two-dimensional integral can be calculated by using a product rule [20]. Consider for example the double integral I:

$$I = \int_{x_1}^{x_2}\int_{y_1}^{y_2} F(x,y)\ dydx = \int_{x_1}^{x_2} g(x)\ dx$$

The inner integral g(x) is now obtained by using an one-dimensional integration routine. Because it is not possible in FORTRAN to call subroutine A in subroutine A (=recursion), the two one-dimensional integration routines used here must have different names.

An absolute error estimate of the two dimensional integral I is given by:

$$\text{error} \leq \text{errx} + (x_2 - x_1) \max_x(\text{erry})$$

where errx is the absolute error in the outer integral and $\max_x(\text{erry})$ is the maximum absolute error in the inner integral.

CQK411,CQK412,CQK611,CQK612.

These subroutines are complex fixed-point integration routines and uses 41- and 61-points Gauss/Kronrod integration rules. These routines are based on the routines given in Quadpack [20].
An estimate of the absolute error in the calculated integral is also determined.

DQK611,DQK612.

Same as the above routines, except for the fact that double precision (real*8) variables are used instead of complex*16 variables.

LUDCMP and LUBKSB.

These subroutines solve the general matrix equation [A][X] = [B], where [A] is a NxN matrix and [X] and [B] are Nx1 matrices [21].
First the LU decomposition is computed by the routine LUDCMP. Subroutine LUBKSB then tries to find the solution of matrix equation [LUA][X] = [B], where [LUA] is the LU-decomposition of the original matrix.
Apart from solving a matrix equation it is also possible to calculate the determinant of [A] by using LUDCMP.

All the programs and subroutines mentioned here can be found in

5. CONCLUSIONS.

-The spectral domain moment method presented in this report can, in theory, be used to analyze an arbitrarily shaped single layered microstrip structure with a protective dielectric cover. Two types of basis functions have been considered, namely entire domain sinusoidal basis functions and rooftop sub domain basis functions. For the case of rooftop basis functions, a efficient method is presented for the evaluation of the matrix elements [Z] and [V]. This technique is called "Source term extraction".

-In the case of a single rectangular microstrip antenna or in the case of an array of rectangular microstrip antennas, the best choice for the type of basis function is the entire domain sinusoidal basis function. Now only 2 basis functions have to be used in order to obtain good results for the resonant frequency and input impedance of the antenna.

-If one wants to analyze an arbitrarily shaped microstrip antenna (for example a crossed-slot microstrip antenna) sub domain rooftop basis functions can be used. However, due to the simple source model of the (coaxial- or stripline-) feed, the prediction of the input impedance is more difficult in this case.
Therefore more research has to be done on the modeling of the source.

REFERENCES.

[1] H.J. Visser
Circularly polarized microstrip phased array antennas for mobile communications.
Graduate report no.ET.3-89, Professional group Electromagnetism and Circuit theory, Department of Electrical Engineering, Eindhoven University of Technology, Netherlands, 1989.

[2] A.B. Smolders
Microstrip array geschikt voor ontvangst van satelliet tv-signalen.
Research report no. ET.20-88, Professional group Electromagnetism and Circuit theory, Department of Electrical Engineering, Eindhoven University of Technology, Netherlands, 1988 (in dutch).

[3] J. Huang and Y. Rahmat-Samii
'Recent array antenna developments at JPL'
Proceedings of the COST 213/KUL phased array workshop, Leuven Belgium, october 1988, pp.53-61.

[4] I.J. Bahl and P. Bhartia
Microstrip Antennas.
Artech House, Massachusetts, 1980.

[5] M.C. Bailey and M.D. Deshpande
'Integral equation formulation of microstrip antennas'.
IEEE Trans. on Antennas and Propagation, vol. AP-30, no.4, july 1982, pp. 651-656.

[6] D.M. Pozar
'Input impedance and mutual coupling of rectangular microstrip antennas'.
IEEE Trans. on Antennas and Propagation, vol. AP-30, no.6, november 1982, pp. 1191-1196.

[7] T. Zwemstra
Analysis of a dual stacked rectangular microstrip antenna.
Graduate report no.ET.14-89, Professional group Electromagnetism and Circuit theory, Department of Electrical Engineering, Eindhoven University of Technology, Netherlands, 1989.

[8] M.E.J. Jeuken
Electromagnetische golven en antennes.
Professional group Electromagnetism and Circuit theory, Department of Electrical Engineering, Eindhoven University of Technology, Netherlands, 1983 (in dutch).

[9] J.R. Mosig and F.E. Gardiol
'A dynamical radiation model for microstrip antennas'
In P. Hawkes, Advances in electronics and electron physics.
Academic Press, New York, 1982, pp. 139-237.

[10] M.D. Deshpande and M.C. Bailey
'Input impedance of microstrip antennas'
IEEE Trans. on Antennas and Propagation, vol. AP-30, no.4, july 1982, pp. 645-650.

[11] R.F. Harrington
Time harmonic fields.
McGraw-Hill, New York, 1961

[12] I.H. Sneddon
The use of integral transforms.
McGraw-Hill, New York, 1972

[13] T. Itoh and W. Menzel
'A full-wave analysis method for open microstrip structures'
IEEE Trans. on Antennas and Propagation, vol. AP-29, no.1, january 1981, pp. 63-67.

[14] E.H. Newman, J.H. Richmond and B.W. Kwan
'Mutual impedance computation between microstrip antennas'
IEEE Trans. on Microwave theory and tech., vol. MTT-31, no.11, november 1983, pp. 941-945.

[15] G. Gronau
Theoretische und experimentelle untersuchung der verkopplung in streifenleitungsantennen.
PH.D. Dissertation, Duisburg University, Germany, 1987 (in German).

[16] J.J. More, B.S. Carbow and K.E. Hillstrom
User guide for MINPACK-1.
ANL-80-74, Angonne National Laboratory.

[17] J.R. Mosig and T.K. Sarkar
'Comparison of quasi-static and exact electromagnetic fields from a horizontal electric dipole above a lossy dielectric backed by an imperfect ground plane'.
IEEE Trans. on Microwave theory and tech., vol. MTT-34, no.4, april 1986, pp. 379-387.

[18] E.H. Newman and D. Forrai
'Scattering from a microstrip antenna'
IEEE Trans. on Antennas and Propagation, vol. AP-35, no.3 march 1987, pp. 245-251.

[19] D.M. Pozar
'Improved computational efficiency for the moment method solution of printed dipoles and patches'.
Electromagnetics, vol.-3, september 1984, pp. 299-309.

[20] R. Piessens, E. de Doncker-Kapenga, C.W. Uberhuber and D.K. Kahaner
Quadpack.
Springer Verlag, Berlin, 1983.

[21] W.H. Press, B.P. Flannery, S.A. Teukolsky and W.T. Vetterling
Numerical Recipes.
Cambridge University Press, Cambridge, 1986.

[22] J.R. Mosig and F.E. Gardiol
'General integral equation formulation for microstrip antennas and scatterers'
IEE Proceedings, vol. 132, no.7, december 1985, pp. 424-432.

[23] B. Nauwelaers, J. Dewachtere, G. Vandenbosch and A. v.d. Capelle
'Microstrip antennas: A C.A.D. Approach'
Proceedings of the COST 213/KUL phased array workshop, Leuven Belgium, october 1988, pp.71-84.